Analysis of the Antigenic Composition and Differential Incorporation of Host Membrane Proteins into Murine Leukemia Virus by Flow Virometry

Mariam Maltseva

This thesis is submitted to the Faculty of Medicine in partial fulfillment of the requirements for the degree of Master of Science with specialization in Microbiology & Immunology.

Department of Biochemistry, Microbiology and Immunology
Faculty of Medicine
University of Ottawa

Abstract

Traditionally, viral particles have been primarily analyzed as a whole population according to their biochemical, genetic, and biophysical properties. Here, we describe single particle phenotypic analysis using surface markers found on Murine Leukemia Virus (MLV) by flow virometry. We used this technology to show differential incorporation of host surface markers between wild type MLV and glycosylated Gag (glycogag) deficient MLV. Moreover, we analyzed differential uptake efficiency of host proteins between two cell lines and primary lymphocytes. We hypothesize that the phenotypic profiling and quantification of antigens on the surface of individual viral particles will provide crucial information on the identity of the infected parental cells. Furthermore, we demonstrate that the MLV accessory protein glycogag is associated with the upregulation of surface antigen incorporation during assembly and release. Aside from possible evolutionary implications of glycogag, we demonstrate presence and varying antigenic composition on the surface of MLV viral particles reflective of the cell phenotype that they were released from.

Acknowledgements

I would like to express my great appreciation to Dr. Marc-André Langlois for accepting me to pursue my master's thesis in his laboratory group at the University of Ottawa and supervising my research project.

My thesis advisory committee, Dr Carolina Ilkow and Dr Robin Parks, thank you for your support, guidance and advice.

I would also like to thank Dr. Vera Tang, Anna Fritzsche and Dr. Tyler Renner for all your help with setting up the experimental design and providing me with insightful information and guidance for my experiments.

I would like to thank my family, friends and colleagues who have shown continued support throughout this journey. Thank you Andrew Norrie for the revisions on my thesis. To Matt, Yannick, Ricardo and Andrew thank you for your friendship and support in the lab.

List of Abbreviations

AIDS: Acquired immune deficiency syndrome
APOBEC: apolipoprotein B
ART: Antiretroviral therapy

BSA: Bovine serum albumin

CD: Cluster of differentiation
CXCR4: C X-C chemokine receptor type 4

DMEM: Dulbecco's modified Eagle medium
DNA: deoxyribonucleic acid

EDTA: Ethylenediaminetetraacetic acid
ELISA: Enzyme-linked immunosorbent assay
Env: Envelope
ERV: Endogenous Retrovirus
ESCRT: endosomal sorting complex required for transport
EV: Extracellular vesicle

FBS: Fetal bovine serum
FSC: Forward scatter
FVM: Flow virometry

Gag: Group Antigen
Glycogag / gPr80: glycosylated Gag
gRNA: genomic RNA

HEK 293T: Human embryonic kidney cells 293T
HIV-1: Human immunodeficiency virus type 1
HLA-DR: Human lymphocyte antigen-DR
HTLV: human T-lymphotropic virus

IgG: Immunoglobulin G
IFITM: interferon-induced transmembrane protein
IN: integrase

MA: Matrix
MFI: Mean fluorescence intensity
MHC: Major histocompatibility complex
MLV: (Moloney) Murine leukemia virus

nm: nanometer
Nef: Negative factor

PBS: Phosphate-buffered saline
PCR: Polymerase chain reaction
Pol: Polymerase

RNA: ribonucleic acid
RT: Reverse transcriptase

SIV: Simian immunodeficiency virus
sfGFP: super folder green fluorescent protein
SSC: Side scatter light

Vif: Viral infectivity factor
VLPs: Virus-like particles
Vpr: Viral protein R
Vpu: Viral protein U
Vpx: Viral protein X
VSSC: Violet Side Scatter Light

Table of Contents

Abstract ..... *ii*

Acknowledgements ..... *iii*

List of Abbreviations ..... *iv*

List of Tables ..... *viii*

List of Figures ..... *ix*

1 General Introduction: *1*

1.1 Introduction **1**

1.1.1 Viruses 1

1.1.2 Retroviruses 1

1.1.3 Morphology and life cycle of HIV-1 3

1.2 Techniques for Viral Characterization **6**

1.2.1 Flow Virometry 9

1.3 Murine Leukemia Virus **15**

1.3.1 Group Specific Antigen 15

1.3.2 Viral Polymerase and Integrase 16

1.3.3 Envelope glycoprotein 16

1.3.4 Glycosylated Group Specific Antigen 17

1.4 Aim of the current study **19**

1.4.1 Hypothesis 21

1.4.2 Approach 22

1.4.3 Implications 22

2 Methods *24*

2.1 Cell Culture **24**

2.1.1 NIH 3T3 Mouse Embryonic Cells 24

2.1.2 EL4 Mouse T lymphocyte Cells 24

2.1.3 Primary CD4 + T cells 24

2.2 Generation of Chronic Cell lines **24**

2.2.1 Generation of NIH 3T3 Chronic cell line 24

2.2.2 Generation of EL4 Chronic Cell line 25

2.3 Viral Analysis by Flow Virometry **27**

2.3.1 Virus Production 27

2.3.2 Flow Virometry Analysis and Staining 27

2.4 Primary CD4+ T Cell Activation and Infection **38**

2.5 Data and Statistical Analysis **39**

3 Results *40*

3.1 Characterization of NIH 3T3 fibroblast cell line **40**

3.2 Characterization of wild type and glycogag-deficient MLV released from NIH 3T3 cells **42**

3.3 Characterization of EL4 lymphoma cell line 51

3.4 Characterization of wild type and glycogag-deficient MLV virions released from EL4 cells 53

3.5 Characterization of primary murine CD4+ T cells 60

3.6 Characterization of wild type and glycogag-deficient MLV released from primary CD4+ T cells 63

3.7 Analysis of Endogenous Retroviruses in murine primary cells and lymphocyte cell line. 71

4 Discussion 86

5 References: 96

6 CV 105

List of Tables

Table 1: List of Antibodies used for cell and viral stainings...... 31

List of Figures

Figure 1: Infection and generation of EL4 Chronic Cell Line. 26
Figure 2: Gating strategy for phenotypical analysis of MLV virions. 30
Figure 3: Determination of optimal temperature for viral staining. 33
Figure 4: Effect of Fc Blocking reagent during viral staining on gating. 35
Figure 5: Optimization of controls to assess background fluorescence during viral staining. 37
Figure 6: Characterization of NIH 3T3 fibroblast cell line 41
Figure 7: Scatter and fluorescence quantification between wildtype and glycogag deficient MLV virions released from chronic NIH 3T3 cells. 43
Figure 8: Surface antigen phenotypic analysis of virions released from NIH 3T3 cells. 49
Figure 9: Detection of a discrete EV population positive for the CD81 and CD63 EV tetraspanin markers in supernatant released from NIH 3T3 cells. 50
Figure 10: Characterization of EL4 T lymphocyte cell lines. 52
Figure 11: Two populations are detected in wildtype and glycoGag deficient MLV virions released from chronic EL4 cells. 54
Figure 12: Surface antigen phenotypic analysis of virions released from EL4 cells. 59
Figure 13: Characterization of murine primary total CD4+ T cells. 61
Figure 14: Scatter and fluorescence quantification between wildtype and glycoGag deficient MLV virions released from primary murine CD4+ T cells. 64
Figure 15: Surface antigen phenotypic analysis of virions released from primary murine CD4+ T cells. 70
Figure 16: Detection of endogenous retroviruses in supernatant released from activated murine primary splenocytes and splenocytes infected with exogenous MLV virus by flow virometry. 74
Figure 17: Detection endogenous retroviruses in supernatant released from murine primary splenocytes. 75
Figure 18: Detection of endogenous retroviruses in supernatant released from activated murine primary total CD4+ T cells and cells infected with exogenous MLV virus by flow virometry. 79
Figure 19: Evaluation of endogenous retroviruses in supernatant released from untreated EL4 T lymphocytes and infected with exogenous MLV virus by flow virometry. 81
Figure 20: Detection of ERVs in murine EL4 lymphocytes. 82
Figure 21: Evaluation of NIH 3T3 fibroblast as negative control for detection endogenous retroviruses release. 84

1 General Introduction:

1.1 Introduction

1.1.1 Viruses

Viruses are the most abundant and genetically diverse entities in the earth's biosphere. Pathogenetic in origin, viruses are cellular parasites incapable of independent replication without a suitable host. The first identification and characterization of viruses as infectious agents occurred in the 1890s(1). Earlier bacteriophage research and electron microscopy development were instrumental in the pursuit of animal viral research (2).

Enveloped viruses egress through the host cell plasma membrane, from which they derive their lipid envelope and cellular imbedded proteins. Many of these enveloped viruses represent some of the deadliest human viruses; the most notable are Influenza, Ebola, Sars-Cov-2 and HIV (3–5).

1.1.2 Retroviruses

Retroviruses are a diverse group of enveloped single stranded RNA viruses that infect a wide variety of mammals. The hallmark that distinguishes the *Retroviradae* family of viruses from others is that they guarantee their genetic survival through permanent integration of their viral nucleic acid in the genome of the cell(6). The viral RNA is first reverse transcribed to double stranded DNA, which is then integrated into the genome. Once localized within the host genome, it is termed a provirus. The more notable viruses belong to the *Orthoretrovirinae* subfamily, which is more pathogenetic often leading to severe symptoms such as immunodeficiency, inflammation and cellular oncogenic transformation.

Human Immunodeficiency type-1 Virus (HIV-1) is one of the most infamous retroviruses; it leads to immune cell depletion and acquired immunodeficiency syndrome (AIDS). Since its initial discovery in 1983, HIV has afflicted more than 75 million people worldwide, and more than 35

million have died as a result of HIV-related causes(7). HIV-1 is a member of the *Orthoretrovirinae* subfamily of the Lentivirus genera. It has been extensively studied since its isolation, yet researchers are still on the quest to find a cure. Simian Immunodeficiency Virus (SIV) is the retrovirus that naturally infects African Primates and is the virus from which HIV-1 is derived from(8). The biggest hurdle in eradicating HIV-1 infection is the establishment and persistence of cellular reservoirs that harbor the latent HIV provirus within their genome. Presently, very little is known on the identity and anatomical location of these rare dormant cells. Several cell subtypes have been suggested to constitute the latent reservoir, with the resting CD4+ T cells being the critical majority (9).

Murine Leukemia Virus (MLV) is often used as a prototypical mouse reference model to study retroviruses such as HIV. MLV was initially presumed to code for only three essential genes and lacked any accessory genes. Consequently, MLV has been extensively studied to understand better more complex retroviruses such as HIV-1, HIV-2 and human T-cell lymphotropic virus (HTLV).

All genera of *Orthoretrovirinae* subfamily with the exception of the Lentiviruses have been suggested to be oncogenic. In fact, research on the *Orthoretrovirinae* and associated animal tumor viruses led to the Nobel Prize-winning discovery of oncogenes.

Approximately 10% of the human and mouse genomes account for endogenous retroviruses (ERV). While many ERVs are inactive in humans, ERVs still play an active role in mice to this day. In fact, murine ERV presence likely resulted from a retroviral infection and integration in the host's germline cells, which guaranteed its genetic survival and propagation to offspring via vertical transmission(10). ERV's role as transposable elements led to random integration events during cell division and de novo mutations, giving rise to different mouse phenotypes observed today (11). Viral and host immune interplay resulted in ERVs conferring beneficial functions to

the murine host defense against exogenous viruses through various functions such as receptor interference (12). The majority of murine ERVs share closest homology to exogenous *Gammaretroviruses*, including members of the MLV family (13).

1.1.3 Morphology and life cycle of HIV-1

At its core, HIV-1 harbors two genome copies of RNA, viral proteases, reverse transcriptase and integrases which are enclosed by an icosahedral capsid and enveloped with a lipid bilayer. The viral components are essential for the maturation of the viral particles ensuing their budding, and for successful infection of target cells. The viral genome encodes for the three essential genes know as group-specific antigen (Gag), polymerase (Pol) and envelope glycoprotein (Env), which are conserved sequences among all retroviruses (as reviewed later in more detail). In addition to the above, the HIV-1 genome contains a greater number of sequences which encode for additional proteins such as: viral infectivity factor (Vif), negative factor (Nef), viral protein U (Vpu), R (Vpr), tat and rev. These accessory proteins play several different roles during *in vivo* infections, such as conferring virulent and pathogenetic viral properties. These genes have likely further evolved during the cross-species transmission of SIV to humans, which significantly contributed to the increase in virulence and pathogenicity of the resulting HIV-1 virus while counteracting several human host restriction factors(8).

Upon HIV-1 infection in cells, the virus can accomplish two different tasks: actively replicate and release progeny or enter a latency state. HIV-1 will begin to transcribe, produce viral proteins and replicate leading to the release of progeny and its further propagation to secondary susceptible cells, consequently inducing cytopathic effects on the host cell (14, 15). In contrast, retroviruses can enter a latent state in which the replication competent virus integrates within the host's genome but remains quiescent and transcribes viral protein at a minimal level. The low levels of viral

protein transcription go undetected by the host immune system and are less susceptible to antiretroviral therapy (ART)(15, 16). Due to the latent HIV provirus's ability to reactivate from its dormant state, produce new infectious progeny and infect susceptible cells. The barrier to HIV eradication results from the inability to identify this latent cellular reservoir. To further complicate the situation, dormant resting CD4+ T cells are scarce. As little as 1 to 10 cells harbor the provirus found among one million circulating CD4+ T cells in patients undergoing ART (17). Yet, this latent reservoir is virtually devoid of any robust and definitive biomarkers that distinguish the latently infected cells from the uninfected lymphocyte population.

1.1.3.1 Host Protein Acquisition

Studies from as early as 1960s demonstrated biologically functional host cellular proteins on the surface of enveloped viruses through the means of immunoelectron microscopy(18). However, the majority of studies on HIV-1 analyzed the viral glycoprotein on its envelope with the main incentive to further our understanding of viral tropism, binding, infectivity and development for vaccine designs. Valuable information has been gained by analyzing HIV-1 host derived surface antigens and the maintenance of their biological role for viral pathogenesis (5, 19–22).

Egress is the final step in the replication cycle. It is mediated by a family of cellular endosomal sorting complex required for transport (ESCRT) machinery proteins, which are recruited by Gag (23–25). A majority of newly assembled retroviral particles will bud through the cell surface. In doing so, they will pick up a portion of the lipid bilayer of the cell and the associated host surface markers. This process ensures a highly controlled and specifically executed colocalization, incorporation, and assembly of all the virions' structural components (26). However, the underlying mechanism that impacts cellular antigen uptake has been under much speculation. Several different theories have been postulated, including the passive inclusion model raised by

Trembley and colleagues, which suggests the release of viral particles at specific domains highly enriched with certain molecules(27). Similar evidence has been illustrated indirectly in other observational studies of host derived antigens on the retroviral envelope. In particular, Arakelyan et *al.* stipulates that the cell's phenotype predominantly determines viral envelope's protein expression. These findings imply that the infected cell's phenotype has a critical role in determining the degree of host-derived imbedded proteins in the viral envelope and predominates over the role of genetic differences between two HIV-1 variants used in this particular study. This is in line with Linde *et al.* 's findings conducted on HIV-1 derived from macrophages and T cells by tandem mass spectrometry and quantitative proteomic analysis(28). Linde and colleagues insinuate that despite the conservation of specific host-derived proteins, ultimately, the viral phenotype is dictated by the cellular phenotype and direct protein-protein interactions between host and viral proteins, however these were only noted to be few. Thus, this results in a broad virion phenotypic diversity allowing HIV-1 virions to be incredibly fluid in its protein composition. Taken together, these findings support the overarching hypothesis that viral phenotype is predominantly determined by the cell type it is produced by.

In contrast, many studies have shown that surface cellular antigen uptake is not a passive outcome of the viral egress. These observations rather reveal a selective mechanism of incorporation as observed by the extent of viral phenotypic variability and its effect on infectivity, adhesion, neutralization and pathogenesis(5, 19, 20, 22, 27, 29, 30). Many of these studies note that the concentration levels of antigen expression on the host cell's surface do not necessarily correlate to the abundance of the said protein on the viral envelope. For example, CD45 is known to be abundantly expressed on a lymphocyte's cell membrane, covering as much as 10-25% of the total surface(31). Thus, if egress mechanisms were passive or random, a significant amount of

virion-incorporated CD45 antigens would be observed on the viral envelope; however, this is not observed(5). Although the cell type from which the viral particles are released from is an important determinant of the viral envelope composition, viral factors may play an active role in influencing the marker composition of the envelope. To further add to the undeniable body of evidence, conserved host derived antigens have been observed between HIV-1 and SIV, even when released by different cell lines. Observations on whether host protein acquisition was virus-specific revealed that a set of antigens was conserved between the two viruses, highlighting the possible beneficial physiological function of these proteins for downstream infection (19). Taken together, this indicates that host protein incorporation is a selective process, modulating the enrichment of particular host-derived proteins in the virus membrane and exclusion of others.

Although the primary pathway of egress for enveloped viruses is through the host cell plasma membrane, both MLV and HIV-1 have been recognized to assemble at the endosomal compartment of the cell and bud using multivesicular bodies depending on which cell type they egress from (32, 33). Proposed as the Trojan Horse hypothesis, this alternative release mechanism could alter the viral envelope's composition. Hence the viral phenotype observed can differ depending on the egression pathway.

Many different technologies have been used for host-derived proteins detection thus far, the most notable one being immunoelectron microscopy which initiated these investigations(2). Although these studies have generated a wealth of knowledge on viral biology, viral phenotype has been traditionally characterized indirectly and using bulk methodology.

1.2 Techniques for Viral Characterization

The primary reason that delayed viral research, compared to other organisms, is their very small size. Animal viruses can range from 20 nanometers (nm) to the larger viruses of up to 400 nm in

diameter. Nevertheless, research has come a long way from the earlier viral analysis tools to present-day advanced technology and bioinformatics tools.

Current methods of detecting and identifying host proteins on viruses' surface include immunoelectron microscopy, immunomagnetic capture assays, and mass spectrometry. Research on viruses has predominantly focused on viral population analysis, in part due to the relative lack of technologies capable of characterizing viruses directly on a single particle level. Furthermore, traditional approaches that sought to characterize viruses, such as Western Blots and polymerase chain reaction (PCR), analyze all virions within a sample, both defective and infectious particles. Since viral stocks can contain both defective and infectious viral particles, this becomes a significant confounding factor, especially since defective particles' protein and genetic content may vary and be unrepresentative of the infectious counterparts(34). Bulk analysis methodologies lack the required sensitivity to provide critical information on the protein composition, characteristics of individual viral particles, heterogeneity of viral populations and presence of subpopulations (35). Despite what has been uncovered about cellular heterogeneity, viral particles have yet to be analyzed on single-particle resolution and in high throughput fashion, although enveloped virions are probably as individualized as the cells they are budding from.

Advancements in bioinformatics led to the conceptualization and development of mass spectrometry (MS), a tool of tremendous capabilities for high throughput analysis and quantification of viral populations. MS has propelled the field of proteomics, functional studies, and our understanding of protein-protein interactions with its unparalleled ability to determine protein composition, molecular mass, and post-translational modifications. Identification and quantification of total viral and cellular protein content associated with a given viral population makes MS a powerful tool through the lens of virology research(36). Consequently, MS techniques

have been applied to identify and quantify total protein content in HIV and MLV studies (28, 37–39). However, MS is not designed to determine the location of the host-derived proteins on the virus or measure the abundance of its incorporation at the single virion level.

In contrast, immunomagnetic capture enables protein abundance on the viral envelope to be quantified by first binding magnetic particles that target host-derived proteins and the subsequent capsid targeted (p24) ELISA readout (5, 19, 20, 22). Although this technique's sensitivity was capable of differentiating HIV virions released from different cell lines, it lacks the capability of analyzing incorporation of these cellular constituents on a single particle scale(20, 22). However, most immunoassay technologies' detection limits are limited by both the amount of signal produced and the level of background fluorescent signal produced by the assay(40).

The techniques as mentioned above have their advantages and variations in their degree of sensitivity. For example, coupling MS with other analyses can enhance its sensitivity compared to immunomagnetic capture assays(41, 42). Nevertheless, the most significant limitation of these bulk methods is their inability to analyze viral particles on a single virion scale, consequently obscuring sub-populations' phenotype and negating the extent of viral heterogeneity.

Before the advent and development of modern flow cytometers, there was a lack of appreciation for cell heterogeneity. Flow cytometry has revolutionized the field of immunology. Its capabilities for phenotypic analysis of extracellular and intracellular markers at a single-cell level allowed researchers to quantify, differentiate, and characterize different states and subsets of cells. Over the last few decades, flow cytometry has become well established and standardized among the scientific community, with a multitude of available antibodies. Its high throughput capability to measure a multitude of parameters simultaneously, characterizing transition states and phenotypic profiling has been instrumental in understanding disease pathogenesis and

treatments(43). Flow cytometry techniques have not changed considerably since its development. Flow cytometers analyze samples by detecting the light scattering and produced fluorescence in a given sample by focusing a stream of particles to an interrogation point intersecting with one or more lasers. Thus, the instruments can detect various properties such as relative size, granularity, and the emitted fluorescence produced by selective antibodies, which enables the degree of surface or intracellular protein expression at a single-cell resolution to be determined.

1.2.1 Flow Virometry

In 1978, Hercher *et al.* designed the first custom cytometer with several modifications that allowed for the detection and discrimination of bacteriophages by light scattering properties (44). Initiated with Hercher direct viral analysis, quantification and characterization of viruses were appealing and booming research venues. Since then, flow cytometry principles have been adapted for the analysis of nanoscale particles, such as viruses, a technique coined as flow virometry (FVM). The first viral stainings targeting the genome resulted in the successful detection of larger DNA viruses(45–47). More so, the field of nanoscale flow cytometry was expanding due to the concurrent popularity and recognized importance of extracellular vesicles (EV). EVs have critical biological functions and have been observed in both healthy and pathological processes(48). EV transfer is one of the forms of intercellular communication in multicellular organisms. EVs can range in size between 30 to 1000 nm and have been compared to retroviruses in shared functional and structural aspects (48). Presently, FVM remains a multifaceted, rapidly developing, and open-ended endeavor. Although it has shown significant success in recent years, FVM still faces several significant technical challenges, hindering the full deployment of its potential.

Conventionally, flow cytometers were designed to analyze cells or particles greater than 500 nm in diameter. Hence, analysis of much smaller particles, such as retroviruses, presents numerous

inherent challenges as they are at the limit of detection or may fall within the background noise of conventional flow cytometers. Consequently, it has been shown that even the more sensitive of conventional cytometers were incapable of detecting biological particles smaller than 300 nm in diameter(49, 50). In most cases, light scatter properties alone, such as the forward scatter traditionally used as a detection trigger to register an event, would be insufficient to distinguish viral particles from machine noise or other cellular contaminants(51). Thus, improvements in cytometer designs and the addition of new technology have led to the development of state of the art cytometers such as the Beckman Coulter CytoFLEX, which enables detection and resolution of nanoparticles in the 30-150 nm range by both light scatter and fluorescence at a single particle analysis (49). One of the several modifications to the CytoFLEX is that light signals bypass the traditionally used filters and are instead directed to their final destination. Furthermore, the use of violet side scatter (VSSC), collection of scattered light at an angle of 30-150° relative to the light source, decreases background noise and greatly enhances nanoparticle resolution(49). Thus, analysis using the CytoFLEX gained unprecedented sensitivity allowing discrimination of viral particles like adenovirus and HIV (49).

Flow cytometers were initially designed for the analysis of cells. Thus, an analysis of smaller particles such as viruses can lead to multiple viruses being analysed at the interrogation point at the same time leading to fewer events registered, a phenomenon termed swarm detection. This coincidence of viral particle acquisition leads to a decrease in total events but a concurrent increase in mean fluorescence intensity (MFI). The concurrent increase in MFI is a predictor of false positive events especially in the case of antibody labelling. One method to prevent coincidence is by diluting the viral sample; thus, serially diluted samples should maintain a constant MFI but have differing viral counts.

In the case of enveloped viruses, identifying the viral envelope proteins is an appealing research venture due to their instrumental role in determining viral tropism and antigenic targets for vaccine development. Furthermore, quantifying the abundance of the viral glycoproteins on the envelope is highly relevant for viral entry during viral-cell fusion (50, 52). However, since the viral surface area is 10 000 times smaller than that of a lymphocyte, the relative abundance of surface antigen expression is much lower. Size plays an essential role in analyzing these distinct biological entities relative to one another: a lymphocyte is roughly 7 μm (larger if activated) compared to a retrovirus that falls in the range of 90-150 nm in diameter (45, 53). Consequently, the ten-thousand-fold difference in the surface area profoundly impacts the ability to detect the virions and surface antigen expression.

Lastly, due to many overlapping characteristics with viruses, EV contamination is a significant confounding factor in most viral analysis, since they share many similar biophysical characteristics and egression pathways(48, 54). Much like retroviruses, EVs incorporate lipid membranes' content and the cytosolic portion of their parental cells. Furthermore, microvesicles, one of the EV family members, also egress at the surface of the cell(55). Moreover, EVs have also been shown to incorporate genomic content and viral proteins when released from infected cells(48). To further the narrative, there is no current consensus on a definitive way to distinguish EVs from non-infectious viral particles, termed virus-like particles (VLP)(56, 57). Thus, analysis of viral preparations can lead to false-positive results with traditional analytical methods solely targeting viral protein or nucleic acid components(58). Physical or analytical methods of separation have been employed to ensure viral purity; however, the former techniques have been proven to be labor-intensive and potentially damaging to viral particles (21, 28, 54, 59, 60). Alternatively, the latter method utilized EV markers such as CD45, which is highly expressed on vesicles released

from hematopoietic cells, but observed at very low abundance or not at all on HIV virions(5, 19, 22, 61, 62). Since the overall challenge lies with the inability to characterize viral populations with certainty, the use of genetically modified viral structural components (capsid, matrix/tegument, or envelope glycoproteins) tagged with a fluorescent reporter marker allows for better discrimination of the viral population of interest from background noise and EVs (26, 51, 58, 63–66). However, the onus falls on the researcher in ensuring that the chosen tagged viral component is not incorporated into EVs. Lastly, some groups directly target the surface viral glycoprotein or nucleic acid to resolve fluorescently labeled viral particles from the background(50, 52, 62, 65, 67, 68).

Nevertheless, several studies have revealed the power and utility of FVM as an important technique in a virologist's toolbox. Although initially used for the overarching purpose of enumerating viruses, FVM was employed for viral characterization and was instrumental in revealing the extent of viral heterogeneity. For instance, Landowski *et al.* showed receptor-induced conformational changes and differential incorporation of the attachment and fusion viral glycoproteins dependant on Nipah's size enveloped viral particles(52). This study also highlights that the differential incorporation of the viral glycoproteins allows for better elucidation of viral kinetic assay interpretation and entry kinetic phenotype determination. Gaudin *et al.* further showed particle size and glycoprotein concentration on the viral surface correlate to differences in infectivity of Junin enveloped viruses through fluorescently activated cell sort (FACS) and subsequent functional infectivity assay(50). FACS allows the separation of sub-populations within viable cells for downstream functional assays. Gaudin *et al.* demonstrated sorting of nanoscale particles while preserving their biological activity. Furthermore, they reveal that Junin viral particles egress at specialized lipid membrane microdomains. Interestingly, the viral particle

infectivity is influenced by the decrease in surface abundance of both surface viral glycoprotein and host-incorporated lipid microdomain markers CD9 and Cholera Toxin B(50).

Additionally, FVM was employed to assess the differential incorporation of host derived proteins LFA-1 and HLA-DR on the viral envelope of HIV-1 virions. Following the previously reported high association of the above-mentioned host proteins to HIV virions by bulk analysis, Arakelyan *et al.* confirmed their presence. Most importantly revealed differential antigenic distribution among the individual viral particles(62). First, they demonstrated conservation of these select cellular antigens among viral particles released from different cell lines as observed by several other studies; however they revealed variability in antigenic distribution between these virions(20, 22, 28). Interestingly, Arakelyan *et al.* showed similar host derived antigenic makeup on the viral envelopes between two different HIV-1 genotype variants.

In a later study, Arakelyan *et al.* put an end to the debate whether HIV-1 can express either functional, defective or both Env glycoproteins on its viral envelope. They demonstrated that most HIV-1 particles carry either conformation on their viral envelope. These findings have critical implications on the type of neutralizing antibodies generated and on the development of prophylactic strategies(69).

Similarly, Bonar *et al.* employed FVM to sort fluorescently tagged HIV-1 subpopulations for downstream functional assay to assess Env stability. Moreover, they revealed that the detection and quantification of viral particles by NFC is 1000-fold more sensitive than an ultra-sensitive enzyme linked immunosorbent assay (ELISA), whilst comparable to PCR(51). Some groups employed fluorescent selection markers such as CD45 or other EV markers to discriminate EVs. In contrast, others directly labeled viruses with antibodies against the viral glycoprotein or nucleic acid fluorescent dyes to resolve the viral population of interest.

Tang and colleagues proposed the use of a genetically modified retrovirus that expresses a fluorescent envelope glycoprotein as a selection marker(26, 58, 65). They demonstrated that through the use of a fluorescently tagged Env, they are able to discern the viral population from the background and EVs while ensuring that the structural protein is not incorporated in EVs through a series of transfection and transduction assays(58, 65). Tang and colleagues proposed using genetically modified MLV as a positive biological control and as a size standard to the beads in EV and FVM (26).

Additionally, Renner *et al.* employed FVM to calculate genome packaging efficiency and individual particle infectivity of MLV(58). Consequently, the study of the viral envelope in the context of latent viruses such as HIV-1 has important implications not only as it plays an integral role during viral entry, but also could provide crucial information on the infected cell's identity. Therefore, FVM could potentially identify cellular reservoirs that harbor the HIV-1 provirus, which currently has no robust biomarkers.

From a therapeutic application standpoint, FVM can be applied as a novel analytical tool to allow for enhanced characterization of viral heterogeneity in vaccine production(70). Vlasak *et al.* show differential incorporation of two viral key antigens instrumental for vaccine efficacy in human cytomegalovirus preparations, known to release different particle types. While, Tang *et al.* demonstrated that oncolytic vaccinia virus can aggregate during handling procedures such as freeze-thaw cycles, revealing the extent of FVM capabilities for quality and consistency control in the assessment of vaccinia vaccine preparations(71).

Consequently, FVM is a powerful tool that enables viral enumeration, characterization and phenotypical analysis of proteins at the surface of the viral envelope. It has many advantages over current methods used to characterize viruses and offers many benefits of traditional flow cytometry

while analyzing a single virion level. As mentioned above, these studies demonstrate unprecedented viral heterogeneity that has been previously negated using bulk and indirect analysis. Additionally, FVM has the advantage of ignoring the presence of free proteins and low magnitude protein aggregates as it counts the events based on passing the light scatter triggering(58). Furthermore, viruses could be sorted for downstream biochemical and functional analysis to assess their infectivity. (50, 51, 72). Previously, this has been challenging due to confounding factors such as the presence of VLP and defective virions, which skewed the measurements of viral fitness and infectivity. Lastly, FVM has the added benefit of tracking drastically greater numbers of discrete viral particles than the described techniques, providing greater statistical significance in experiments. Taken together, these results demonstrate the reliability of NFC as a method of detecting, quantifying, and phenotyping unique viral populations while addressing current gaps in knowledge on viral heterogeneity.

1.3 Murine Leukemia Virus

MLV is a simple enveloped retrovirus that has been extensively studied and characterized. This prototypical virus is a gammaretrovirus that falls in the same diameter as HIV-1 and has been used as a reference model to study more complex retroviruses. The MLV genome encodes for the three essential genes required for the retroviral replication cycle: Gag, pol and env.

1.3.1 Group Specific Antigen

Gag is a polyprotein which orchestrates viral structural assembly and encompasses four structural subunits: matrix, capsid, p12 and nucleocapsid. Gag alone can generate VLPs, although, without incorporating other viral components, these particles are non-infectious (73, 74). Matrix protein plays essential roles in viral assembly, such as localizing gag molecules to the plasma

membrane and ensuring Env incorporation. The myristoylation sites detected in the MA domain are essential for targeting Gag assembly to detergent resistant microdomains and lipid rafts, from which retroviral viruses like MLV and HIV-1 preferentially egress (21, 75, 76). Mutations to MA resulted in inhibition of transport of the Gag polyprotein to the plasma lipid membrane and its incorporation into MLV virions(77). Interestingly, deleterious mutations in the matrix protein did not impact the assembly of HIV particles, but significantly impaired envelope glycoprotein incorporation(78, 79). Jalaguier et al, found that MA is essential for ICAM-1 incorporation in HIV-1 viral envelope, elucidating on the potential role of the matrix protein on host protein incorporation (80). Whilst p12 and capsid proteins ensure the viral core structure's assembly in the immature virion, subsequent proteolytic cleavage by the viral protease leads to rearrangement of the capsid lattice and viral maturation(81, 82). Furthermore, the nucleocapsid, which has a strong affinity for nucleic acids, is responsible for recognizing and packing the viral genome (83).

1.3.2 Viral Polymerase and Integrase

Pol is a polyprotein which encodes for three enzymes indispensable in the replication cycle. The first enzyme, the RNA-dependant DNA polymerase, is essential for the reverse transcription of a positive strand RNA genome into a double stranded DNA, which is integrated into the target cell's genome. The reverse transcriptase discovery led to the Nobel prize awarded to David Baltimore, Renato Dulbecco, and Howard Martin Temin in 1975. Lastly, the viral protease and integrase genes are essential in the viral life cycle for viral maturation and the earlier mentioned integration of proviral DNA into the host genome, respectively(84).

1.3.3 Envelope glycoprotein

Env is critical for the entry step of the viral infection. This is the only essential viral protein that is found on the surface of the viral envelope(85). Env is inserted in the cellular membrane as

a trimeric transmembrane protein as a cleavage product by protease, which results in covalently linked surface and transmembrane subunits. This cleavage is essential for ensuring localization and incorporation of Env at the site of viral assembly, which is critical in regulating the consistent level of 80-120 Env trimeric spikes, which are incorporated into each budding virion (86, 87). Its expression is conserved among several retroviral viruses such as SIV, which expresses 73-98 spikes per virion, while HIV-1 shows only 14-21 spikes(88, 89). Interestingly, in the HIV-1 viral envelope , Env only accounts for 0.1 % of total protein content found on the viral envelope, while host-derived human lymphocyte antigen-DR (HLA) constitutes 20%(90). Furthermore, coordination between Gag and Env in the endosomal compartment and at the cellular lipid membrane ensures Env selective incorporation in virions over EVs. This has been selectively illustrated by both transfection and retroviral transduction assays, accentuating Env as a highly advantageous discrimination marker as discussed earlier on.

1.3.4 Glycosylated Group Specific Antigen

Some strains of MLV express a glycosylated gag (glycogag), a protein with an additional 88 amino acid sequence. Recognition of a start codon upstream of Gag directs this precursor for N-glycosylation. Upon glycogag's post-translational modification in the endoplasmic reticulum, it is cleaved and inserted as a transmembrane protein in infected cells. Glycogag has been postulated as an accessory protein of MLV since it is not required for viral replication, but enhances replication and pathogenesis in vivo (91). In a similar fashion to the HIV-1 accessory proteins, glycogag has been suggested to aid in the pathogenesis and resistance to host restriction factors to facilitate efficient replication. It has also been suggested that glycogag influences viral budding, directing virion assembly and release at the highly saturated cholesterol and lipid environment of lipid rafts (92, 93). The exact role remains an enigma, although glycogag has been established to

provide viral core stability and circumvent the antagonistic functions of host restriction factor apolipoproteins (APOBEC3) and serine incorporated proteins (Serinc). The degree of glycosylation influenced the susceptibility of the antagonistic effect of APOBEC3, where higher glycosylation resulted in retroviral resistance to APOBEC3 (57, 94). Interestingly, glycogag has been shown to be incorporated in a different orientation in virions than EVs(57). Renner *et al.* revealed that in virions, glycogag was oriented in a type I membrane protein orientation, which inserted the structural domain of Gag into the viral core, while EVs glycogag were type II membrane proteins. These findings further the narrative on the importance of structural glycogag domain for viral core stability and protection from host retroviral restriction factors.

Interestingly, glycogag has been shown by several groups to counter the selective pressures of another novel host retroviral restriction Serinc, responsible for inhibiting viral replication. Glycogag, similar to the HIV-1 accessory protein Nef, first delocalizes Serinc from the plasma membrane by endocytosis and subsequent lysosomal degradation of Serinc(57, 95–97). Interestingly, initially, Nef's pathogenetic functions have been attributed for its effect on the downregulation of CD4, MHC I and tetherin much in a similar function to Serinc. However, through the means of convergent evolution, both of these differing retroviruses reveal similar methods to counteract the effects of Serinc. Additionally, Ahi *et al.* demonstrated that glycogag has significantly impacted viral entry of MLV in conjunction with Env, enhancing its infectivity with select Env proteins (97).

Consequently, each of the components, as mentioned above, serves a concrete function in the replication cycle and altering these could affect viral composition and be detrimental to viral infectivity and replication. Strikingly, through the long co-evolution and interplay between host and virus, both have evolved different strategies to circumvent one another in their continued arms

race. However, MLV is a very well established and characterized virus that is often employed as a prototypical retroviral model.

1.4 Aim of the current study

In recent years, interest in FVM has been reignited, and it has since become a useful tool for the analysis of viruses. FVM makes profiling of antigens and biomarkers on the surface of viruses a possibility. Consequently, we believe that FVM could make a critical contribution for its ability to immunophenotype nanoscale particles, such as EVs and retroviruses. Additionally, it raises the possibility of identifying the specific lymphoid cell types that constitute the latent HIV-1 cell reservoir. To establish the necessary framework for retroviral immunophenotyping, we propose to use MLV, which shares a similar diameter with HIV-1, as a model reference retrovirus. Our laboratory has genetically engineered MLV virus to expresses a super folder GFP fusion protein with the viral-encoded envelope glycoprotein. This serves as a positive control and selection marker to discriminate from EVs and background noise(26, 58, 65). The intricate process of viral capsid assembly in retroviruses ensures consistent stoichiometry of released viral particles. Hence, MLV has been shown to have a highly monodisperse profile on VSSC due to controlled assembly and consistent size (26, 81). Thus, MLV presents as a suitable model retrovirus for flow virometry as it has two-pronged identification by both size homogeneity and Env incorporated GFP fluorescence.

Our laboratory has previously shown successful detection and quantification of cell-derived tetraspanins on MLV from a chronically infected murine fibroblast cell line. Although these tetraspanins have been previously observed on EVs, our lab demonstrated their presence and abundance on the viral envelope of MLV. Taken together, these results demonstrate the reliability

of FVM as a method of detecting and quantifying viral particles of low antigenic density. Consequently, we propose FVM for the analysis of viruses to phenotypically analyze and characterize surface markers at a single-viral particle level.

1.4.1 Hypothesis

We hypothesize that the phenotypic profiling and quantification of antigens on the surface of individual viral particles will provide crucial information on the identity of the infected parental cells.

1.4.2 Approach

For the optimization and phenotypic profiling, we will analyze supernatants from chronically infected cell lines and primary CD4+ T cells using an antibody panel targeting highly expressed tissue-specific antigen markers by FVM. We will first probe for known abundantly expressed antigens, like tetraspanins, and proceed to weakly expressed host antigens. Additionally, as negative and specificity controls, we will stain abundantly found host markers such as CD4 and CD45, which have not been observed on egressed HIV-1 virions yet have been documented on EVs.

1.4.3 Implications

Our study elucidates on key questions such as what receptors are taken up during viral egress and whether there is conservation, selective upregulation and uptake of specific host antigens. We demonstrate that the infected cell's phenotype plays an important role in determining the viral envelope's protein composition. Yet, the abundance of antigen expression does not necessarily correlate to the viral expression. Thus, this work highlights that FVM is an effective tool for phenotypic characterization and quantification that provides valuable information on the parental cell's phenotype. However, further experiments are required which consider a broader array of antigens in order to assess the extent of FVM's capability in deciphering the parental cell identity. Future studies will shed light on current gaps in knowledge and test the capability of FVM to identify infected producer cells based on surface marker expression on enveloped viruses. Thus, raising the possibility for the identification of HIV latent reservoirs that presently have no robust or defining biomarkers. It remains unknown which factors govern the cellular antigen uptake during viral egress. We uncovered the intriguing possibility that glycosylated gag protein is associated with the increase in the incorporation of host derived antigens during viral release.

These findings highlight the need for further research into the intricate complexities of glycogag protein's role during viral assembly and egress. Furthermore, this project paves the way for future development and optimization of prognostic tools by means of immunophenotyping disease biomarkers of EVs.

2 Methods

2.1 Cell Culture

2.1.1 NIH 3T3 Mouse Embryonic Cells

NIH 3T3 mouse embryonic fibroblasts were cultured in Dulbecco's Modified Eagle Medium (DMEM) (Wisent) with 4.5 g/l glucose, L-glutamine and sodium pyruvate(Wisent), supplemented with 10% Fetal Bovine Serum (FBS) (Corning), 100U/mL penicillin and 100µg/mL streptomycin (Wisent) and propagated in an incubator at 37°C with 5% CO_2.

2.1.2 EL4 Mouse T lymphocyte Cells

EL4 mouse T lymphocytes were cultured in Roswell Park Memorial Institute (RPMI) (Wisent) 1640 Medium with 4.5 g/l glucose, L-glutamine and sodium pyruvate (Wisent), supplemented with 10% Fetal Bovine Serum (FBS) (Corning), 100U/mL penicillin and 100µg/mL streptomycin (Wisent) and propagated in an incubator at 37°C with 5% CO_2.

2.1.3 Primary CD4 + T cells

Primary CD4+ T lymphocytes were cultured in RPMI 1640 Medium with 4.5 g/l glucose, L-glutamine and sodium pyruvate (Wisent), supplemented with 10% Fetal Bovine Serum (FBS) (Corning), 100U/mL penicillin and 100µg/mL streptomycin (Wisent) and propagated in an incubator at 37°C with 5% CO_2.

2.2 Generation of Chronic Cell lines

2.2.1 Generation of NIH 3T3 Chronic cell line

Chronic NIH 3T3 producer cells were generated as described in previously by our group(26, 58, 65) . In short, NIH 3T3 cells were infected with either MLVsfGFP WT or MLVsfGFP CTG at a high multiplicity of infection (MOI). Briefly, 10mL of MLVsfGFP- containing cell supernatant was produced by transfection of 293T cells in a 10cm dish for 72 hours. Upon collection, viral

supernatant was filtered through a 0.45μm filter and ultra-centrifuged at 100,000xg for 3h in a 70Ti rotor at 4°C. Lastly, the viral pellet was resuspended in DMEM and used to infect NIH 3T3 cells seeded in 6-well dished seeded at 500 000 cells per well.

2.2.2 Generation of EL4 Chronic Cell line

Chronic EL4 cells (ATCC cat. #TIB-39) were generated in similar fashion to the producer cell line. Briefly, 60 ml of viral supernatant produced by NIH 3T3 chronic cell line for 72 hours in a 10 cm dish was collected, filtered through a 0.45μm filter and ultra-centrifuged at 100,000xg for 3h in a 70Ti rotor at 4°C. Lastly, the viral pellet was resuspended in RPMI and used to infect EL4 cells seeded in 6-well dished seeded at 500 000 cells per well. Infected cell population was plated in a 10 cm dish upon reaching confluency and population-cell sorted based on sfGFP expression and expanded.

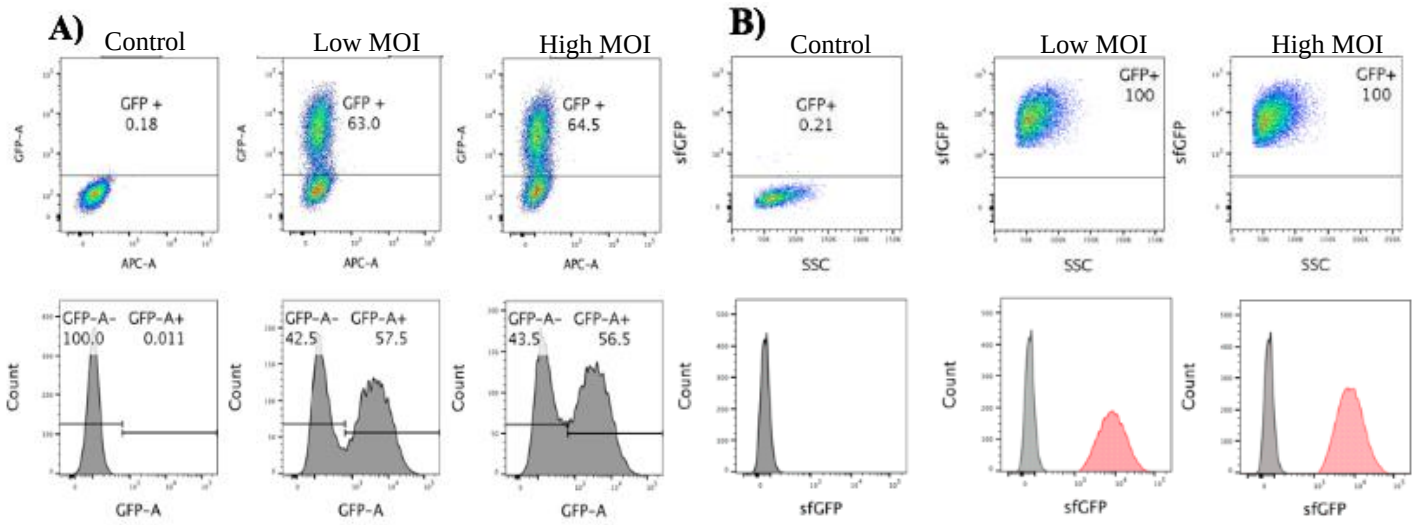

Figure 1: Infection and generation of EL4 Chronic Cell Line.
Analysis of EL4 T lymphocytes cells infected with viral supernatant collceted from the NIH 3T3 producer cells at high and low MOI. Cell infection was monitored with GFP expression. B) Analysis of infected EL4 cells that were population cell sorted for GFP expression.

2.3 Viral Analysis by Flow Virometry

2.3.1 Virus Production

For viral supernatant released from NIH 3T3 cells, cells were seeded at $5x10^6$ cells in 10 cm dish in 10 mL of non-phenol DMEM media (Wisent) 10% EV-depleted FBS for a 72 hour incubation. Viral supernatant was collected, centrifuged at 900xg for 5 mins and filtered with 0.45μm filter. For flow virometry analysis, viral supernatant was diluted 1 in 1000 in 0.1 μm filtered phosphate buffered saline (PBS) (Thermo Fisher Scientific). Similar approach was used for viral supernatant released from the EL4 cell line, however $5x10^6$ cells were plated in a 10 cm dish in 10 mL of non-phenol RPMI media (Wisent) supplemented with 10% EV-depleted FBS for a 48-hour incubation period. For flow virometry analysis, viral supernatant was diluted 1 in 200 in 0.1 μm PBS.

2.3.2 Flow Virometry Analysis and Staining

Detailed methodology has been published to BioRxiv preprint server with a description on viral antibody staining and instrument settings. FVM analysis was conducted employing the CytoFLEX S (Bekman Coulter) using the 405nm SSC-H as the threshold parameter (threshold of 1500). For our instrumental platform, small particles were preferentially displayed in the height measures as the intensity of the signal generated is more accurate compared to the often used area measurement for cells(71). This is explained by the principal that area is an integrated value of height and width (the time that a particle spends in flight during the generation of the electronic pulse), and due to the much smaller size and time in flight of viruses to cells, the width measurement decreases in precision. Lastly, according to the Mie Scatter theory, for cellular analysis the forward scatter is the preferred angle of detection, as more light is captured. However the inverse is true for particles within 100 to 200 nm diameter, in which case side scatter angle is

preferred to capture more light(98, 99). Briefly, all viral supernatants were filtered and centrifuged prior to dilution in 0.1 μm PBS. For viral antibody staining, 50μL viral supernatant aliquots were mixed with 2X concentred PE-conjugated antibodies in a total volume of 100 μL at a final concertation of 1.6 μg/mL for $1x10^9$ viral particles for 60 mins at 37°C. Stained viral supernatant was diluted in 0.1 μm PBS and acquired for 60 seconds at low setting at a sampling rate of 10 μL/min. Prior to viral staining, the antibody was centrifuged at 17 000 xg for 10 min to decrease presence of antibody aggregates and Table 1 includes detailed description of all PE-fluorophore conjugated antibodies employed. **Figure** 2 illustrates two gating strategies utilized for the analysis of viral population of interest stained for tetraspanin marker CD81, an isotype control for CD45 marker and positive control for GFP marker.

The first strategy employs initial gating on the viral population based on GFP fluorescence and subsequent analysis for the degree of staining, this strategy was used for phenotypic analysis unless otherwise indicated. This allows the for immediate discrimination of viral particles from background and EVs, however additional negative control is required to set up the gating for staining analysis. As such, the gating was set manually for each sample analyzed. In this manner, the gating strategy was set up to contain 99.5% of the negative control in the PE negative quadrant and only allow 0.5% of any higher fluorescent background in the PE positive quadrant.

Panel B highlights second gating strategy to first identify viral population of interest by violet side scatter and then discern for positively stained viral particles from negative particles (internal negative control). Although the latter method allows to remove antibody aggregates, this gating can have confounding variables in case of internal control staining for EVs, providing skewing signal intensity and altering the gating strategy. Viral particle count, included in the analysis, shows consistent results between GFP stained viral particles in two gating strategies. However, in

CD81 viral staining there are different viral particles counts between two strategies as result of higher fluorescence in background and a separate CD81 positive EV particles which becomes problematic when setting definitive gates. Consequently, the first approach was employed to avoid this effect by setting the gates with media and antibody controls that are run in same session with the stained viral samples.

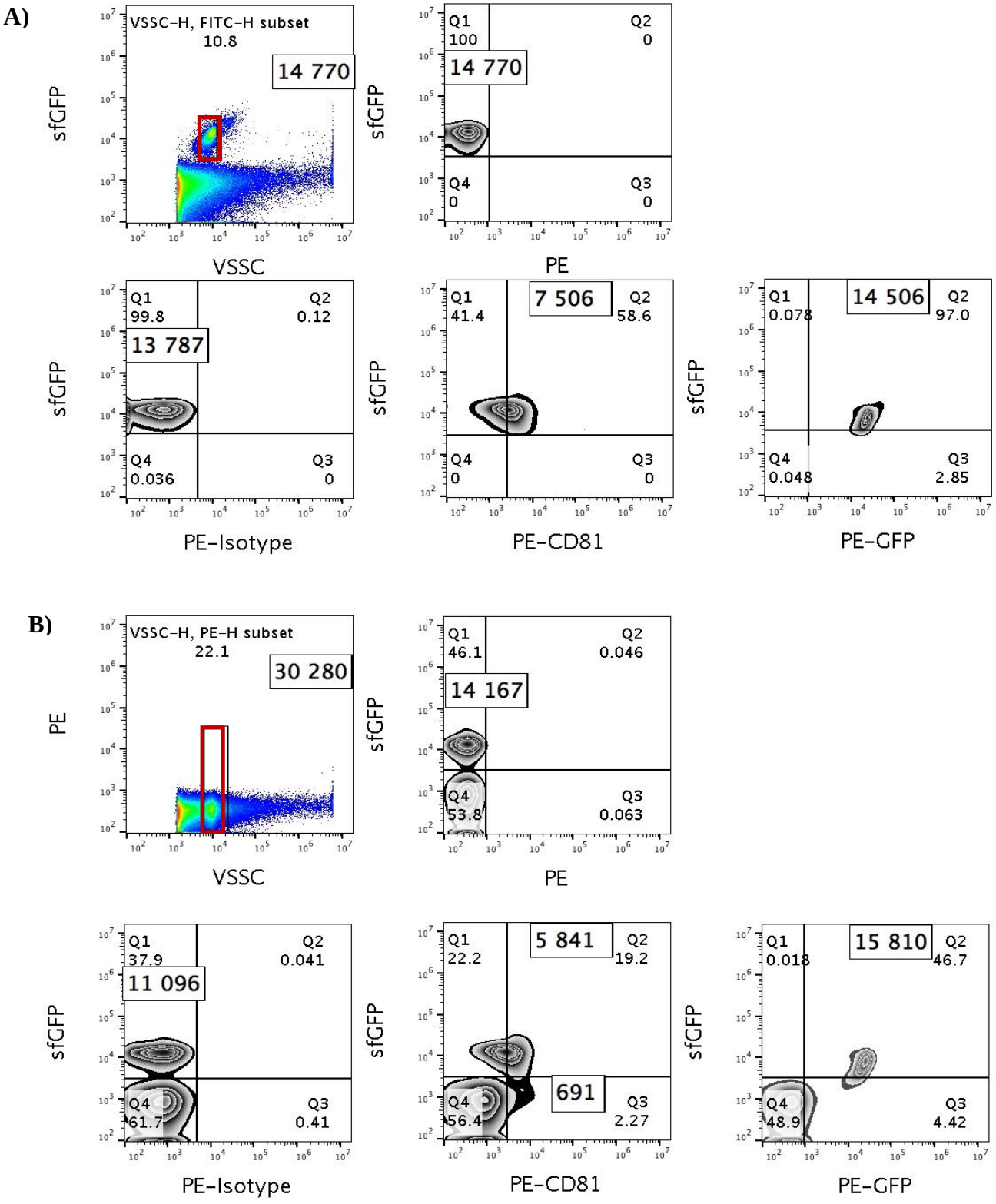

Figure 2: Gating strategy for phenotypical analysis of MLV virions.
Viral population of interest was identified and gated (red gate) on by either **A)** GFP expression or **B)** violet side scatter intensity. Panel A gating was set based on media and antibody controls that were run separately, whilst panel B gating was set using the internal background control.

Table 1: List of Antibodies used for cell and viral stainings.

Antibody Name	Clone	Company
PE–Conjugated monoclonal anti-CD81	Eat2	BioLegend
PE–Conjugated monoclonal anti-CD63	NVG-2	BioLegend
PE–Conjugated monoclonal anti-CD9	KMC8	BioLegend
PE–Conjugated monoclonal anti-CD3	17A2	BioLegend
PE–Conjugated monoclonal anti-LFA-1	H155-78	BioLegend
PE–Conjugated monoclonal anti-CD45	30-F11	BioLegend
PE–Conjugated monoclonal anti-CXCR4	2B11	BioLegend
PE–Conjugated monoclonal anti-CD29	HMB1-1	BioLegend
PE–Conjugated monoclonal anti-CD69	H12F3	BioLegend
PE–Conjugated monoclonal anti-CD4	RM4-5	BioLegend
PE–Conjugated monoclonal anti-Thy1.2	53-2.1	BioLegend
PE–Conjugated monoclonal anti-CD55	RIKO-3	BioLegend
PE–Conjugated monoclonal anti-CD59	mCD59.3	BioLegend
PE–Conjugated monoclonal anti-CD317	129c1	BioLegend
PE–Conjugated monoclonal anti-GFP	FM264G	BioLegend
PE–Conjugated polyclonal Isotype	Ab72480	Abcam

During cell staining, temperature is a key determinant as it can induce internalization of surface protein, causing varying results during staining. For viral staining, several differing temperature conditions (4°C, room temperature and 37 °C) used for cell staining were analysed to determine optimal staining conditions. Although, the room temperature staining condition resulted in higher number of viral particles stained for CD81 antigen, there was also an increase in non-specific binding whereas staining at 37°C had slightly lower CD81 positive viral particles yet a reduction in non-specific staining as illustrated in **Figure 3**. Thus, for future phenotypic analysis of retroviral surface markers we performed viral staining at 37°C.

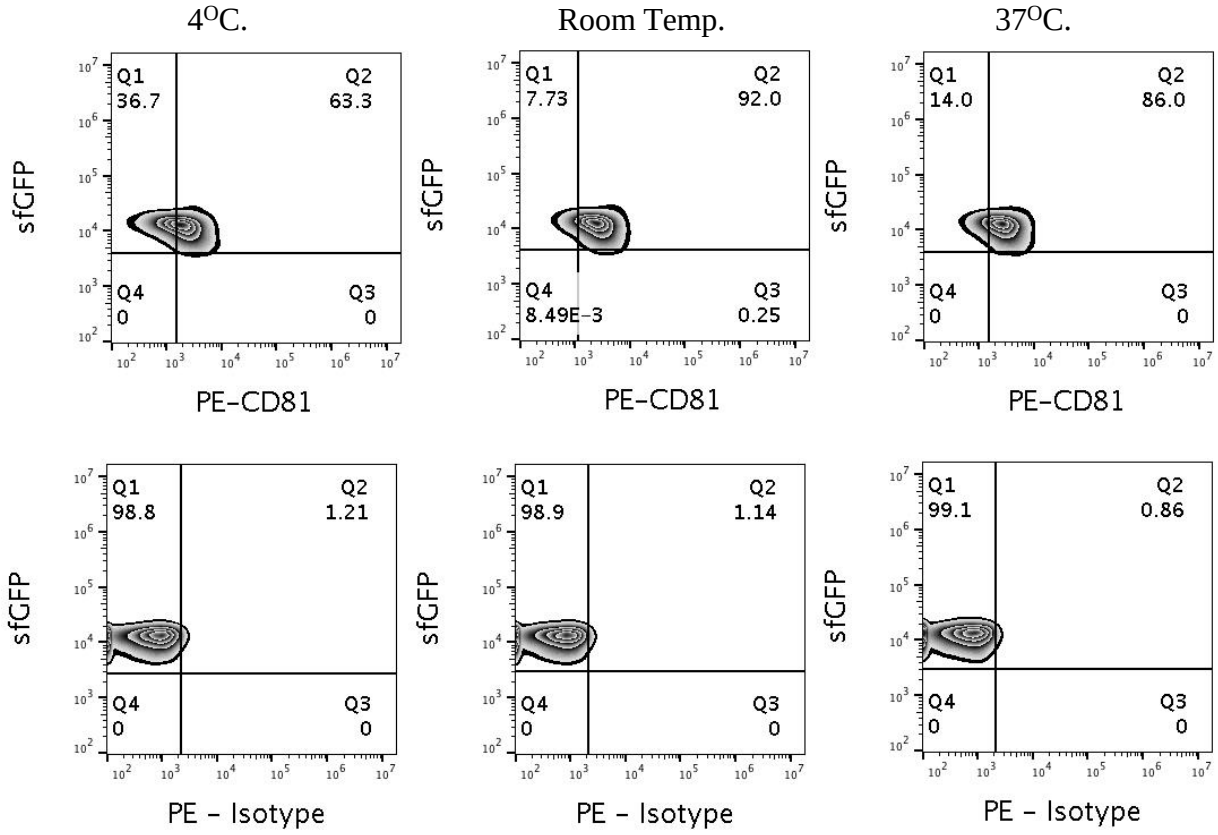

Figure 3: Determination of optimal temperature for viral staining.
MLV supernatant was stained with CD81 and isotype antibody at the three different temperatures (4^{O}C, room temperature and 37 ^{O}C) to assess highest CD81 staining and lowest non-specific staining.

During small particles analysis and staining, it is critical to reduce the number of particles that contribute to background noise and decrease resolution of submicron particles. These can impact the gating strategy as described earlier on, thereby increasing background fluorescence and obscuring the presence or count of particles expressing low abundant antigens. For this purpose, all reagents such as sheath, PBS and viral samples are filtered during staining as described in detail in Tang *et al* (65). Thus, in order to reduce the number of background particles we want to minimize the number of reagents used during staining. Nevertheless, we sought to use the fragment crystallizable region (**Fc** region) blocking reagents during viral staining to assess whether it can decrease non-specific staining and its impact on the background fluorescence. We tested three different concentrations of a serum-based blocking reagent traditionally used for cell staining and noted that, as expected, it increased background noise and fluorescence intensity therefore shifting the gating as a result decreasing the percentage of positively stained CD81 MLV virions as shown in **Figure 4**. All three concentrations tested had similar apparent reduction of positively stained particles. Although we did observe an apparent decrease in non-specific staining with an isotype control, however this was a by-product of adjusting the gating based on the media, antibody and Fc blocking agent control. Furthermore, since the cells analyzed in this project were either fibroblasts, T lymphocytes and primary CD4 T cells which don't express high abundance of **Fc** gamma receptors characteristic of B lymphocytes, myeloid and granulocytes, Fc region blocking reagents were not employed during the viral staining procedure.

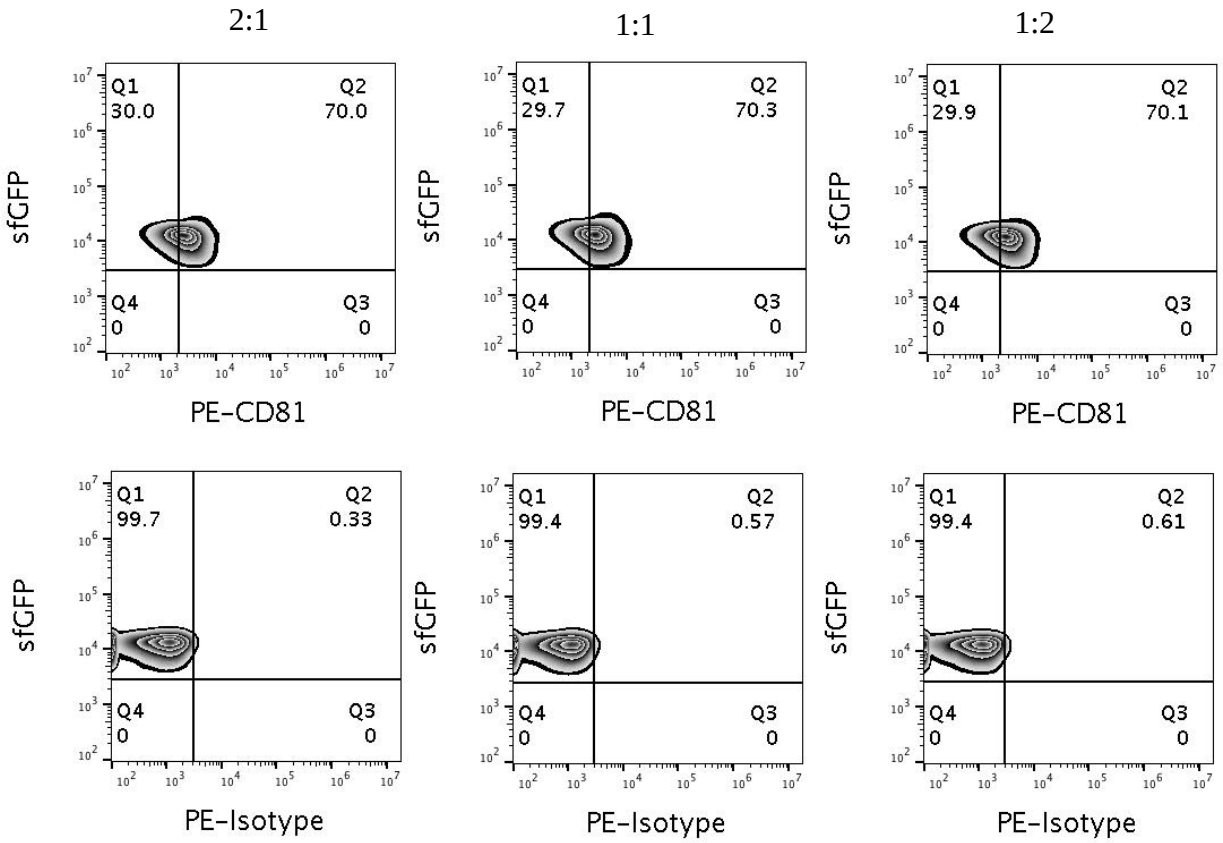

Figure 4: Effect of Fc Blocking reagent during viral staining on gating.
Three concentrations of serum-based Fc block reagent (diluted 1:1, 1:2, 2:1) was tested during viral staining, MLV supernatant was stained with CD81 and isotype antibody to assess highest CD81 staining and lowest non-specific staining.

2.3.2.1 Flow Virometry Controls

Previously, our lab employed stained PBS with antibody as a negative control which included background noise and fluorescence contributed from antibody staining to set the gates for analysis. However, we set out to compare different controls to ensure all variables contributing to the fluorescence were included for. Thus, we assessed differences in background and fluorescence from PBS, DMEM, RPMI and antibody controls. Moreover, to account for potential EV specific staining, supernatant was collected from NIH 3T3 fibroblast cell line and primary CD4+ T cells and stained for a marker common on EVs, CD45. Both media and antibody controls, while giving similar results, displayed higher background fluorescence than PBS and antibody control as illustrated in **Figure 5**. Consequently, to account for an increase in background event numbers of stained media and shift in fluorescence, media and antibody controls were utilized to set gates during viral staining. Alternatively, staining the viral supernatant with an isotype antibody will provide similar effect for gating, as it will account for increase in fluorescent intensity as a result for any non-specific binding. Thus, it is crucial to set proper gating to avoid yielding false positive results especially in the case of nanoparticles staining, which have much small dynamic range of resolution compared to that of positively stained cells.

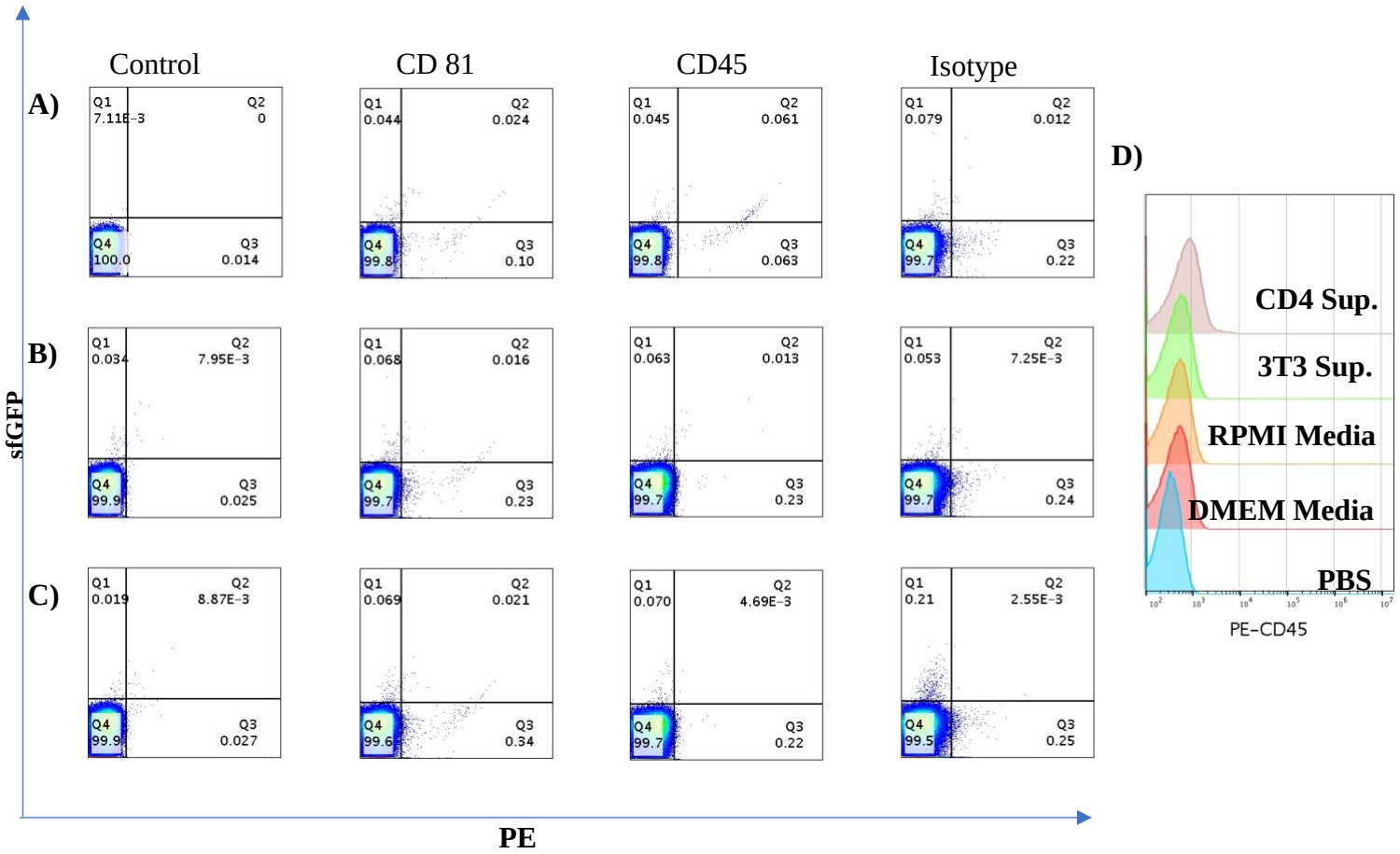

Figure 5: Optimization of controls to assess background fluorescence during viral staining. A) PBS and antibody B) DMEM and C) RPMI media and antibody were assessed for background and antibody fluorescence. Media control displayed higher fluorescence than PBS and antibody. Gates were adjusted to media and antibody controls as reference of antibody and media background for future experiments. D) CD45 expression comparison of A), B) and C) shown as overlaid histograms with 3T3 NIH and CD4 primary cell supernatants to assess for extracellular vesicle staining.

2.4 Primary CD4+ T Cell Activation and Infection

Mouse splenocytes were isolated from either wild type (mA3 WT) or APOBEC3-deficient (mA3 KO) 12 day old C57BL/6 mouse pups. Briefly, spleens were homogenized by enforcing passage through a 70 μm nylon cell strainer. Cells were washed with ice cold PBS substituted with 1 % FBS (denoted 1% PBS herein) and centrifuged at 330xg for 5 mins. The cell pellet was resuspended with 1 mL Ammonium Chloride Potassium (ACK) lysis buffer (Thermo Fisher Scientific) per spleen of for 1 minute and neutralized with 1% PBS. The remaining splenocytes were centrifuged at 330xg for 10 mins and counted. Splenocytes were isolated for total or naïve CD4 T cells using either Miltenyi Biotec total CD4 T (cat. # 30-095-130) or naïve CD4 T isolation kit (130-104-453) following manufacturer's instructions. Following isolation, cells were resuspended in RPMI media substituted with human Il-2 50 units/mL (Peprotech), 0.01 M Betamercaptoethanol (BME) (Sigma) and CD28 1 μg/mL (BioLegend) at a concentration of $2x10^6$ cells/mL. Cells were plated in a total volume of 250 μl per well in a 96 well round bottom plates pre-coated with 1 μg/mL CD3 (BioLegend). After a 2-day incubation 37°C with 5% CO_2, activated cells were infected with either wild type MLVsfGFP or glycogag deficient MLVsfGFP at a high MOI. Briefly, 20 mL of viral supernatant produced by the chronic NIH 3T3 producer cell line in a 10 cm dish for 72 hours was collected, centrifuged at 900xg, filtered through a 0.45μm filter and ultra-centrifuged at 100,000xg for 3h in a 70Ti rotor at 4°C. The viral pellet was resuspended in RPMI medium (Il-2 50 units/mL, 0.01 M BME) and used to infect the activated total or naïve primary CD4 T cells. After 24 hours, cells were aliquoted in 15 mL falcon tubes (Fisher Scientific) and washed thoroughly 3 times with 10 mL room temperature PBS. Subsequently, infected cells were resuspended in RPMI media supplemented with (Il-2 50 units/mL, 0.01 M BME and 1 ng/mL Il-7 (Miltenyi Biotec)) at a concentration of $2x10^6$ cells/mL

and plated in a total volume of 450 μL per well in 48 well plate. After 48 hours, viral supernatant was collected from the infected primary CD4+ T cells and used for flow virometry analysis as described earlier.

2.5 Data and Statistical Analysis

Flow cytometry data was analyzed with FlowJo v.10.0.7 (FlowJo, Ashland, OR). For cell analysis, FSC-height versus FSC-area and SSC-area versus FSC-area were used to exclude cell aggregates and debris. Statistical analysis to test for normal distribution and unpaired Mann-Whitney test was performed using GraphPad Prism (GraphPad Software, San Diego, CA).

3 Results

3.1 Characterization of NIH 3T3 fibroblast cell line

Since the cell's own surface marker composition influences the viral envelope composition, we first sought out to characterize the uninfected and chronically infected NIH 3T3 embryonic fibroblast cell line. The cellular surface phenotype was characterized with a panel of 12 antibodies against tetraspanin markers, adhesion molecules, integrins and lipid raft markers as shown in **Table 1**. The phenotypic characterization is presented as both histogram plots and summarized as mean fluorescent PE intensity as shown in **Figure 6**. Non-infected and chronically infected cells demonstrated similar phenotypic profiles. Both cell lines tested positive for tetraspanin and lipid microdomain markers (CD81, CD63 and CD9), CD29 integrin marker, CD55 and Thy1.2 lipid raft markers. Of note, CD81 and CD63 were the most abundantly expressed markers comparable to GFP expression which was the most abundantly detected antigen on the surface of these chronic cells.

A)

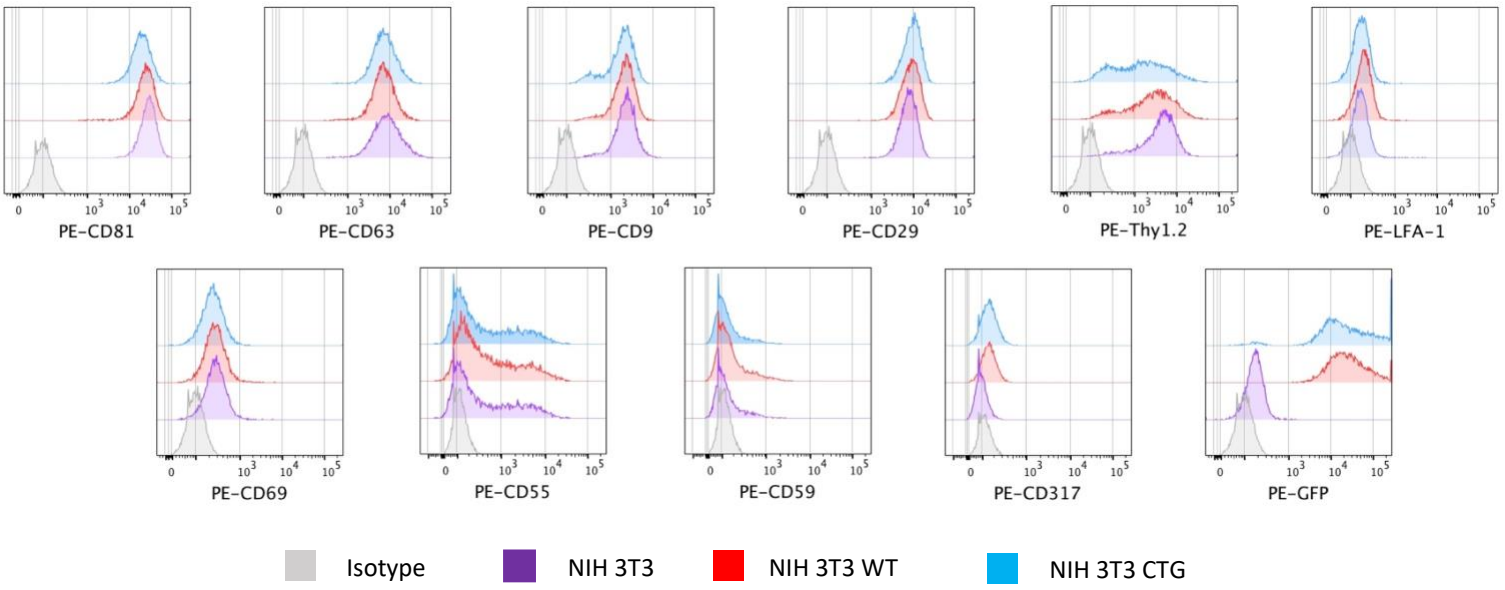

B)

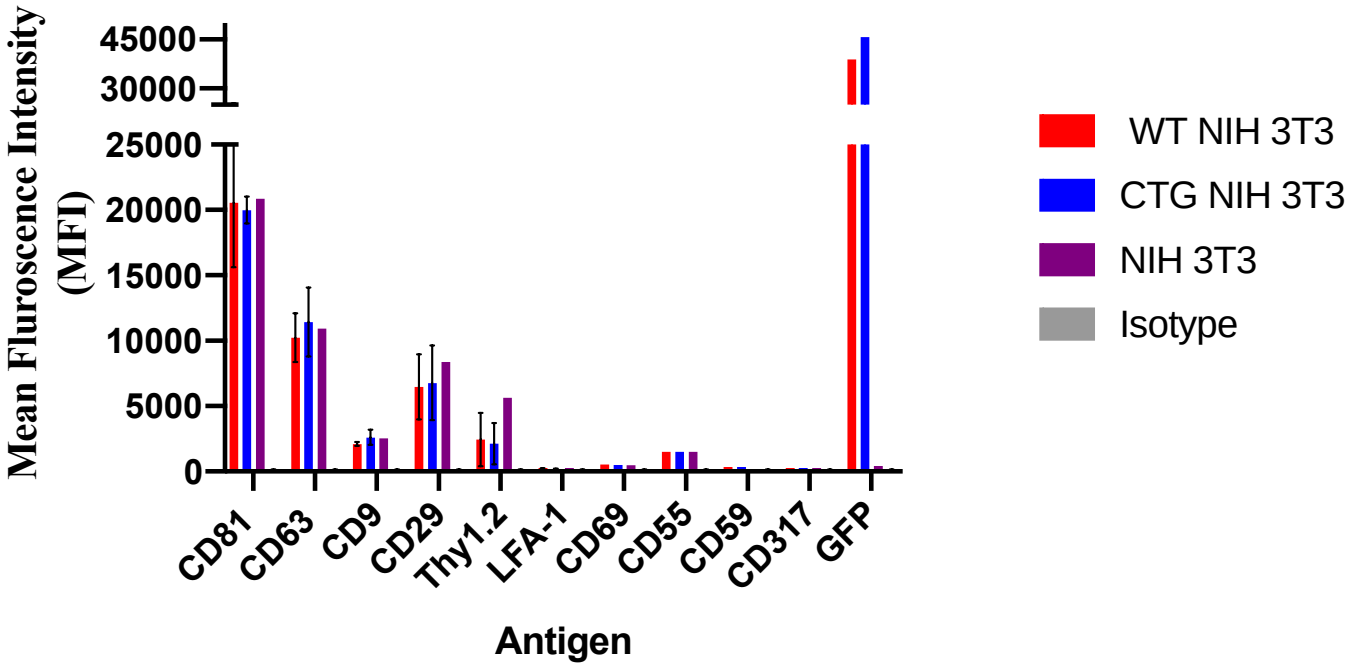

Figure 6: Characterization of NIH 3T3 fibroblast cell line.
Surface antigen analysis of uninfected and chronic NIH 3T3 cell line by flow cytometric analysis with an antibody screen targeting for tetraspanin,lipid microdomain markers, lipid raft proteins and integrins. A) Histogram analysis and B) Mean fluorescence intensity analysis of cellular surface antigens on wild type (WT) and glycogag deficient (CTG) chronically infected and uninfected NIH 3T3 fibroblast cells.

3.2 Characterization of wild type and glycogag-deficient MLV released from NIH 3T3 cells

Next, a viral phenotypic analysis was conducted directly on supernatant collected from chronically infected wild type and glycogag deficient fibroblast cell lines with FVM. Firstly, the viral population of interest was resolved from background by both scatter intensity and GFP fluorescence. Analysis of MLV virions show a highly monodisperse population by violet side scatter intensity (VSSC). This homogeneous expression of VSSC was further reflected in Env-GFP fluorescence intensity as illustrated in **Figure 7**. Although, VSSC profiles between glycogag-deficient and wild type virions were similar, glycogag deficient virions displayed a more monodispersed profile and a higher mean fluorescent intensity (MFI) of GFP expression compared to wildtype (**Figure 7C**).

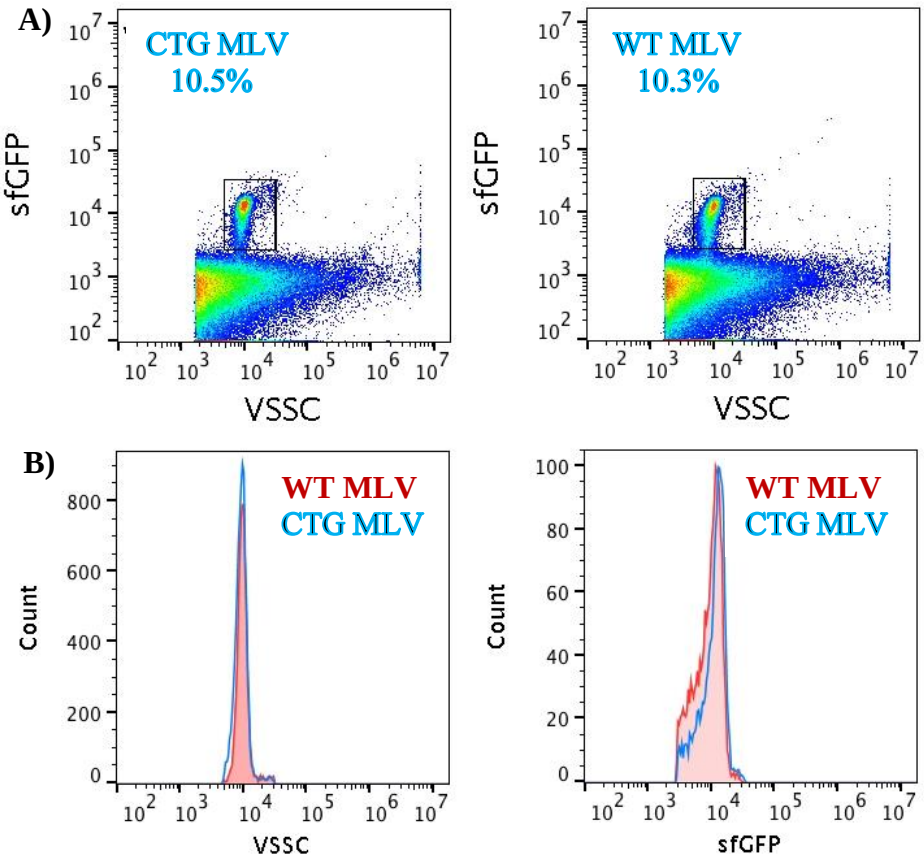

C)

	VSSC Intensity (MFI)	GFP Intensity (MFI)
WT MLV	10 056	9 750
CTG MLV	9 446	11 456

Figure 7: Scatter and fluorescence quantification between wildtype and glycogag deficient MLV virions released from chronic NIH 3T3 cells.

A) Wild type MLV (WT) virions present a similar discrete scatter plot profile to glycogag deficient (CTG) MLV virions. Gated particles express similar **B)** side scatter and GFP intensity as overlaid histograms and **C)** mean fluorescent intensity (MFI) values. Viral supernatant was collected after 72 hours from chronic NIH 3T3 fibroblasts and diluted 1:500 and was subsequently directly run by flow virometry.

Subsequently, to analyze the presence and distribution of host derived antigens on the surface of individual MLV particles, the viral supernatant was stained against the previously described antibodies chosen for the NIH 3T3 cell phenotypic analysis. The results from the viral staining are summarized as mean and median fluorescence intensity bar graph and overlaid histogram plots of PE fluorescence as illustrated in **Figure 8**. Thus, we set out to assess the two separate null hypotheses stipulated as follows:

H_0: MLV viral particles do not uptake cell derived antigens on their viral envelope during budding, thus the signal intensity between stained MLV virus and negative control does not differ.

H_1: MLV viral particles do uptake cell derived antigens on their viral envelope during budding, thus the signal intensity between stained MLV virus and negative control is different.

H_0: The glycogag protein on wild type virus does not upregulate incorporation of the cell derived antigens when compared glycogag deficient virus.

H_1: The glycogag protein on wild type virus does upregulate incorporation of the cell derived antigens when compared to the glycogag deficient virus.

Firstly, we need to understand the type of the distribution of the fluorescent intensity produced by these viral particles. For example, if the signal follows the law of Normal (Gaussian) distribution, it is the T-Student test that would be used to verify whether there is differential uptake of cellular antigens between wild type and glycogag deficient MLV. In the case when the signal intensity fails to be normally distributed, the Mann-Whitney non-parametric test was statistically appropriate to be used to compare the differences in distributions between these unmatched groups. Contrary to the Student T test that compares the means of two samples, this test compares their medians. Distribution normality of the samples' data was tested using D'Agostino-Pearson and Kolomogorov-Smirnov statistical criteria. Data distribution of all the samples analyzed was confirmed not to be of Gaussian distribution ($K2>191$, $KS>0.06$ $n>10000$, $p<0.0001$) on a very

high significance level. Therefore, to assess whether the null hypothesis is rejected and whether there is indeed statistically significant difference in signal between the two MLV viruses, the Mann-Whitney test was applied. It needs to be mentioned that for the purpose of this analysis, all data collected across 3-5 independent experiments was pooled together. Since we dealt with the same type of samples each time, which are independent of the day in which the experiment was performed.

Presence and abundance of antigens were determined using the antibody and media sample as a negative control in statistical analysis and for gating as described in detail in the methods section. From the 11 viral stainings performed on wildtype and glycogag deficient MLV virions, both variants displayed presence of the highly abundant cellular tetraspanin marker CD81 ($n=99980$, $p<0.0001$) and CD63 ($n=100011$, $p<0.0001$) as compared to negative control. Only wild type MLV virions were positive for the lipid raft protein marker CD59 ($n= 3140$, $p<0.0001$). Intriguingly, the glycogag deficient particles alone expressed the interferon induced host protein CD317 ($n=2855$, $p<0.001$), known as tetherin which inhibits the release of assembled viral particles at cell surface and has been shown to inhibit a wide range enveloped virus(25, 100–102). Interestingly, CD317 was not detected on the cell surface however it has been shown to assemble at the site of late endosomal release. Furthermore, the integrin marker CD29 ($n>99891$, $p<0.0001$) was only detected on glycogag deficient MLV. Other cellular markers that were present on the cell surface were not detected on the viral envelope of MLV. Furthermore, we observed discrete populations on scatter plots that were positive for the tetraspanin markers CD81 ($n=36245$, $p<0.0001$) and CD63 ($n=33114$, $P<0.0001$) (**Figure 9**). Since this population was negative for sfGFP and these tetraspanin markers are often used for EV characterization studies, we can infer that we were able to stain and observe discrete population of EVs positive for these markers that were produced by

NIH 3T3 cells in both normal and infected conditions. Moreover, using the statistical z-score approach, we calculated with the 99% confidence interval for the percentage of viruses that are positive for the respective host derived cellular antigen analyzed. Thus, FVM revealed that host derived CD81 and CD63 were present on the viral envelope on 69.1 % ± 0.2% (n=168758), and 30.1 % ± 0.2% (n=250415) of wild type virions whereas only 38.5% ± 0.3% (n=217941) and 20.3%± 0.2% (n=226449) of glycogag deficient virions carried these antigens, respectively. Analysis of CD81 expression demonstrates a more monodisperse population on wildtype MLV compared to CD81 expression on glycogag deficient MLV; whereas the inverse was seen for CD63 antigen expression (**Figure 8A**). Next, we quantified the mean and median PE fluorescence intensity signal to assess distribution and antigenic variability between wild type MLV and glycogag-deficient virions as illustrated in **Figure 8 B) and C)**. To assess for viral heterogeneity and antigenic variability, the viral count was kept identical across all stainings. Thus, the relative expression of cellular antigen abundances detected on wild type virions were quantified as mean and median PE intensity with the most abundantly detected surface antigen CD81 expressing 2548±6 and 2228 and CD63 expressing 1905±7 and 1455. In contrast, glycogag deficient MLV particles expressed a significantly lower mean and median fluorescence intensity, on average, with CD81 at 1606±5 and 1332 (n=99980, $p<0.0001$) and CD63 with 1579±6 and 1182 (n=97615, $p<0.0001$), respectively. Lastly, the tetherin marker CD317 was expressed on glycogag deficient virions at a mean MFI of 416±5 and a median intensity of 379. However, when we compared the MFI of the double positive virions to that of stained supernatant collected from uninfected NIH 3T3 cells for those antigens, we observed that only wild type virions expressed a significantly greater relative intensity value for CD81 (n=111421, $p<0.0001$) , CD63 (n=109045, $p<0.0001$) and GFP (n=110023, $p<0.0001$) only. Whereas the expression of CD81 (n=99980, $p<0.0001$) and

GFP (n=100091, $p<0.0001$) alone on glycogag deficient virions displayed significant differences to that of the uninfected stained supernatant. Therefore, it is important to note that the presence of the above-mentioned antigens are based on the significantly greater PE median intensity to the antibody and media negative control ($p<0.0001$). However, this significance was not confirmed for all antigens observed when compared to the PE intensity of the stained supernatant collected from uninfected cells. Thus, it is unclear whether the CD29 was actually expressed on the viral envelope, or whether this signal was a result of non-specific labelling. Nevertheless, all NIH 3T3 cells expressed CD29 antigen at a high abundance, although its expression was lower than that of CD81 and CD63 **(Figure 6)**. Moreover, the observed greater signal of the stained untreated supernatant compared to the negative control could be a result of EV staining which will contribute to the increase in the signal. EV staining for a particular antigen prevents the use of a stained supernatant as a reliable negative control due to potential confounding variables and providing a skewed signal intensity as discussed in methods section 4.3.2 *Flow Virometry Staining and Analysis*. Lastly, due to similar values of PE fluorescence output of other antigens (CD9, Thy1.2 and CD55) analyzed to media control, we could not report differences between the two MLV variants.

A)

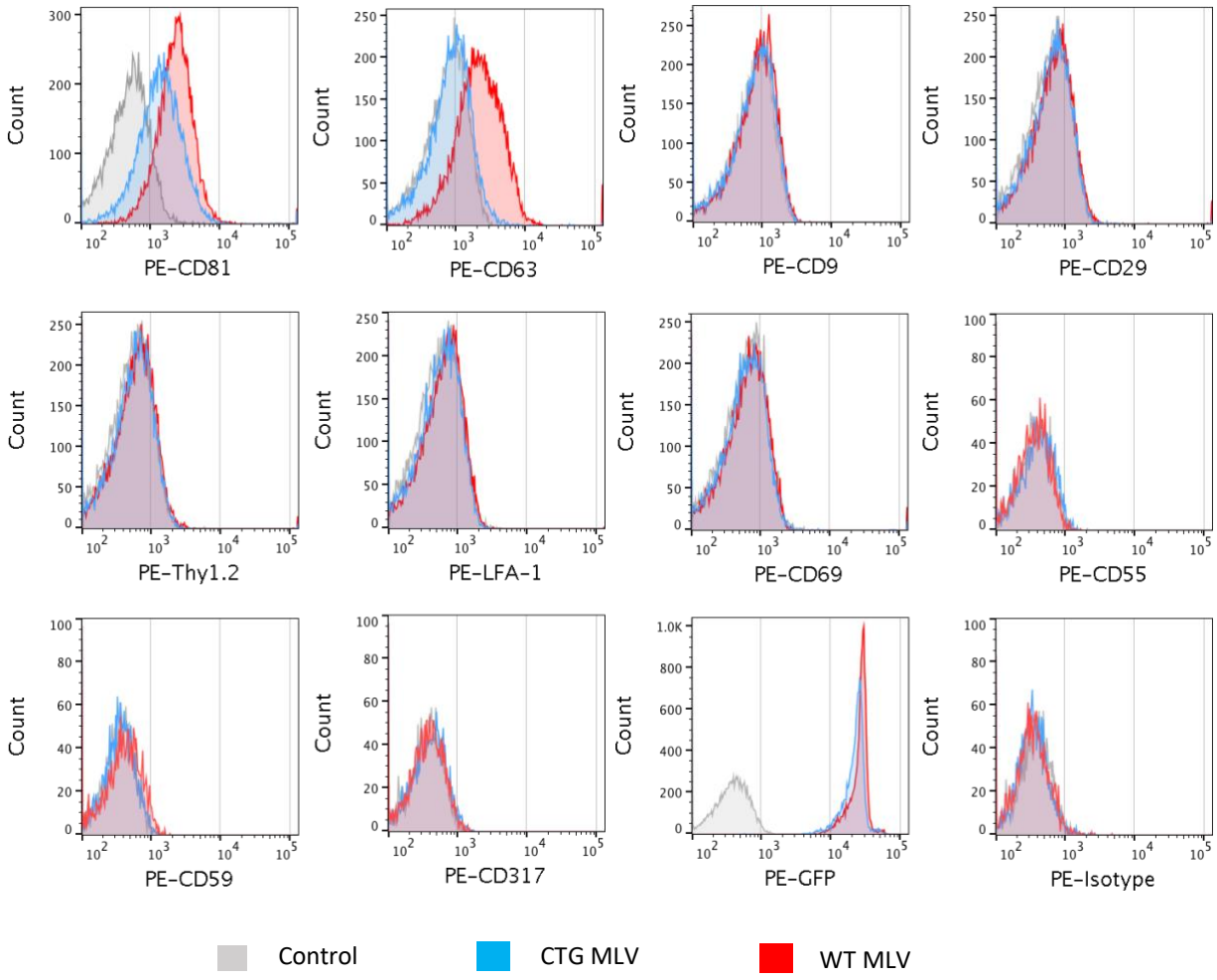
Count
PE-CD81
PE-CD63
PE-CD9
PE-CD29
PE-Thy1.2
PE-LFA-1
PE-CD69
PE-CD55
PE-CD59
PE-CD317
PE-GFP
PE-Isotype
Control
CTG MLV
WT MLV

B)

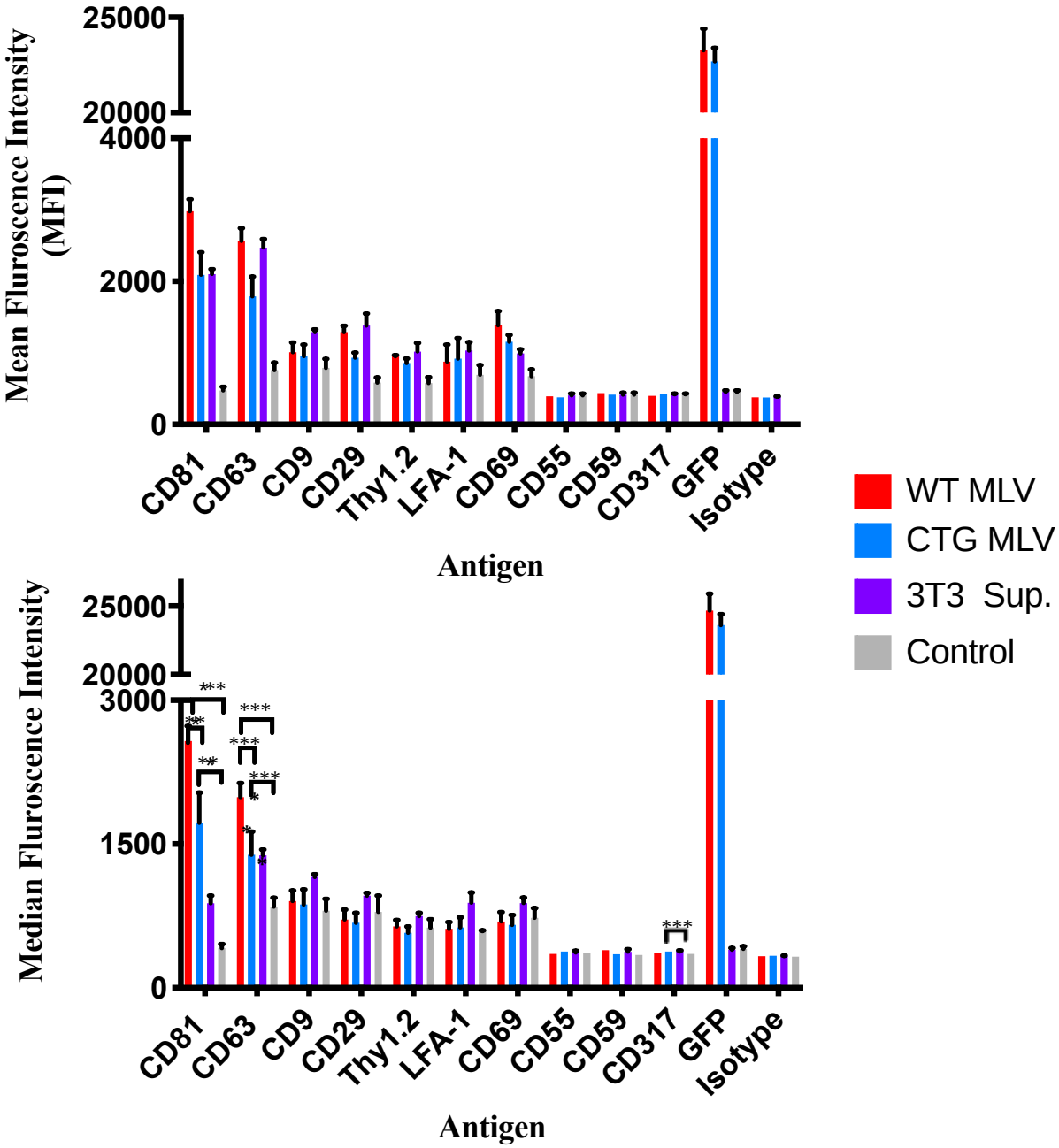

Figure 8: Surface antigen phenotypic analysis of virions released from NIH 3T3 cells. Surface antigen analysis of uninfected and chronic NIH 3T3 cell line by flow virometry with a small panel antibody screen. A) Histogram analysis of antigen expression distribution of overlaid MLV variants and antibody and media control. B) Mean and C) median fluorescence intensity bar graph of surface antigens on virions released from two chronic producer cells: wild type (WT) and glycogag deficient (CTG), uninfected NIH 3T3 fibroblast cells, and antibody and media control. Data normality of samples was calculated by D'Agustiona and Person test and validated by Kolomogorov-Smirnov test. Statistical significance was calculated by a nonparametric Mann-Whitney test as distribution of sample data was not of Gaussian form. ***, P value < 0.0001.

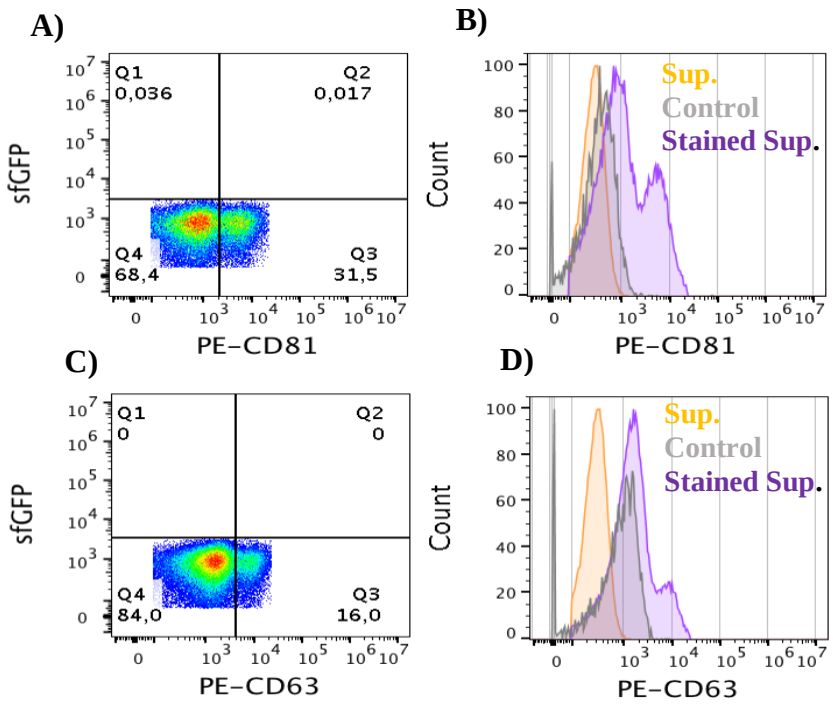

Figure 9: Detection of a discrete EV population positive for the CD81 and CD63 EV tetraspanin markers in supernatant released from NIH 3T3 cells.
Scatter plots of uninfected supernatant stained against A) CD81 and C) CD63 show discrete population that can be resolved by PE intensity. B) and D) Overlaid histogram comparison of stained supernatant against unstained control and negative media and antibody control.

3.3 Characterization of EL4 lymphoma cell line

The phenotypic analysis of MLV genotype variants released from NIH 3T3 fibroblast cells, established the framework for retroviral surface marker characterization by flow virometry. Next, we sought out to evaluate MLV virions released from more physiologically and immunologically relevant cells. Thus, we infected an EL4 murine T lymphocyte cell line with wild type and glycogag-deficient MLV as described in detail in the methods sections. Uninfected and chronically generated EL4 cells were characterized with an antibody panel chosen against highly expressed surface immune markers as well as previously analyzed integrins, adhesion, tetraspanin, lipid microdomain and lipid raft protein markers. The phenotypic characterization of EL4 cells is presented as both histogram plots and summarized MFI as shown in **Figure 10**. Non-infected and chronic cells demonstrated a similar phenotypic profiles, positive for immune markers CD3, CXCR4 and the highly abundant hematopoietic CD45 and Thy1.2 marker. Additionally, cells minimally expressed the tetraspanin CD81, CD63 and CD9, lipid raft protein marker CD59 and tetherin marker CD317. Furthermore, the lipid raft protein markers CD55 and Thy1.2 and adhesion receptor LFA-1 were also presented on non-infected and chronic EL4 cells. However, in contrast to NIH 3T3 cellular phenotype, CD81 and CD63 were not as abundantly expressed, instead CD45, Thy1.2 and LFA-1 antigens in that order had the highest PE intensity signal.

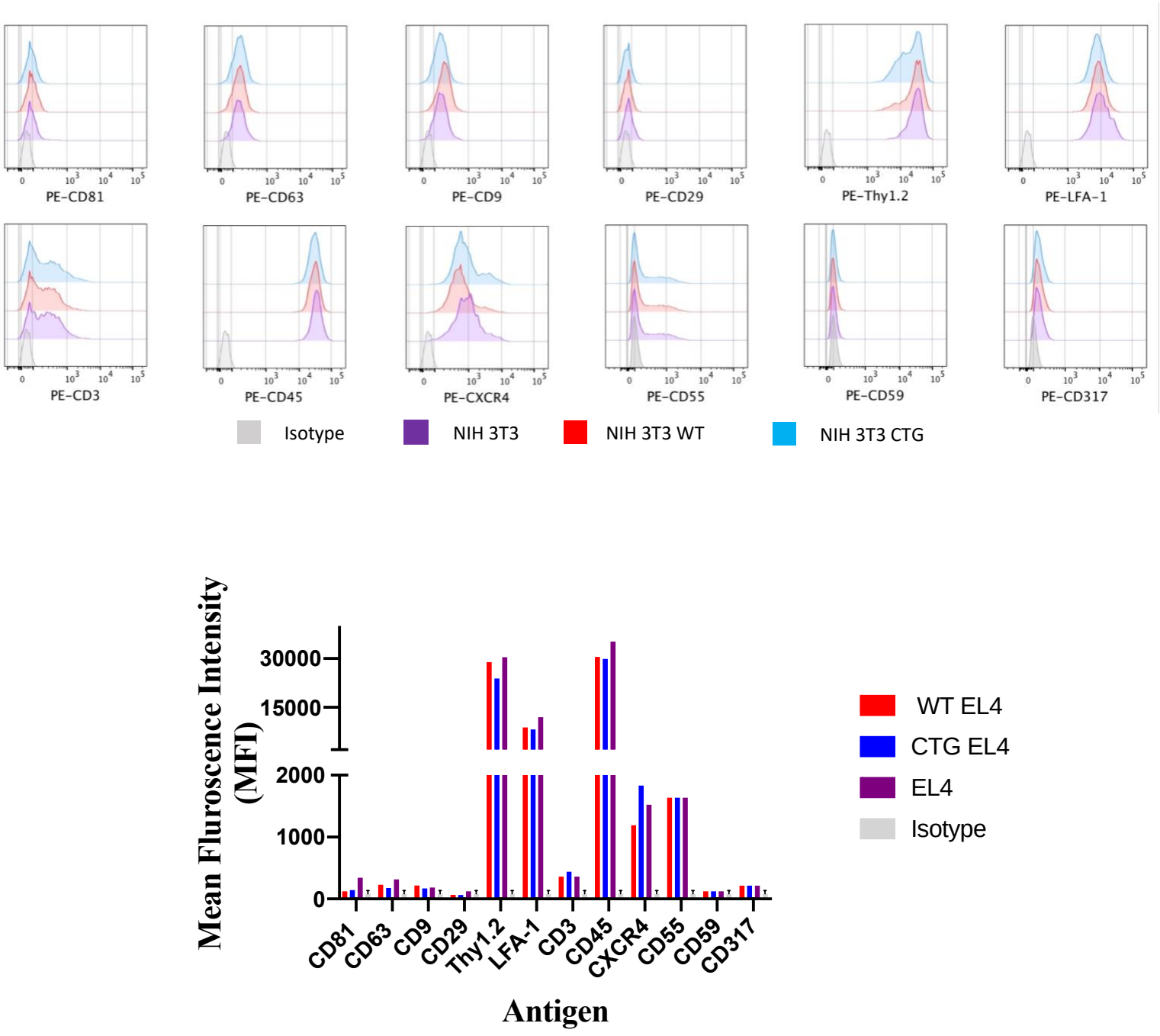

Figure 10: Characterization of EL4 T lymphocyte cell lines.
Surface antigen analysis of uninfected and chronic EL4 cell line by flow cytometry analysis with a small panel antibody screen targeting for immune, tetraspanin and lipid microdomain, lipid raft proteins, integrins adhesion markers. A) Overlaid histogram analysis of PE intensity and B) Mean fluorescence intensity analysis of cellular surface antigens on uninfected and chronically infected with wild type (WT) and glycogag deficient (CTG) virus EL4 cells.

3.4 Characterization of wild type and glycogag-deficient MLV virions released from EL4 cells

A viral phenotypic analysis was conducted directly on the supernatant collected from chronically infected wild type and glycogag-deficient T lymphocyte EL4 cell lines with FVM. The optimized protocol established for virions released from the NIH 3T3 producer cell line was followed. Firstly, the viral population of interest was resolved from background by both scatter and GFP intensity similar to the virions released from chronic NIH 3T3 cells. Interestingly, the chronic EL4 cells produced approximately 20-fold less of viral particles as analyzed by FVM compared to the amount of the virus released by the similarly plated quantity of NIH 3T3 producer cells. Furthermore, analysis of MLV virions show one monodispersed population by VSSC and GFP fluorescence intensity as shown by the orange gate. Interestingly additional heterogenous viral particles were detected that showed higher scatter and GFP intensities as shown by the red gate (**Figure 11**). Wild type and glycogag virions displayed similar VSSC and GFP expression profiles mean fluorescence intensities which was consistent between the two population of MLV particles.

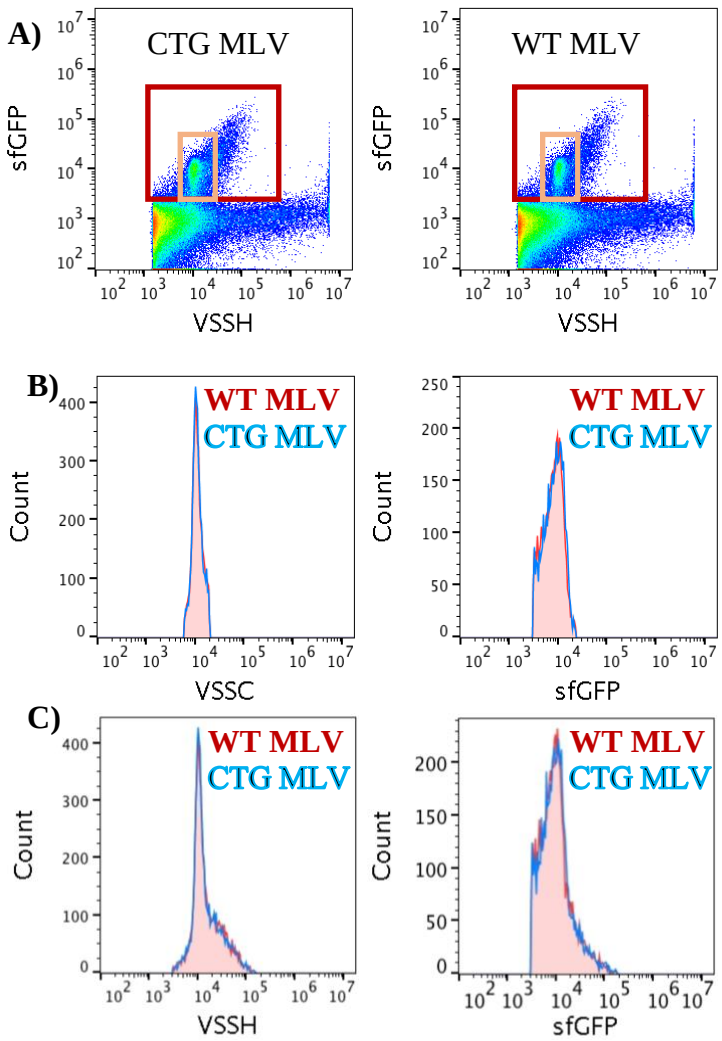

D)

	VSSC Intensity (MFI)	GFP Intensity (MFI)
WT MLV	11 175	8 410
CTG MLV	11 113	8 770
WT MLV	19 497	13 360
CTG MLV	19 127	13 783

Figure 11: Two populations are detected in wildtype and glycoGag deficient MLV virions released from chronic EL4 cells.

A) Wild type MLV (WT) virions present a similar discrete scatter plot profile to glycogag deficient (CTG) MLV virions. Two population are detected by flow virometry: **B)** a monodisperse population gated in orange and **C)** a more heterogenous particles express similar side scatter and GFP intensity as overlaid histograms and **D)** mean fluorescent intensity (MFI) values.

Subsequently, viral supernatant was stained against the previously described antibodies used for the EL4 cell phenotypic analysis. Additionally, to validate the analysis of the viral population, we stained against the abundantly found host marker CD45 which has not been observed on egressed HIV-1 virions yet documented on EVs. The results from the viral staining are summarized as a mean and median fluorescence intensity bar graph and overlaid histogram plots of PE fluorescence as illustrated in **Figure 12**. Virions released from EL4 cells also follow a non-Gaussian distribution and were analyzed with a Mann-Whitney nonparametric unpaired test as previously described. Similarly, presence and abundance of antigens were determined utilizing the antibody and media sample as a negative control. From the 13 viral stainings performed on the two MLV genotype variants, the highly abundant mouse T cell and lipid raft marker Thy1.2 ($n=9319$, $p<0.0001$), T cell marker CD3 ($n=9193$, $p<0.0001$) and the adhesion marker LFA-1 ($n=6047$, $p<0.0001$) were observed as compared to negative control. Interestingly, T cell marker CD45 ($n=4840$, $p<0.0001$) was present on both wildtype MLV virions and glycogag deficient particles. Lastly, only glycogag deficient virions displayed presence of the lipid raft marker CD55 ($n=3407$, $p<0.0001$) and CD59 ($n=3576$, $p<0.0001$) as compared to the negative control. Interestingly, as observed for on MLV virions released from NIH 3T3 cells, tetherin host factor CD317 ($n=3295$, $p<0.0001$) was detected on glycogag deficient MLV only as compared to the control, although it was not expressed on the cell surface on either cell type. Other cellular markers that were present on the cell surface were not detected on the viral envelope of MLV.

Furthermore, as we observed for supernatant collected from the uninfected NIH 3T3 cells, we detected discrete EV populations on scatter plots positive for the commonly employed EV CD45 marker MFI=491 ($n=230429$, $p<0.0001$), Thy1.2 MFI =613 ($n=72714$, $p<0.0001$), and LFA-1 MFI=447 ($n=267797$, $p<0.0001$). Thus, flow virometry revealed that host derived Thy1.2 and

LFA-1 were present on the viral envelope, with a probability of 99% confidence, on 69.2%±0.84% (n=11998) and 3.27%± 0.28% (n=16040) of wild type virions whereas only 64.4%±1.09% (n=12801) and 3.83%± 0.44% (n=12571) of glycogag deficient virions carried these antigens, respectively. Intriguingly, the CD45 EV marker was present on sfGFP positive wild type and glycogag deficient MLV virions, on 7.82%±0.43% (n=15867) and 9.16%±0.68% (n=12020) of particles, respectively. Lastly, the lipid raft protein markers CD55 and tetherin marker CD317 were observed on 0.92%±0.42% (n=3389) and 1.5%±0.55% (n=3277) of glycogag deficient MLV virions, which showed a more heterogenous incorporation profile compared to its wild type counterpart. To assess for viral heterogeneity and differential antigen incorporation, viral count was kept identical across all stainings. Analysis of Thy1.2 expression reveals a similar highly heterogenous distribution of this cellular antigen between both MLV variants. Whereas, the form of LFA-1 and CD45 between the two MLV genotypes is similar, the antigenic distribution reveals one dominant monodisperse population and a separate discrete population expressing an increased PE signal as shown in **Figure 12A**. For other host derived cellular antigens, both MLV variants displayed a similar form which showed one monodisperse population.

Next, we quantified mean and median PE fluorescence intensity signal to assess distribution of antigen expression between wild type MLV and glycogag-deficient virions. Thus, the relative expression of cellular antigen abundance detected on wild type virions was quantified as mean and median PE intensity with the most abundant Thy1.2 expressing 3945±97 and 1926, followed by CD45 with 879±23 and 441, and LFA-1 with 718±82 and 420, respectively. In contrast, glycogag deficient MLV particles expressed a significantly lower mean and median fluorescence intensity with Thy1.2 at 3669±97 and 1639 (n=9319, $p<0.0001$) and LFA-1 with 647 and 393 (n=6047,

$p<0.0001$). Whereas there was no significant difference between the two genotypes for the CD45 and CD3 antigen expression. Lastly, lipid raft marker CD55 and CD59 was expressed on glycogag deficient virions alone at an MFI of 451 ± 4 and 416 ± 3 and a median intensity of 422 and 390. As previously, when we compared the MFI of the double positive virions to that of stained supernatant collected from uninfected NIH 3T3 cells for those antigens, we observed that only wild type virions expressed a significantly greater relative intensity value for Thy1.2 ($n=9319$, $p<0.0001$), CD45 ($n=4840$, $p<0.0001$), CD3 ($n=10565$, $p<0.0003$), LFA-1 ($n=10913$, $p<0.0001$) and GFP ($n=11102$, $p<0.0001$) only. Whereas the expression of Thy1.2 ($n=9319$, $p<0.0001$), CD45 ($n=8667$, $p<0.0001$), CD3 ($n=91393$, $p<0.0024$), CD55 ($n=3407$, $p<0.0001$) and GFP ($n=10090$, $p<0.0001$) alone on glycogag deficient virions displayed significant differences to that of the uninfected stained supernatant. When we stained either wildtype or glycogag deficient MLV with an isotype, and compared it to control or stained supernatant, we did not observe any statistical significance between samples. Lastly, due to similar low expression of other cellular antigens tested, we could not reliably report presence or differences between the two MLV variants. The low PE intensity values detected could be a result of non-specific staining since signal is similar to control or reflects the decreased concentration of these surface antigens on the EL4 cells themselves.

A)

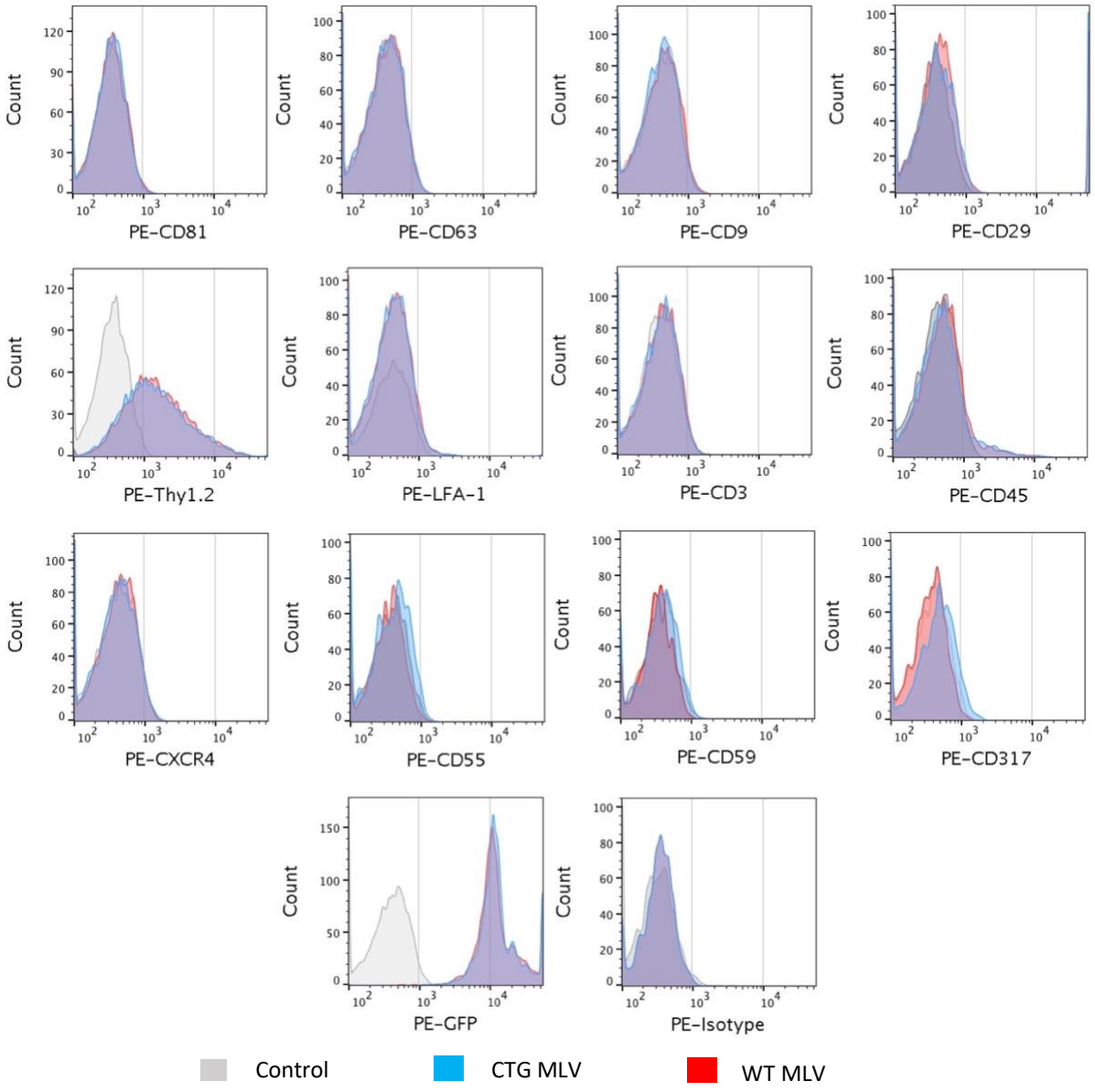
Count
PE-CD81
PE-CD63
PE-CD9
PE-CD29
PE-Thy1.2
PE-LFA-1
PE-CD3
PE-CD45
PE-CXCR4
PE-CD55
PE-CD59
PE-CD317
PE-GFP
PE-Isotype
Control
CTG MLV
WT MLV

B)

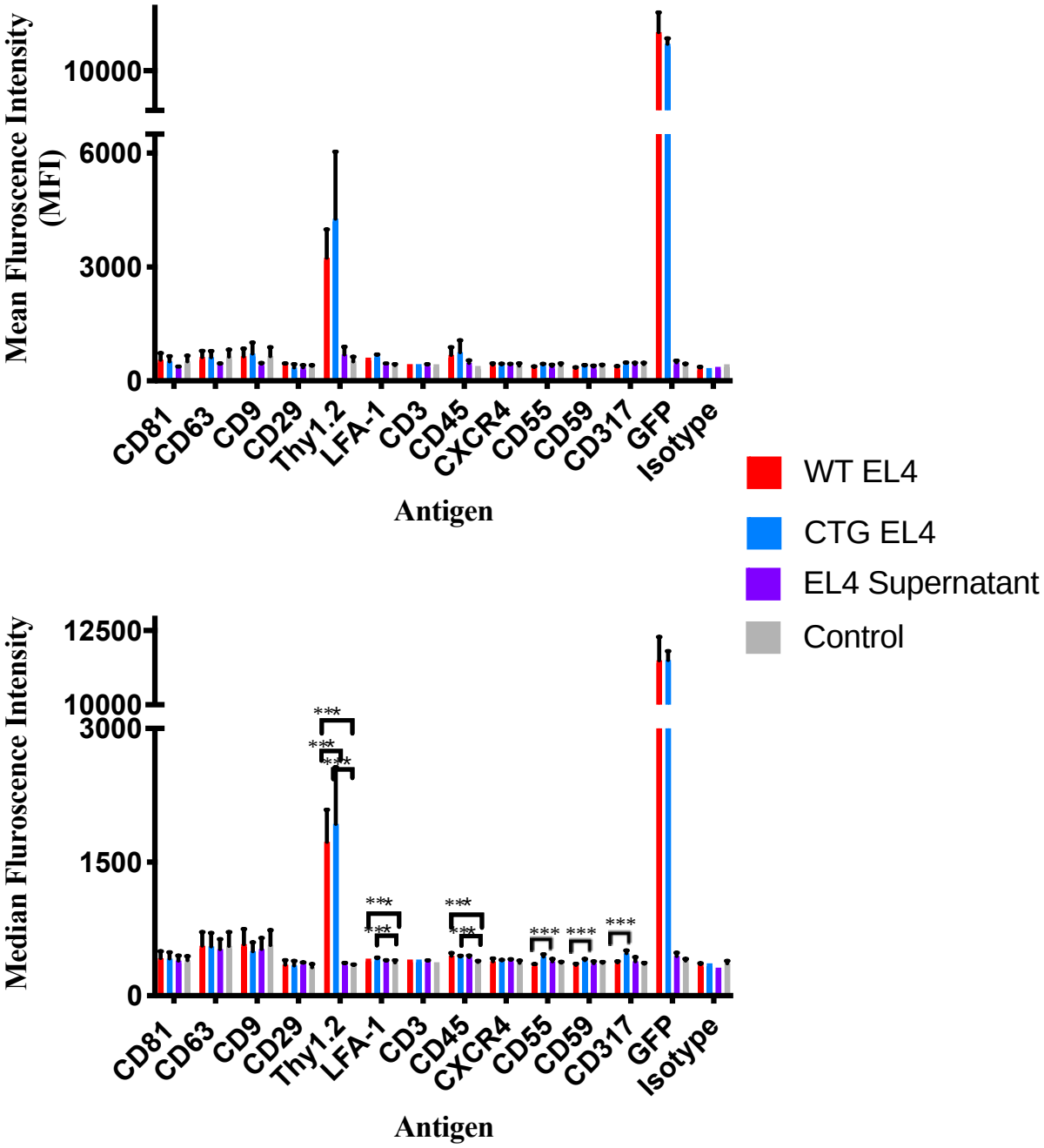

Figure 12: Surface antigen phenotypic analysis of virions released from EL4 cells.
Surface antigen analysis of uninfected and chronic El4 cell line by flow virometry with a 14 panel antibody screen. A) Histogram analysis of antigen expression distribution of overlaid MLV variants and antibody and media control. B) Mean and median C) fluorescence intensity analysis of cellular surface antigens on two chronic producer cells: wild type (WT) and glycoGag deficient (CTG), uninfected EL4 cells, and antibody and media control. Statistical significance was calculated by a nonparametric Mann-Whitney test as distribution of sample data was not of Gaussian form. ***, P value < 0.0001.

3.5 Characterization of primary murine CD4+ T cells

Next, we evaluated whether retroviral phenotypic analysis using FVM could be performed directly on virions released from primary cells in an *ex vivo* infection. Toward this goal, we first optimized activation and expansion protocols for murine primary total and naive CD4+ T cells. Then we infected these activated cells with either wild type or glygogag-deficient MLV as described in the methods section. First, non-infected and infected primary CD4+ T cells were characterized with an antibody panel chosen against highly expressed surface immune markers as well as previously analyzed integrins, adhesion, tetraspanin, lipid microdomain and lipid raft protein markers. The phenotypic characterization of CD4+ T cells is presented as both histogram plots and summarized with mean fluorescent intensity as shown in **Figure 13**. Chronic cells demonstrated an upregulated phenotypic profile compared to the uninfected cells, positive for immune markers such as CD3, CXCR4, CD4 and the highly abundant hematopoietic CD45 and Thy1.2 marker. Additionally, all cells expressed the tetraspanin CD63 minimally, however the infected cells had an upregulation of CD81, CD9 and the integrin marker CD29 compared to the uninfected CD4+ T cells. Furthermore, the lipid raft protein markers CD55 and Thy1.2 and adhesion receptor LFA-1 were also present in all cells, following the similar trend of upregulation in the infected cells. However, in contrast to NIH 3T3 phenotype, CD81 and CD63 were not as abundantly expressed, instead similar to the EL4 lymphoma T cell profile CD45, Thy1.2, LFA-1, CD4 and GFP antigens had the highest PE intensity signal.

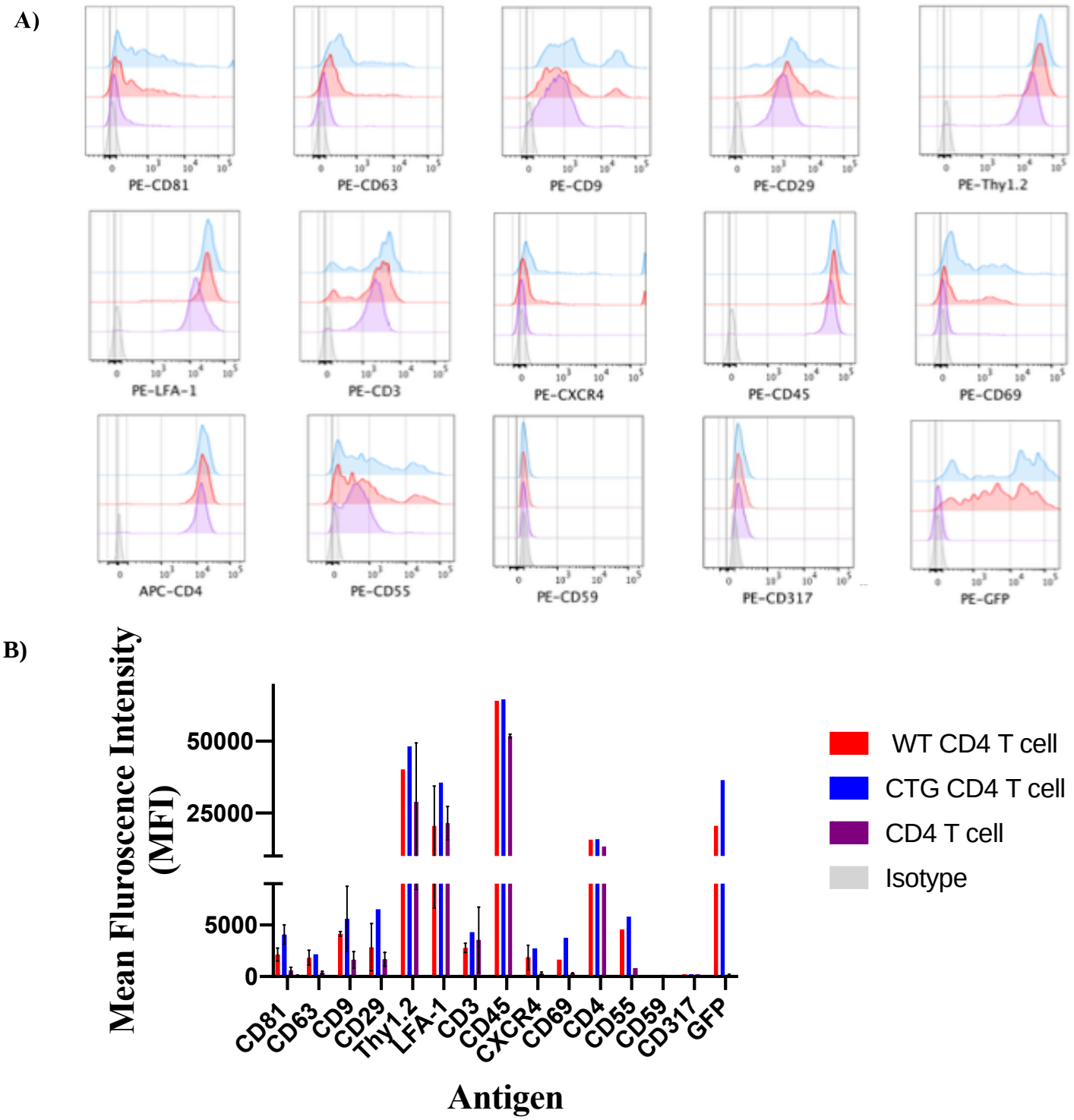

Figure 13: Characterization of murine primary total CD4+ T cells.
Surface antigen analysis of uninfected and infected CD4+ T cells by flow cytometry analysis with an antibody screen targeting for immune, tetraspanin and lipid microdomain, lipid raft proteins, integrins and adhesion markers. A) Overlaid histogram analysis of PE intensity and B) mean fluorescence intensity (MFI) analysis of cellular surface antigens on CD4 T cells infected with wild type (WT) and glycoGag deficient (CTG) and uninfected CD4 T cells. CD4 T cells were

isolated from C57/BL 12- day old mice, activated with CD3/CD28 stimulation and infected with two MLV variants.

3.6 Characterization of wild type and glycogag-deficient MLV released from primary CD4+ T cells

Next, a viral phenotypic analysis by FVM was conducted directly on the supernatant collected from untreated and infected with wild type and glycogag deficient virus CD4+ T cells. Firstly, the viral population of interest was resolved from background by both scatter intensity and GFP fluorescence as observed in **Figure 14 A)** and **B)**. However, we observed much lower viral production in *ex vivo* infections compared to the amount of virus produced by the NIH 3T3 producer cells (two orders of magnitude lower) and EL4 chronic cells (an order of magnitude lower). Analysis of MLV virions show a monodispersed population by VSSC intensity, this homogeneous expression is further reflected in Env-GFP fluorescence intensity as shown in **Figure14**. Although, VSSC profile between glycogag deficient and wild type virions was similar, glycogag-deficient virions displayed a more monodispersed profile and a higher MFI of GFP expression compared to wildtype (**Figure 14C**).

A)

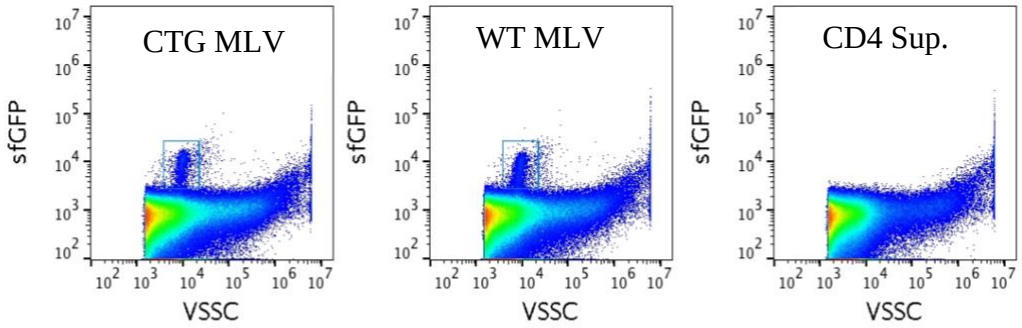

B)

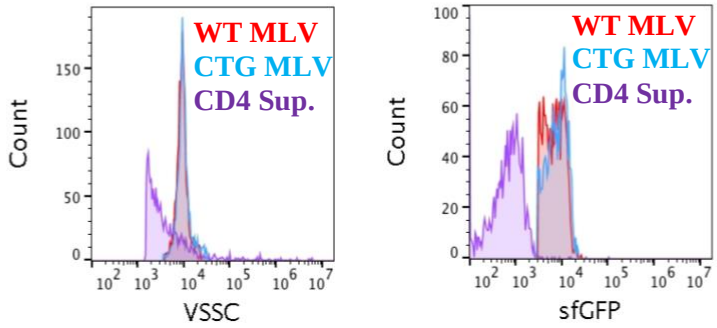

C)

	VSSC Intensity (MFI)	GFP Intensity (MFI)
WT MLV	9457	8493
CTG MLV	10387	7506
CD4 T cell Sup.	61696	848

Figure 14: Scatter and fluorescence quantification between wildtype and glycoGag deficient MLV virions released from primary murine CD4+ T cells.
A) Wild type MLV (WT) virions present a similar discrete scatter plot profile to glycogag deficient (CTG) MLV virions. Gated particles express similar **B)** side scatter and GFP intensity as overlaid histograms and **C)** mean fluorescent intensity (MFI) values. Supernatant was collected after 48 hours from infected and non-infected CD4+ T cells and diluted 1:100, and was subsequently directly run by flow virometry.

Subsequently, viral supernatant was stained against the previously described antibodies used for the CD4+ T cell phenotypic analysis. Virions released from murine primary CD4+ T cells also follow a non-Gaussian distribution and were tested with the Mann-Whitney nonparametric unpaired test as previously described. The results from the viral staining are summarized as mean and median fluorescence intensity bar graph and overlaid histogram plots of PE fluorescence as illustrated in **Figure 15**. As previously shown, presence and abundance of antigens were determined utilizing the antibody and media sample as a negative control. From the 14 viral stainings performed on the MLV variants, the highly abundant mouse T cell and lipid raft marker Thy1.2 ($n=2078$, $p<0.0001$), T cell marker CD3 ($n=2098$, $p<0.0011$) and the integrin marker CD29 ($n=1855$, $p<0.0001$) were observed as compared to the negative control. Interestingly, as observed on EL4 virions, the T cell marker CD45 ($n=1820$, $p<0.0001$) was present on both wildtype MLV virions and glycogag deficient particles. The tetraspanin markers CD81 ($n=1789$, $p<0.0001$), CD63 ($n=1679$, $p<0.0001$) and CD9 ($n=12761$, $p<0.0001$) were observed on both MLV variants as compared to the negative control. Lastly, both wild type virions ($n=5326$, $p<0.0001$) and glycogag deficient MLV ($n=1761$, $p<0.0001$) displayed the presence of the lipid raft marker CD55 as compared to the control. Other cellular markers that were present on the cell surface were not detected on the viral envelope of MLV. Furthermore, as observed for supernatant collected from the uninfected NIH 3T3 and EL4 cells, we detected discrete EV populations on scatter plots positive for the previously observed EV marker CD45 MFI=760 ($n=125511$, $p<0.0001$), Thy1.2 MFI =1013 ($n=105038$, $p<0.0001$), LFA-1 MFI=675 ($n=113867$, $p<0.0001$), CD81 MFI=607 ($n=153271$, $p<0.0001$) and CD9 MFI=473 ($n=113867$, $p<0.0001$). Moreover, using the statistical z-score approach, we calculated the 95% confidence interval for the percentage of viruses that are positive for the respective host derived cellular antigen analyzed. As a result, we conclude that

host derived CD81 and CD63 present on the viral envelope on 16.3%±1.5% (n=7709) and 4.2%± 0.8% (n=2499) of wild type virions whereas only 11.1% ± 1.5% (n=1789) and 4.9%± 1.0% (n=1679) of glycogag deficient virions carried these antigens, respectively. Contrary to the previously observed virions released from NIH 3T3 and EL4 cells, both wild type and glycogag deficient viruses showed presence, although minimal, of the tetraspanin marker CD9 on 1.72%± 0.6% (n=1932) and 2.7%± 0.7% (n=2153). Furthermore, flow virometry revealed that host derived Thy1.2 and LFA-1 were present on the viral envelope, on 21.1%±1.6% (n=7709) and 4.1%± 0.8% (n=2188) of wild type virions whereas only 6.5%±1.1% (n=2078) and 4.4%± 1.0% (n=1744) of glycogag deficient virions carried these antigens, respectively. Intriguingly, the CD45 EV marker was also present on sfGFP positive wild type and glycogag deficient MLV virions, on 15.5%±1.5% (n=2187) and 17.1%±1.7% (n=1820) of particles, respectively. Lastly, the lipid raft protein markers CD55 was observed on 3.0%±0.6% (n=7501) wild type and 2.6%±0.7% (n=1761) of glycogag deficient MLV virions. The latter showed a more monodispersed antigenic variability profile compared to its wild type counterpart. However, other cellular markers that were present on the cell surface were not detected. To assess for viral heterogeneity and differential antigen incorporation, viral count was kept identical across all stainings. Analysis of Thy1.2 expression reveals a slighter greater heterogenous distribution of this antigen on wild-type MLV, however both variants displayed one more dominant monodisperse population and a separate discrete population expressing an increased PE signal (**Figure 15A**). This distribution of signal intensity was reflected in both wildtype and glycogag deficient MLV stained for CD45. For other host derived cellular antigens, both MLV variants displayed a similar form which showed one monodisperse population. Next, we quantified mean and median PE fluorescence intensity signal to assess distribution of antigen expression between wild type MLV and glycogag-deficient

virions. Thus, the relative expression of cellular antigen abundance detected on wild type virions was quantified as mean and median PE intensity with the most abundant CD81 expressing 866±8 and 733, followed by Thy1.2 with 596±59 and 427, and CD45 with 566±18 and 429, respectively. Moreover, mean and median signal intensity of host derived integrin CD29 was expressed at 497±84 and 367, CD55 expressed at 485±4 and 450, while CD63 was expressed at 457±6 and 413 and CD3 was expressed with the lowest MFI of 428±6 and a median of 403. In contrast, glycogag deficient MLV particles expressed significantly lower mean and median fluorescence intensity with CD81 at 555±9 and 461 ($n=1789$, $p<0.0001$), Thy1.2 at 483±28 and 380 ($n=2078$, $p<0.0001$) and CD55 ($n=1761$, $p<0.0019$) at 452±6 and 415. Lastly, although CD29 and CD3 were expressed at a lower MFI and median fluorescence intensity at 425±7 and 372, and 423±5 and 388, respectively, there was no statistical significance between the two MLV variants. We did not calculate any significant difference between the two MLV variants for the CD45 expression, however glycogag deficient MLV had an MFI of 647±28 and a median of 441. Additionally, the tetraspanin CD9 was expressed at greater intensity than on wild type with a MFI of 527±13 and a median of 436 ($n=1932$, $p<0.0180$). Although a greater amount of glycogag particles showed presence of CD9 antigen and significant higher median fluorescent intensity, it is important to note that relative to its cellular expression, wild type MFI viral expression was approximately 1.8-fold higher than that of glycogag MLV. When we compared the MFI of the double positive virions to that of stained supernatant collected from uninfected CD4 T cells for those antigens, we observed that only wild type virions expressed a significantly greater relative intensity value for CD81 ($n=4147$, $p<0.0001$), CD55 ($n=5326$, $p<0.0003$), CD9 ($n=4840$, $p<0.0001$), and GFP ($n=2127$, $p<0.0001$) only. Whereas the expression of CD81 ($n=1789$, $p<0.0001$), CD9 ($n=8667$, $p<0.0001$) and GFP ($n=1989$, $p<0.0001$) alone on glycogag deficient virions displayed significant difference

to that of uninfected stained supernatant. Intriguingly, supernatant collected from uninfected CD4+ T cells had significantly greater PE signal than that observed of either MLV variant for Thy1.2 ($n=105008$, $p<0.0007$), CD45 ($n=125511$, $p<0.0001$) and LFA-1 ($n=113867$, $p<0.0001$). When we stained either wildtype or glycogag deficient MLV with an isotype, and compared it to control or stained supernatant, we did not observe any statistical significance between samples.

A)

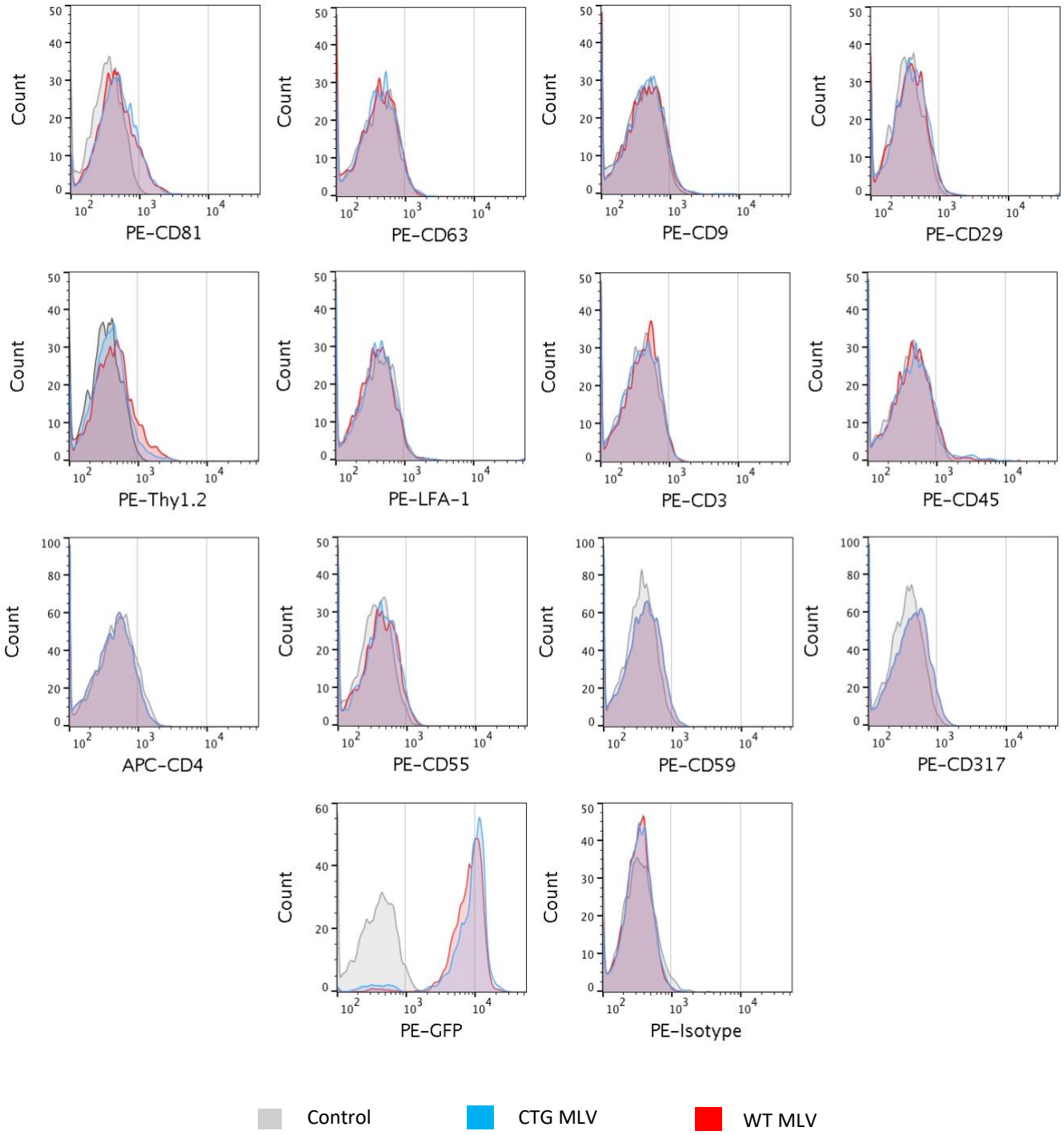
Count
PE-CD81
PE-CD63
PE-CD9
PE-CD29
PE-Thy1.2
PE-LFA-1
PE-CD3
PE-CD45
APC-CD4
PE-CD55
PE-CD59
PE-CD317
PE-GFP
PE-Isotype
Control
CTG MLV
WT MLV

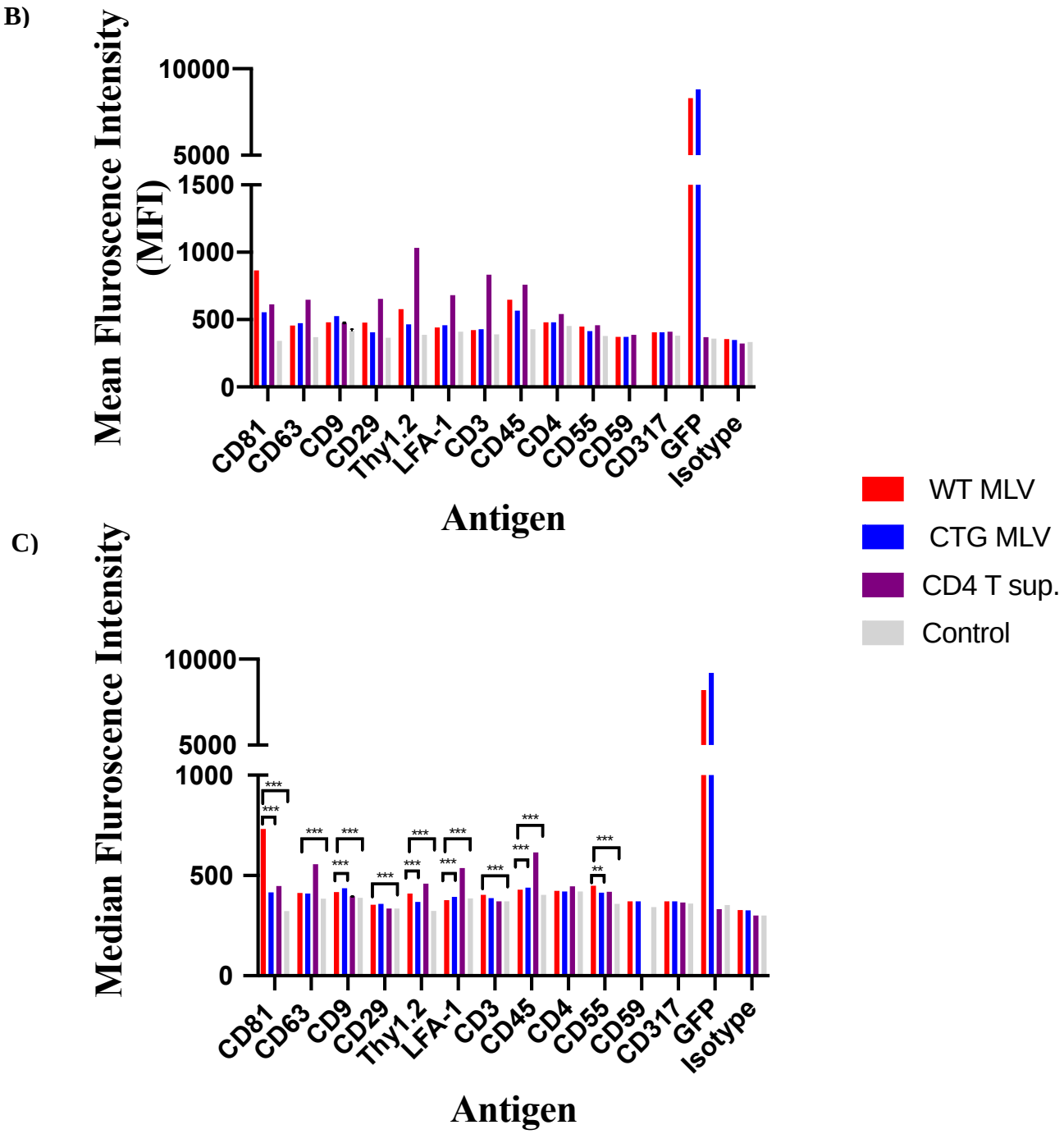

Figure 15: Surface antigen phenotypic analysis of virions released from primary murine CD4+ T cells.

Surface antigen analysis of uninfected and uninfected primary murine total CD4+ T cells by flow virometry with a 14-panel antibody screen. A) Histogram analysis of antigen expression distribution of overlaid MLV variants and antibody and media control. B) Mean and median C) fluorescence intensity analysis of cellular surface antigens of CD4+ T cells infected with wild type (WT) and glycogag deficient (CTG), uninfected CD4+ T cells, and antibody and media control. Data normality of samples was calculated by D'Agustiona and Person test and validated by Kolomogorov-Smirnov test. Statistical significance was calculated by a nonparametric Mann-Whitney test as distribution of sample data was not of Gaussian form. ***, P value < 0.0001, **, P value < 0.001.

3.7 Analysis of Endogenous Retroviruses in murine primary cells and lymphocyte cell line.

Although humans' endogenous retroviruses (ERV) are mostly inactive, ERVs still play an active role in mice to this day. Since approximately 10% of mouse genome's account for ERVs, this remains an important topic of research. Majority of ERVs share close resemble to gammaretrovirus' homology, in particular the MLV family (13). During our phenotypic analysis of host derived antigens on the viral envelope of MLV, we observed a discrete and dense population in the supernatant collected from both uninfected and infected primary murine cells by FVM. In particular, this discrete concentrated population was resolved on density scatter plots and histograms by VSSC intensity from uninfected and infected primary splenocytes and isolated CD4+ T cells as shown in the graphical illustrations **Figure 16 and 18**. ERVs have not been documented on NIH 3T3 fibroblast cells, and as such supernatant collected from this cell line was used as a negative control for gating in our flow virometry analysis (**Figure 21**).

Consequently, we demonstrated in **Figure 16** a discrete population of ERVs that is resolved by VSSC in supernatant collected from non-infected and infected primary splenocytes. Splenocytes were activated with either a T cell stimulant, lipopolysaccharide (LPS), or with a CD3/CD28 antibodies as discussed in detail in the methods. We show that activation of murine cells leads to the release of ERVs and this was further enhanced with infection with an exogenous MLV virus. Thus, we collected supernatant from either a 24-hour and 48-hour incubation period post plating from uninfected splenocytes and infected splenocytes. We detected a discrete population in infected cells at a 24-hour period that was resolved by VSSC. This formation was observed on both a density scatter plot and further reflected on the histogram plot (purple histogram) in which a discrete peak was detected between 6000-10000 VSSC intensity interval. Since ERVs closely

resemble MLV virus in composition, we superimposed the ERV and background population gated in purple to the whole sample population containing the MLVsfGFP discrete population and background (blue histogram) (**Figure 16C**). For the purpose of this analysis, the viral count between the gated sample and the whole population sample was kept identical to compare the exogenous and endogenous viral population. Thus, we illustrated that exogenous MLVsfGFP peak formation is detected within the 6000 -10000 VSSC intensity interval and that the ERV peak occurs immediately below it within this interval, however at a much lower count. In particular, the mean and mode of the exogenous MLVsfGFP of VSSC intensity is expressed at of 7955 ± 8 and 8170, whereas that of endogenous ERV was at 6739 ± 11 and 6127, respectively. Next, we analyzed supernatant from infected cells at a 48-hour time point. We observed this peak formation on the histogram plot at the previously indicated interval, however with an increased amplitude that is comparable to that of the exogenous MLVsfGFP virus. Consequently, when the count was kept identical for the gated population between the two time points, we calculated a 9.8% increase of ERV particles relative to 24-hour time point. This was further confirmed by the density plot analysis, which shows a discrete dense ERV sub-population in the background (purple gate) (**Figure 16B**). Analysis of supernatant obtained at 48 hours from noninfected splenocytes does not show a discrete population on either the density plot or the histogram plot. Interestingly, the histogram analysis illustrates a different slope of regression at the interval of interest at which point a kink is observed that drops and this pattern is not reflected in the supernatant of the negative control (NIH 3T3 supernatant) observed in **Figure 21C**. This band could suggest a formation of a peak, however the number of ERV particles is not sufficient enough to generate a discrete form. This could be a result of greater number of events from the background noise attributed to EV and other components in the media compared to the diminutive number of events that make up ERV

population. As discussed previously, a small population of interest could be obscured by the background noise without a selection marker, whilst tagging the population of interest with a GFP fluorescent antibody will allow the population to be resolved by both side scatter and GFP intensity from background.

Consequently, to further investigate the possible presence of ERVs in the supernatant, we conducted an alternative approach to flow virometry by western blot analysis and blotted for the viral capsid p30 protein (**Figure 17)**. Since, ERV closely resemble MLV in composition, the capsid viral protein of molecular mass of 30 kDa is conserved between endogenous and exogenous gammaretroviruses. Thus, we blotted the cell lysate, supernatant and ultra-centrifuged supernatant collected from untreated and activated splenocytes at a 48-hour time point with a monoclonal p30 capsid antibody. Our results show that cell lysate of the activated splenocytes show presence of the immature form Pr65 of the gag capsid polyprotein, whereas both the untreated and activated supernatant and supernatant concentrated by ultracentrifugation exhibited the immature form of capsid protein (~65 kDa), yet only a faint a band for the mature of form of p30 (~30 kDa) was observed in the supernatant of activated splenocytes. As reported by Marin *et al.*, the polyclonal antibody has been shown to detect the immature form of the gag polyprotein by western blot analysis(103). Thus, these findings support our observation of the peak formation in the uninfected splenocytes and allude to the presence of the ERV population in the 6000 -10000 VSSC intensity interval. Although this population cannot be fully resolved due to its lower frequency in comparison to the overall background noise.

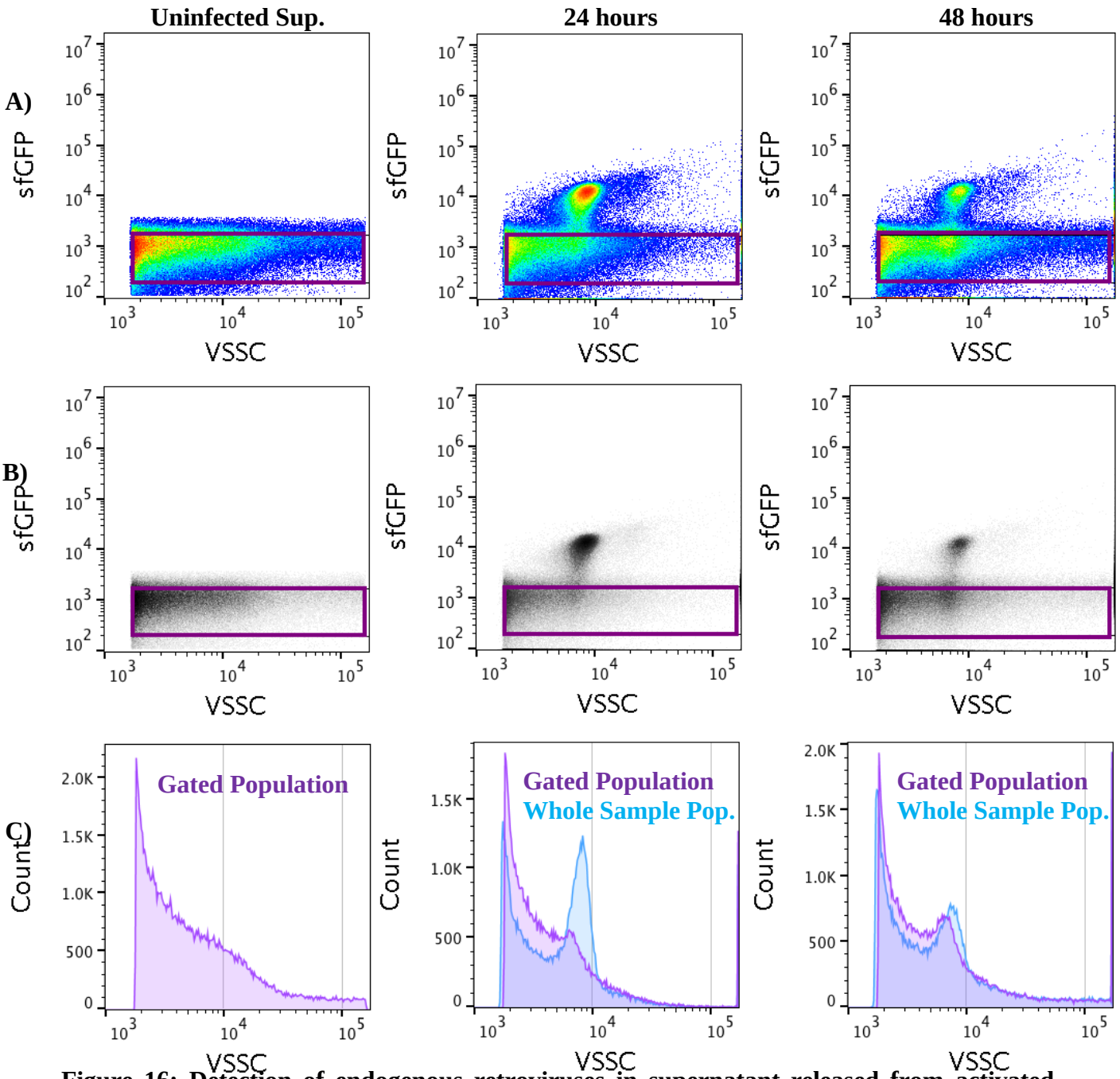

Figure 16: Detection of endogenous retroviruses in supernatant released from activated murine primary splenocytes and splenocytes infected with exogenous MLV virus by flow virometry.

A) Pseudocolor and **B)** density scatter plots of supernatant collected from uninfected and infected primary murine splenocytes at 24-hour and 48-hour time point. Uninfected supernatant collected at 48-hour time point is show only. C) Histogram analysis of overlaid gated population (purple gates) of background noise and ERVs (purple histogram) and the whole sample population containing the MLVsfGFP (blue histogram).

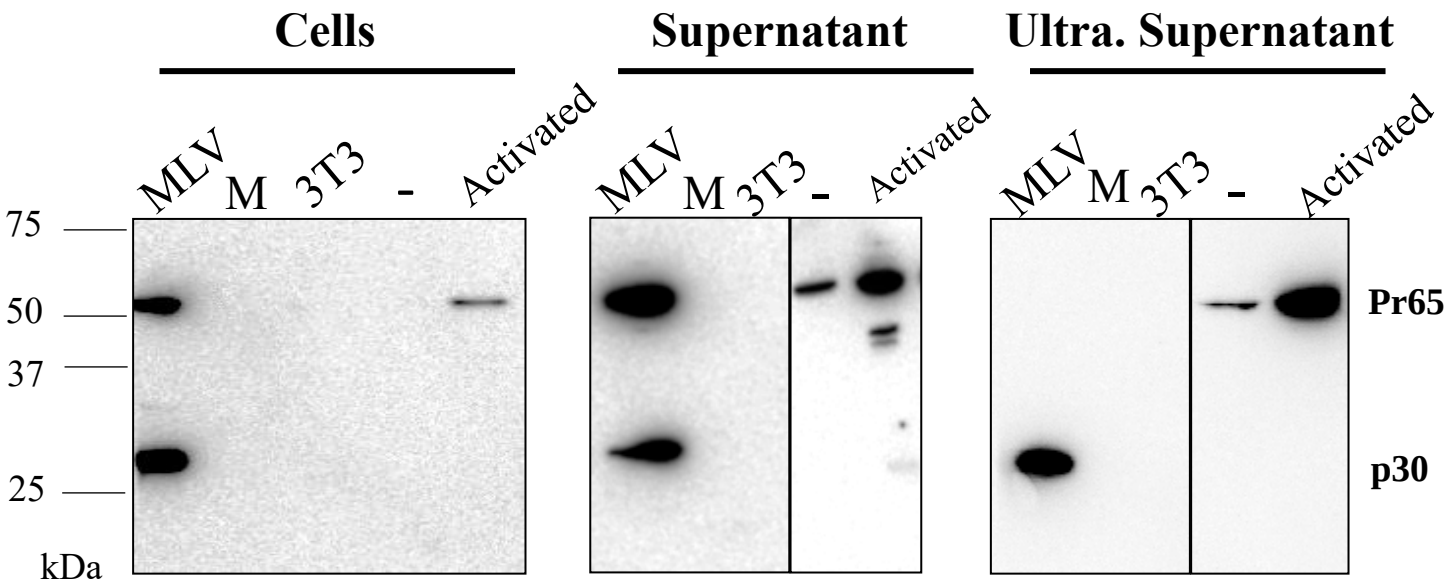

Figure 17: Detection endogenous retroviruses in supernatant released from murine primary splenocytes.

Detection of the capsid protein precursor Pr65 by Western Blot in murine primary splenocytes from C57/BL6 mouse in untreated (-) and activated cell lysate, supernatant and ultra-centrifuged (ultra.) supernatant. Positive control of NIH 3T3 infected with MLVsfGFP exhibit both the p30 capsid protein and its precursor Pr65, whilst NIH 3T3 cells were used as negative control.

Next, we sought out to analyze the release of ERVs from a specialized subset of immune cells, and for this purpose we isolated and activated total CD4+ T cells. In our observations, we detected a discrete ERV population at the previously noticed signal range of 6000 – 10000 VSSC intensity on both the density and histogram plots in supernatant released from uninfected and infected cells as illustrated in **Figure 18**. In particular, we observed a formation of a peak in the infected cell supernatant at 24-hour point, which was further increased by 40.1% at the 48-hour interval. At the 24-hour point, the superimposed whole sample population containing the MLVsfGFP virus (blue histogram) and the gated background and ERV (purple histogram) sample showed a similar profile pattern which was reflected at the 48h-hour time point (**Figure 18C**). Although, in comparison to the ERV population observed in infected splenocytes at this time point, the peak was not as discretely detected, however the apparent dip just prior to the interval of interest, change in regression slope and the drop ensuing do not follow the pattern of the negative control as illustrated in **Figure 21C**. Thus, these are clear indicators that the band appearance and peak formation reflects the development of the ERVs in smaller quantity compared to the number of particles that constitute the background. However, this ERV population is readily resolved at the 48-hour time point, where the ERV peak was directly superimposed on the MLVsfGFP apex (**Figure 17C)**. Intriguingly, we detected the presence of a discreate population of ERV in a supernatant of activated uninfected murine primary CD4+ T cells collected at the 48-hour time point, which was not as readily observed in supernatant released from uninfected whole splenocytes. Although this population is not as clearly detected in either of the scatter plots due to high presence of other particles in the background, it is readily resolved in the histogram plot by the apparent peak at the 6000-10000 VSSC intensity interval **Figure 18C**. Furthermore, when we compare the ERV population of interest from uninfected CD4+ T cells to those released from cells infected with

exogenous MLVsfGFP, we observed that these populations have different side scatter signal, in particular when the particle count is identical, the former has the mode and mean expressed at 8170 and 7523±16 VSSC intensity, whereas the latter is significantly lower at 6466 and 7344±15 (n=17057, $p<0.0001$), respectively **Figure 18D**. Furthermore, we report that staining with a fluorophore conjugated antibody affects the side scatter signal of the ERV population and aids in further defining the observed peak of this sub-population as shown in **Figure 18E**. For this purpose, we analyzed both stained and unstained supernatant collected from uninfected and infected CD4+ T cells. Thus, we observe that the staining with a fluorescently labelled PE antibody modulates the scatter intensity of the ERV population of interest **Figure 18E**. This effect was additionally noted when supernatant was stained with an APC conjugated antibody **Figure 18E**. As such, we infer that labelling with an antibody either leads to an increase in the apparent size of ERV or modulation of its refractive properties when labelled with fluorescent antibody consequently enhancing its signal by VSSC intensity.

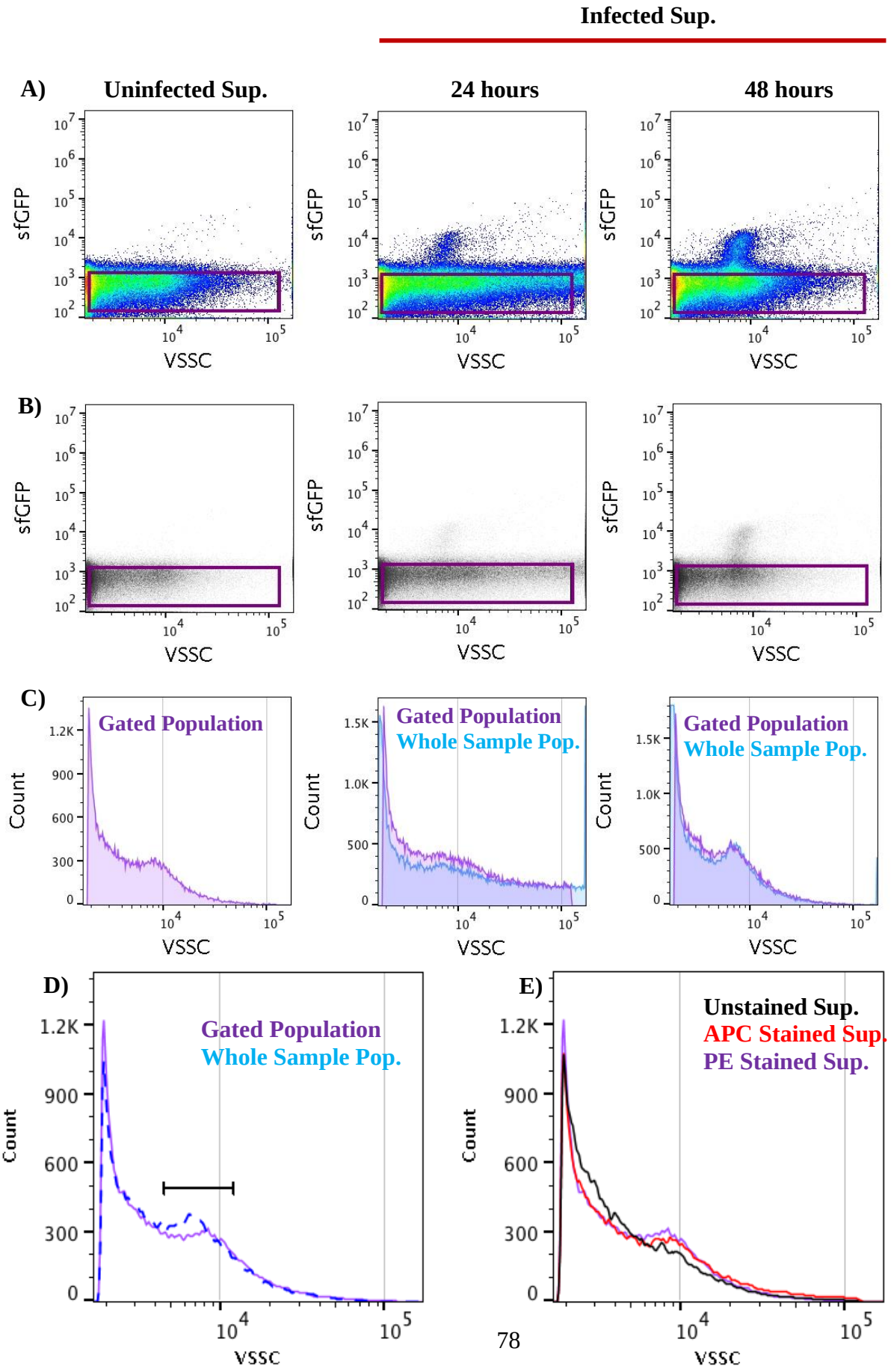
Infected Sup.
A)
Uninfected Sup.
24 hours
48 hours
sfGFP
VSSC
B)
C)
Gated Population
Gated Population
Whole Sample Pop.
Count
D)
Gated Population
Whole Sample Pop.
E)
Unstained Sup.
APC Stained Sup.
PE Stained Sup.

Figure 18: Detection of endogenous retroviruses in supernatant released from activated murine primary total CD4+ T cells and cells infected with exogenous MLV virus by flow virometry.

A) Pseudocolor and **B)** density scatter plots of supernatant collected from uninfected and infected primary murine CD4+ T cells at 24-hour and 48-hour time point. Uninfected supernatant collected at 48-hour time point is show only. **C)** Histogram analysis of gated population of background noise and ERVs (purple gates) and overlaid gated population and whole sample population containing the MLVsfGFP. **C)** Histogram analysis of gated population of background noise and ERVs (purple gates) activated CD4+ T cells and infected CD4+ T cells. **D)** Comparison of VSSC intensity signal between ERVs released by uninfected cells and infected cells. **E)** Modulation of VSSC intensity of ERV sub-population as a result of labelling with conjugated fluorescent antibodies. Supernatant collected from uninfected cells shows a different VSSC signal when unstained or labelled with either PE conjugated antibody or APC conjugated antibody.

Next, we sought to analyze the ERV released from EL4 uninfected and chronic cell lines. For this purpose, we followed a similar experimental set up used for the analysis of primary murine cells, however these cells were not activated with CD3/ CD28 initially. Interestingly, we did not observe any indication of ERV population in noninfected nor in the infected cells as shown in **Figure 19**. Upon analysis of the density scatter plot or histogram overlaid with the whole sample population containing the MLVsfGFP, we observed the peak of the exogenous viral population however the ERV population was not detected (**Figure 19B-D**). As an alternative to flow virometry, we analyzed the cell lysate, supernatant and ultra-centrifuged supernatant collected at 48 hours from uninfected cells by western blot stained with a polyclonal anti-p30 capsid antibody. Intriguingly, our results exhibit presence of both the unprocessed and processed form of the Gag polyprotein in cell lysates and ultra-centrifuged supernatant of uninfected EL4 cells as shown in **Figure 19**. The absence of either form of gag protein in the cell supernatant suggests that the ERVs were released at a low frequency by the EL4 cells, as the viral capsid is only detected in the concentrated ultra-centrifuged supernatant and cell lysate where it is produced in the cytoplasm.

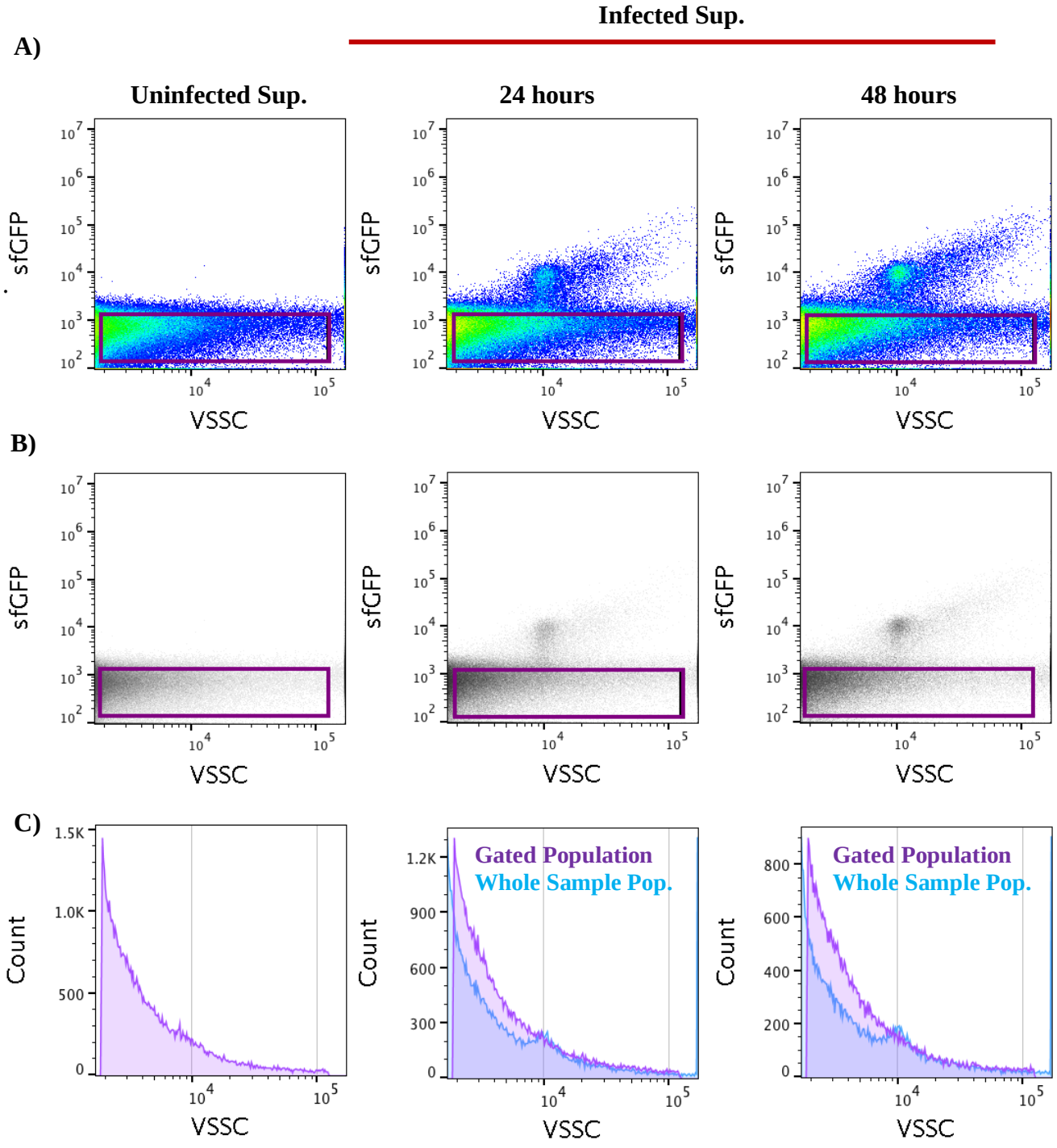

Figure 19: Evaluation of endogenous retroviruses in supernatant released from untreated EL4 T lymphocytes and infected with exogenous MLV virus by flow virometry.
A) Pseudocolor and B) density scatter plots of supernatant collected from uninfected and infected EL4 T at 24-hour and 48-hour time point. Uninfected supernatant collected at 48-hour time point is show only. C) Histogram analysis of overlaid gated population (purple gate) of background noise and ERVs (purple histogram) and the whole sample population containing the MLVsfGFP (blue histogram)

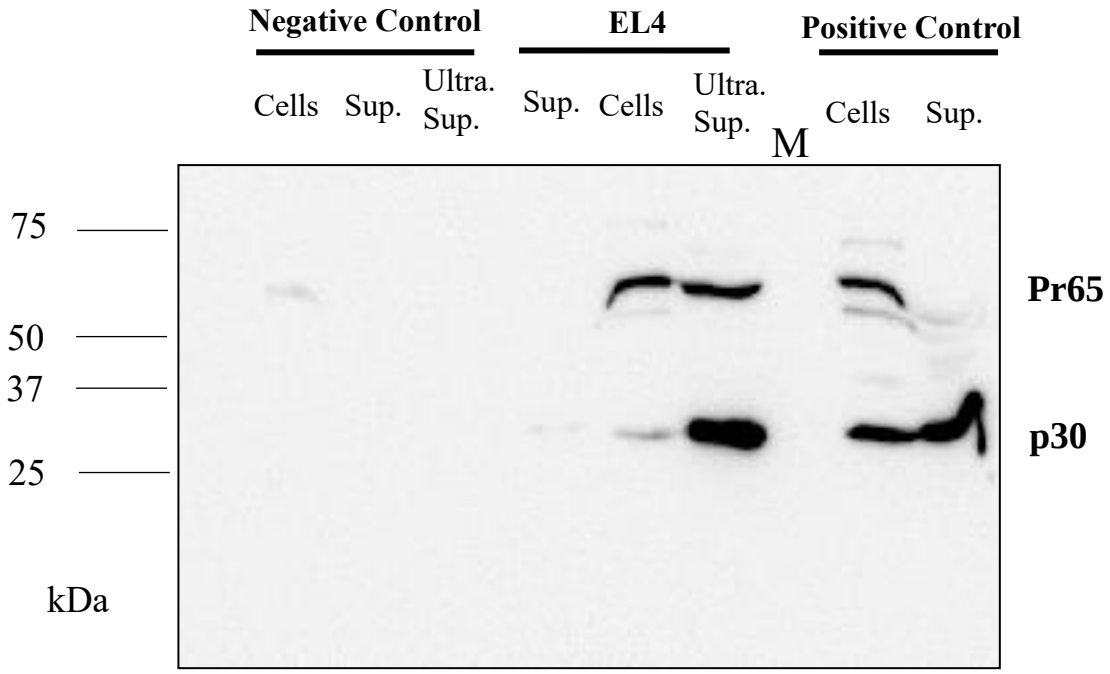

Figure 20: Detection of ERVs in murine EL4 lymphocytes.
Detection of the capsid protein p30 and its precursor Pr65 by Western Blot in EL4 lymphocytes in cell lysate, supernatant (sup.) and ultra-centrifuged (ultra.) supernatant. Positive control of NIH 3T3 infected with MLVsfGFP exhibit both the p30 capsid protein and its precursor Pr65, whilst NIH 3T3 cells were used as negative control.

Lastly, as a negative control we used supernatant that was collected at 48-hour time point from chronic NIH 3T3 cells. For the purposes of flow virometry analysis of ERV detection of primary murine cells and EL4 cell line, we set the control of the purple gate which included the ERV population and background relative to the supernatant collected from NIH 3T3 producer cells as observed in **Figure 21**.

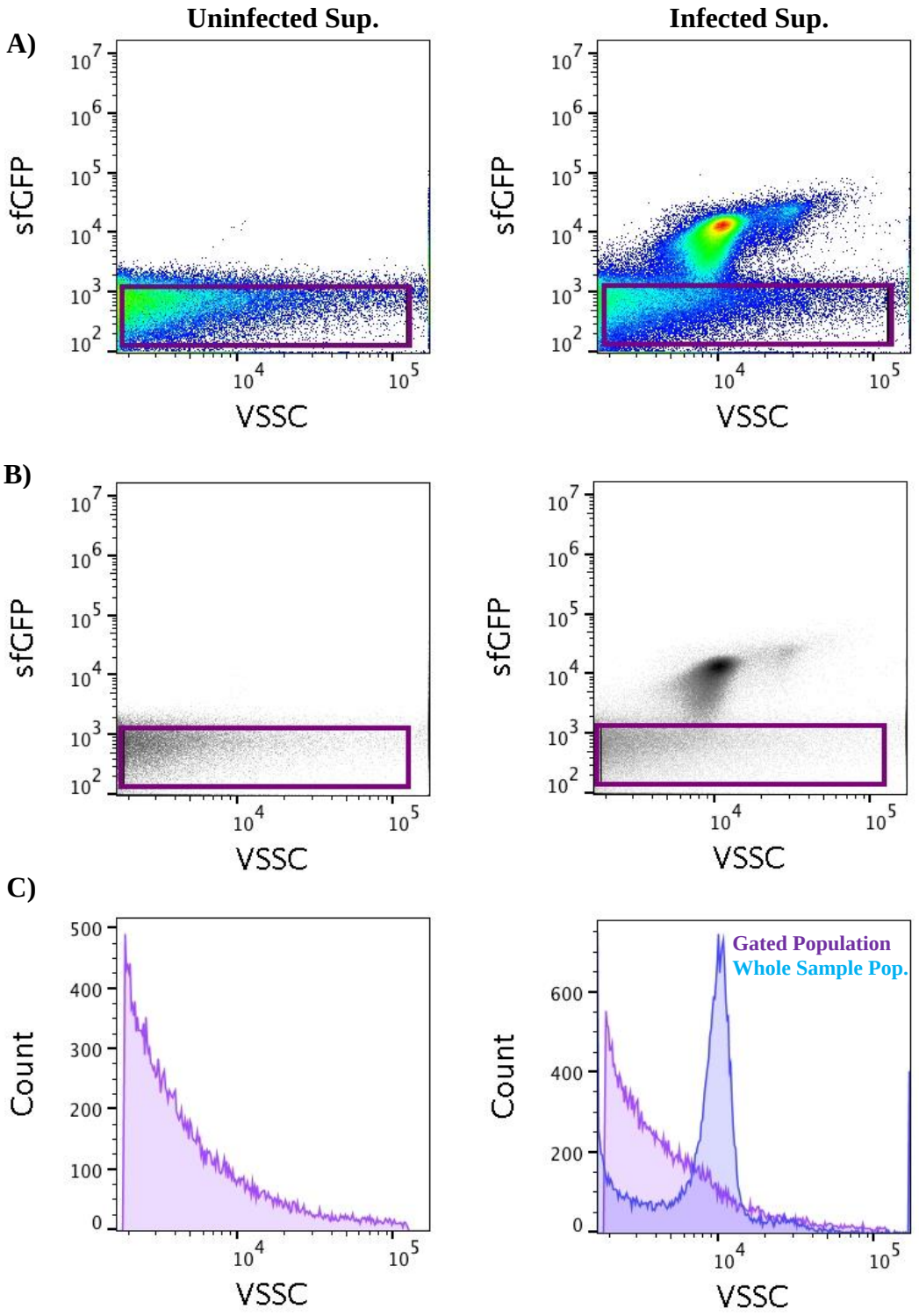

Figure 21: Evaluation of NIH 3T3 fibroblast as negative control for detection endogenous retroviruses release.

A) Pseudocolor and B) density scatter plots of supernatant collected from uninfected and infected NIH 3T3 fibroblasts at 48-hour time point. C) Histogram analysis of gated population (purple gates) of background noise and ERVs (purple histogram) and overlaid gated population and whole sample population containing the MLVsfGFP (blue histogram).

As such, the gate was set to ensure that the exogenous MLVsfGFP virus was not included as we observed in **Figure 21**. For this discrimination, we carefully analyzed the density scatter plot and histogram plot to ensure that MLVsfGFP viral particles were not detected in the previously observed 6000-10000 VSSC intensity range. Consequently, ERV population was not detected in supernatant collected from either untreated or infected NIH 3T3 cells (purple histogram), however the exogenous MLVsfGFP population was readily resolved by side scatter as seen in **Figure 20C**. This was further confirmed in western blot analysis which did not show presence of either the processed not unprocessed form the Gag polyprotein **Figure 17 and 20**.

Consequently, we report for the first time the possibility of ERV detection and quantification by flow virometry as shown in **Figure 16-18**. Here, we show the observation of a monodisperse concentrated sub-population of ERVs that is resolved by VSSC intensity. ERV release was detected in supernatant collected from activated uninfected and infected with exogenous MLV virus whole splenocytes and isolated CD4+ T cells. These observations were further validated by the presence of the immature form of the viral capsid protein Pr65 by western blot analysis. Taken together, our observations demonstrate that flow virometry is a reliable tool to directly identify unique sub-populations within a sample, such as the detection of a low frequency ERV population, for further analysis of its properties.

4 Discussion

In this dissertation, I aimed to detect the presence and abundance of host-derived antigens on the surface of the Moloney strain of murine leukemia virus (MLV) by flow virometry (FVM). This has implications in deciphering the factors which influence antigen uptake during viral egress and provide critical information on the infected cell's phenotype. We uncovered the intriguing possibility that glycosylated gag (glycogag) protein plays a role in increasing the incorporation of host-derived antigens during viral release and assembly. These findings highlight the need for further research into the intricate complexities of this enigmatic accessory protein's role at the last step of MLV viral replication cycle. Moreover, during our observations, we reveal the capability of FVM to detect endogenous retroviruses (ERV). Consequently, we detected and quantified ERV release in both untreated and activated primary murine cells.

RNA viruses are genetically diverse; the extent of this diversity was strikingly shown in the study by Keele *et al.* that illustrates that only one or several HIV viral particles among billions in the seminal fluid are sexually transmitted and lead to an infection(104). This suggests potential unique differences at the viral envelope composition level, which is responsible for productive infections (104). During viral assembly and egress, retroviruses incorporate hundreds of host cell proteins within their capsid and/or membrane(37). Since most analytical approaches described earlier measure global protein content, only a few approaches can investigate the protein distribution on the surface of individual viruses. This analysis is further complicated by contamination with extracellular vesicles (EVs), which have been shown to incorporate viral components such as the genomic content or viral proteins(48, 57). In addition to EV contamination, viral-like particles (VLPs) are a possible confounding factor, which at this point have no definite distinguishing features to EVs or viral particles (48). Due to the overlap in morphology and

biochemical properties between EVs, VLPs and retroviruses, selective resolution of these particles is challenging. Furthermore, most analytical methodologies lack the necessary caliber to effectively analyze pure viral preparations, and as such, the onus falls on the researcher to achieve this robust discrimination.

Despite the plethora of studies conducted on MLV and other retroviruses, there remain important gaps in knowledge. Such as the mechanisms that govern host imbedded cellular protein incorporation on the viral envelope during viral release and whether viral factors play an active role in this determination. Further research is required to assess whether there is conservation, selective upregulation and uptake of specific host antigens. However, most current viral analysis techniques fail to highlight the extent of viral antigenic heterogeneity and lack the capability to provide direct information on individual viral particles in evaluating surface protein composition. Despite the fact that diversity in the antigenic constitution has profound effects on downstream functions in the viral replication cycle, such as such as infectivity as shown by Gaudin *et al*. (50). Characterizing the proteins found on the viral envelope and deciphering the intricacies behind retroviral egress and host protein incorporation are crucial to advancing our knowledge of viral pathogenesis, identifying therapeutic targets and ultimately vaccine development.

In this research, we set out to detect and quantify the abundance of host-derived cellular antigens on the surface of the viral envelope of MLV. We illustrated that wild type MLV virions produced by the NIH 3T3 fibroblasts show presence of the highly expressed cellular tetraspanin markers CD81 and CD63 (**Figure 8**). To investigate whether there was a selective uptake of a specific antigen, we evaluated the abundance of viral surface antigen relative to cellular surface antigens' presence. Despite that approximately 70 % of virions stained positive for CD81 compared to 30 % stained for CD63, the MFI of the former particles was lower than that of the

latter. This could result from higher fluorescent output signal produced by the CD63 antibody compared to the CD81 antibody, which was observed when media and antibody alone were tested. Nevertheless, we observe that the ratio of CD81 positive virions relative to the cellular expression is approximately 7:10, while that of CD63 is roughly 3:10. This suggests that CD81 is likely being selectively incorporated 2.5 times as much as CD63. Upon evaluating the antigenic distribution between these host-derived proteins on the viral envelope, we note a more heterogeneous expression of CD63 compared to the more monodisperse distribution of CD81, as illustrated in **Figure 8A**. Several studies demonstrated the incorporation of tetraspanin proteins within the HIV-1 envelope, revealing their functional role in entry and possible activation of recently infected cells(105–108).

The presence of these cellular proteins also serves as a unique clue that provides insight into the virus's assembly pathway during release. Retroviruses egress primarily at the cell surface; however, they have been noted to use the late endosome pathway. HIV-1 virions released from monocytes are shown to use this egress pathway as well, consequently incorporating tetraspanins and other late endosomal markers (28, 32, 33, 37, 106). This suggests that some of the viruses observed were potentially released through the late endosomal pathway. This was further corroborated by the observations that exosomes are released using multivesicular bodies in both haematic and non- haematic cell types(109).

Next, we assessed the presence and the degree to which host-derived proteins were expressed on the surface of wild type MLV shed by EL4 cells. We observed a high expression of the highly abundant mouse T cell and lipid raft marker Thy1.2, T cell marker CD3, and the adhesion marker LFA-1 (**Figure 12)**. Intriguingly, we also observed the well-known EV marker CD45 that has not been reported on HIV-1 virions, despite its abundance covering as much as 10-25% of the total

surface(19, 22, 31). Taken together, the observed presence of CD45 on the viral enveloped of MLV, yet its selective exclusion in HIV-1 viral envelope suggests that this exclusion mechanism may not be conserved between these retroviruses. Alternatively, HIV-1 virions released from infected T cells have been shown to egress through lipid raft domains, which are highly concentrated with glycosylphosphatidylinositol (GPI)-linked proteins(5,22,111). Interestingly, other transmembrane proteins such as CD45 do not show a preference for these domains(5, 22, 110). All EL4 cells were positive for CD45, Thy1.2, and LFA-1 markers, with CD45 being the most abundant. However, viral antigen expression was highest for Thy1.2, followed by CD45 and LFA-1, respectively. The high abundance of Thy1.2 expression on the virions suggests the egress at the lipid raft junctions, where Thy1.2 is known to partition to preferentially(5, 111, 112). However, Thy1.2 was also the second most abundantly expressed surface on marker on EL4 cells. Yet, these findings are consistent with the notion observed by Fan *et al.*, who demonstrated that wildtype MLV glycogag protein facilitates release of virions through lipid rafts. They hypothesize this release to be more efficient than through other membrane structures or regions (92, 113). Interestingly, Thy1.2 has also been implicated in mouse T lymphocyte activation, where it was observed to partially substitute for TCR activation along with CD28 co-stimulation(111). Given the mitotic requirement of MLV to infect actively dividing cells, the selective upregulation of Thy1.2 could result from an evolutionary pressure forced upon MLV for the priming of potential target cell reservoir(114).

Lastly, analysis of the virions released from EL4 cells by flow virometry showed one monodispersed population and one heterogeneous population that differed in violet side scatter (VSSC) and sfGFP intensity as observed in **Figure 11**. Given these particles' low frequency and highly dispersed profile, these events could represent EVs that have incorporated the Env-sfGFP

on their envelope(57, 58). However, our lab has previously revealed that the amount of EVs with incorporated Env-sfGFP is negligible (1%) compared to the overall MLVsfGFP count in NIH 3T3 cells by both transfection and transduction assays (58, 65). Since MLV particles are shown to be consistent in size by several different methods, VSSC intensity could be influenced by either: the refractive index (RI), protein or genomic composition of the particle, and or lipid content of the envelope(49, 65, 115, 116). As such, several different factors could be contributing to the highly dispersed distribution of these particles.

Next, we assessed the presence and the degree of expression of host-derived proteins on virions released from murine primary CD4+ T cells. We detected the expression of CD45, Thy1.2, LFA-1, and the tetraspanin markers CD81, CD63, and CD9, as illustrated in **Figure 15**. All cells were positive for CD45, Thy1.2, LFA-1, and CD29 markers, with CD45 being the most abundant. However, Thy1.2 displayed the highest viral antigen expression, followed by CD45 and LFA-1. All of the CD4+ T cells labeled for Thy1.2, CD45, and LFA-1; however, not all cells stained for CD81 and CD63. Nevertheless, we still observe a preferential uptake of these tetraspanin markers on the viral envelope **(Figure 13)**. In comparison, the ratio of positive virions relative to the cellular expression of these tetraspanins is lower than the ratio observed in virions released from NIH 3T3 cells. Thus, this attests to the notion that the level of cellular expression does not predict the relative host-derived protein abundance on the viral envelope. As a result of our experimental setup, we performed single stainings on the viral particles with a PE fluorescently labeled antibody. However, next experiments should include co-staining of several lipid rafts markers to infer whether the uptake of these proteins is a direct result of release through lipid raft or whether there is preferential uptake of these antigens for their biologically beneficial role.

The underlying mechanism that governs cellular antigen uptake has been under much speculation. Several different theories have been postulated, including a passive or an active model of host-derived antigen incorporation. The latter suggests that viral components directly influence the uptake. For example, myristylations sites detected in the MA domain were essential for targeting Gag assembly to detergent resistant microdomains and lipid rafts, from which MLV and HIV-1 preferentially egress from (5, 21, 75, 76). In conjunction, Fan and colleagues show that glycogag of wild type MLV facilitated release through lipid rafts(92, 93). Intriguingly, Jalaguier *et al.* showed that matrix deleterious mutations had a significant impact on host-derived ICAM-1 incorporation in the HIV-1 viral envelope, elucidating the matrix protein's potential role in the host protein incorporation (80).

I hypothesize the latter, favoring a more active role of viral factors that predominantly impact the phenotypic expression on the viral envelope of MLV.

We investigated whether glycogag accessory protein modulates the incorporation of host-derived proteins during assembly and release. For this purpose, we evaluated the expression of surface antigens between the wild type MLVsfGFP and a glycogag deficient MLVsfGFP released from three different cell lines. This glycogag MLV has a CTG-CTA mutation, which abolishes the glycogag translation initiation.

In our assessment of antigen expression and abundance of wild type and glycogag deficient MLV virions released from NIH 3T3 cells, we determined that the CD81 and CD63 tetraspanin markers were significantly less expressed on glycogag deficient MLV. More specifically, we detected 2.4-fold less CD81 positive glycogag viral particles when compared to wildtype virions. While CD63 expression was decreased by 1.8-fold in the viral envelope of glycogag virions. Analysis of CD81 expression demonstrates a more monodisperse population on wild type MLV

compared to CD81 expression on glycogag-deficient MLV, alluding to more stringent incorporation of CD81 in wild type virions (**Figure 8A**). In contrast, the inverse was seen for CD63 antigen expression.

Next, we compared host-derived antigens' expression on the wild type MLV to glycogag deficient MLV released from EL4 cells. In line with our hypothesis, we observed a significant decrease in expression of both Thy1.2 and LFA-1 markers on glycogag-deficient MLV. Although there were a similar number of positively stained particles from the antigens between the two variants, we note a significant reduction in viral expression of these antigens when compared to the wild type virions. Moreover, our observations suggest that glycogag selectively increases the uptake of specific host-derived antigens that could aid its infectivity, as there was no selective increase of virion bound CD45 and CD3.

Lastly, we assessed the difference in antigen expression between both MLV variants released from primary murine CD4+ T cells. As observed of glycogag deficient virions released from prior cell types, we revealed a decrease in the number of positive particles for CD81 and Thy1.2 antigens. We note that positively stained CD81 glycogag deficient particles were 1.5 times less abundant, and the level of CD81 expression is reduced by two-fold compared to wild type. Additionally, we observed a 3.4-fold decrease in the percentage of positively stained Thy1.2 glycogag virions compared to the wild type counterpart, despite the fact that the viral expression relative to cellular antigen expression was similar. Consequently, our results provide evidence supporting our hypothesis that the viral phenotype of MLV is positively influenced by its viral factors. Our findings raise the intriguing possibility that glycogag protein is responsible for the increase in the incorporation of specific host-derived proteins incorporated during viral assembly and egress. Several studies show a clear influence of glycogag protein activity on viral assembly

and host proteins' modulation to enhance its pathogenicity(92, 93, 96, 97, 117–120). Furthermore, HIV-1 accessory proteins Nef and viral protein u (Vpu) downregulate host surface antigens such as CD4, MHC-I, tetherin, etc. Additionally, Hogue *et al.* illustrate that HIV-1 gag protein induces portioning of lipid rafts and tetraspanin enriched microdomains(121). Consequently, this raises the intriguing possibility that glycogag protein has evolved functions to positively impact the incorporation of biologically significant cellular proteins to aid in its pathogenicity.

The aim of our study was a phenotypical analysis of retroviral surface markers, the evaluation of their expression to cell phenotype, and between wild type and glycogag deficient viruses. However, important future work should probe on the underlying mechanisms of glycogag protein and its function in regulating host protein incorporation. Therefore, two questions arise from our observations 1) whether glycogag reorganizes cellular microdomains at viral assembly sites, and 2) the determinants that govern glycogag induced cellular microdomains reorganization. These findings will provide critical information in elucidating glycogag's role in selective upregulation and uptake of host incorporation proteins.

Our study reveals that the infected cell's phenotype plays an important role in determining the protein expression of the viral envelope composition. Nevertheless, we show that the abundance of antigen expression does not necessarily correlate to the viral expression. We demonstrate that FVM is an effective tool for phenotypic characterization and quantification that provides valuable information on the parental cell's phenotype. However, further experiments are required which consider a broader array of antigens in order to assess the extent of FVM's capability in deciphering the producer cell identity. Moreover, we reveal selective upregulation of specific host proteins by glycogag protein during viral assembly and release. These host proteins have been previously documented to: maintain their biological activity, improve the efficiency of adhesion during

infection, impact syncytium formation, and increase viral infectivity(19, 122). These findings are not at all surprising, given the propensity of viruses to exploit different host cell factors and their unique ability to adapt to host cell environments in their quest for assuring their survival. A plethora of evidence substantiates glycogag's important role in MLV's replication cycle, such as facilitated release through lipid rafts and enhanced pathogenesis and replication during *in vivo* infections. Aside from possible evolutionary implications, the results shown here demonstrate the presence and varying antigenic distributions of host-derived antigens on the MLV viral particles released from three different cell types.

Unexpectedly, in our observations of retroviral surface markers on MLV, we show for the first-time detection of endogenous retroviruses (ERVs) by FVM. The coevolutionary interplay between host and retroviruses provided beneficial functions to its host, such as in their defense against exogenous retroviruses as reviewed by Stoye(123). In our study, we reveal the presence of ERVs in primary murine splenocytes and isolated CD4+ T cells in activated and infected cells by FVM as illustrated in **Figures 16 and 18**. In particular, we resolved a discrete population of particles by VSSC intensity on both a density scatter plot and histogram plot. Since viral capsid assembly in retroviruses is a highly regulated process that ensures consistent stoichiometry of released viral particles, this discrete population suggests the presence of ERVs. Moreover, MLV has been shown to have a highly monodisperse profile on VSSC due to highly controlled assembly and consistent size, as shown earlier in this thesis (26, 81). We validated our findings with a western blot probing for the viral capsid protein p30 and its unprocessed form Pr65 (**Figure 17**). Thus, we detected the presence of both immature and mature capsid protein in splenocytes activated with lipopolysaccharide (LPS) by western blot. These findings fall in line with Kwon *et al.* 's evidence that revealed the production of ERVs due to stress-induced by LPS on lymphoid cells. This study

analyzed the presence of ERV release in whole murine splenocytes, T cells, and B cells isolated from C57BL/6 mice. In our findings, we show detection of ERVs by both western blot analysis and FVM in whole splenocytes and total CD4+ T cells isolated from C57BL/6 mice.

Furthermore, we took our investigations in ERV release a step further. We infected these primary murine cells with exogenous MLV virus to investigate whether this led to an increase in ERV release. We reveal that we are able to detect both the exogenous and endogenous viral populations by VSSC intensity. Intriguingly, samples collected from splenocytes and CD4 T cells at 24-hour and 48-hour intervals demonstrated a 10% and 40% increase in ERV prevalence, respectively. Although we observed defined peaks for infected samples collected at the 48-hour time point, we only note initial band formation in supernatant collected from activated splenocytes or infected CD4+ T cells at 24-hour time point. This method could further resolve this sub-population of interest by staining with fluorescently conjugated antibodies against viral constituents and with lipid dyes (65, 66).

Given the important role of immunized mice in various immunological experimental designs, flow virometry has proven herein as rapid approach that allows for identification and quantification of ERVs.

5 References:

1. Woolhouse M, Scott F, Hudson Z, Howey R, Chase-Topping M. 2012. Human viruses: Discovery and emeraence. Philos Trans R Soc B Biol Sci https://doi.org/10.1098/rstb.2011.0354.
2. Ackermann H-W, Ackermann H-W. 2011. The first phage electron micrographs. Bacteriophage https://doi.org/10.4161/bact.1.4.17280.
3. Rossman JS, Lamb RA. 2011. Influenza virus assembly and budding. Virology.
4. Noda T, Ebihara H, Muramoto Y, Fujii K, Takada A, Sagara H, Jin HK, Kida H, Feldmann H, Kawaoka Y. 2006. Assembly and budding of Ebolavirus. PLoS Pathog https://doi.org/10.1371/journal.ppat.0020099.
5. Nguyen DH, Hildreth JEK. 2000. Evidence for Budding of Human Immunodeficiency Virus Type 1 Selectively from Glycolipid-Enriched Membrane Lipid Rafts. J Virol https://doi.org/10.1128/JVI.74.7.3264-3272.2000.
6. Coffin JM, Hughes SH, Varmus HE. 1997. The Place of Retroviruses in Biology. Retroviruses.
7. 2018. WHO | Number of deaths due to HIV/AIDS. World Health Organization. Retrieved on April 4th, 2020 from: https://www.who.int/gho/hiv/epidemic_status/deaths_text/en/
8. Sharp PM, Hahn BH. 2011. Origins of HIV and the AIDS pandemic. Cold Spring Harb Perspect Med https://doi.org/10.1101/cshperspect.a006841.
9. Pierson T, McArthur J, Siliciano RF. 2002. Reservoirs for HIV-1: Mechanisms for Viral Persistence in the Presence of Antiviral Immune Responses and Antiretroviral Therapy. Annu Rev Immunol https://doi.org/10.1146/annurev.immunol.18.1.665.
10. Boeke J, Stoye J. 1997. Retrotransposons, Endogenous Retroviruses, and the Evolution of Retroelements. Retroviruses. Retrieved from http://www.ncbi.nlm.nih.gov/pubmed/21433351
11. MacLachlan NJ, Dubovi EJ, Barthold SW, Swayne DE, Winton JR. 2017. Chapter 14 – Retroviridae. Fenner's Vet Virol https://doi.org/10.1016/B978-0-12-800946-8.00014-3.
12. Stocking C, Kozak CA. 2008. Endogenous retroviruses: Murine endogenous retroviruses. Cell Mol Life Sci.
13. Weiss RA. 2013. On the concept and elucidation of endogenous retroviruses. Philos Trans R Soc B Biol Sci https://doi.org/10.1098/rstb.2012.0494.
14. Chun TW, Finzi D, Margolick J, Chadwick K, Schwartz D, Siliciano RF. 1995. In vivo fate of HIV-1-infected T cells: Quantitative analysis of the transition to stable latency. Nat Med https://doi.org/10.1038/nm1295-1284.
15. Archin NM, Sung JM, Garrido C, Soriano-Sarabia N, Margolis DM. 2014. Eradicating HIV-1 infection: Seeking to clear a persistent pathogen. Nat Rev Microbiol.
16. Chun T-W, Engel D, Berrey MM, Shea T, Corey L, Fauci AS. 1998. Early establishment of a pool of latently infected, resting CD4+ T cells during primary HIV-1 infection. Proc Natl Acad Sci https://doi.org/10.1073/pnas.95.15.8869.
17. Finzi D, Hermankova M, Pierson T, Carruth LM, Buck C, Chaisson RE, Quinn TC, Chadwick K, Margolick J, Brookmeyer R, Gallant J, Markowitz M, Ho DD, Richman DD, Siliciano RF. 1997. Identification of a reservoir for HIV-1 in patients on highly active antiretroviral therapy. Science (80-) https://doi.org/10.1126/science.278.5341.1295.
18. NOVIKOFF AB, DE THE G, BEARD D, BEARD JW. 1962. Electron microscopic study

of the ATPase activity of the BAI strain A (myeloblastosis) avian tumor virus. J Cell Biol https://doi.org/10.1083/jcb.15.3.451.
19. Orentas RJ, Hildreth JEK. 1993. Association of Host Cell Surface Adhesion Receptors and Other Membrane Proteins with HIV and SIV. AIDS Res Hum Retroviruses https://doi.org/10.1089/aid.1993.9.1157.
20. Lawn SD, Roberts BD, Griffin GE, Folks TM, Butera ST. 2000. Cellular Compartments of Human Immunodeficiency Virus Type 1 Replication In Vivo: Determination by Presence of Virion-Associated Host Proteins and Impact of Opportunistic Infection. J Virol https://doi.org/10.1128/jvi.74.1.139-145.2000.
21. Graham DRM, Chertova E, Hilburn JM, Arthur LO, Hildreth JEK. 2003. Cholesterol Depletion of Human Immunodeficiency Virus Type 1 and Simian Immunodeficiency Virus with -Cyclodextrin Inactivates and Permeabilizes the Virions: Evidence for Virion-Associated Lipid Rafts. J Virol https://doi.org/10.1128/jvi.77.15.8237-8248.2003.
22. Esser MT, Graham DR, Coren L V., Trubey CM, Bess JW, Arthur LO, Ott DE, Lifson JD. 2002. Differential Incorporation of CD45, CD80 (B7-1), CD86 (B7-2), and Major Histocompatibility Complex Class I and II Molecules into Human Immunodeficiency Virus Type 1 Virions and Microvesicles: Implications for Viral Pathogenesis and Immune Regulation. J Virol https://doi.org/10.1128/jvi.75.13.6173-6182.2001.
23. Bartusch C, Prange R. 2016. ESCRT requirements for murine leukemia virus release. Viruses https://doi.org/10.3390/v8040103.
24. Prescher J, Baumgärtel V, Ivanchenko S, Torrano AA, Bräuchle C, Müller B, Lamb DC. 2015. Super-Resolution Imaging of ESCRT-Proteins at HIV-1 Assembly Sites. PLoS Pathog https://doi.org/10.1371/journal.ppat.1004677.
25. Martin-Serrano J, Neil SJD. 2011. Host factors involved in retroviral budding and release. Nat Rev Microbiol.
26. Tang VA, Fritzsche AK, Renner TM, Burger D, Lannigan JA, Brittain GC, Ouellet C V., Pol E van der, Langlois M-A. 2019. Engineered Retroviruses as Fluorescent Biological Reference Particles for Nanoscale Flow Cytometry. bioRxiv 614461.
27. Tremblay MJ, Fortin JF, Cantin R. 1998. The acquisition of host-encoded proteins by nascent HIV-I. Immunol Today https://doi.org/10.1016/S0167-5699(98)01286-9.
28. Linde ME, Colquhoun DR, Mohien CU, Kole T, Aquino V, Cotter R, Edwards N, Hildreth JEK, Graham DR. 2013. The conserved set of host proteins incorporated into HIV-1 virions suggests a common egress pathway in multiple cell types. J Proteome Res https://doi.org/10.1021/pr300918r.
29. Burger D, Travis S. 2011. Conventional medical management of inflammatory bowel disease. Gastroenterology https://doi.org/10.1053/j.gastro.2011.02.045.
30. Burnie J, Guzzo C. 2019. The Incorporation of Host Proteins into the External HIV-1 Envelope. Viruses https://doi.org/10.3390/v11010085.
31. Hořejší V. 1998. The leucocyte Antigen FactsBook (2nd edn). Immunol Today https://doi.org/10.1016/s0167-5699(97)01240-1.
32. Sherer NM, Lehmann MJ, Jimenez-Soto LF, Ingmundson A, Horner SM, Cicchetti G, Allen PG, Pypaert M, Cunningham JM, Mothes W. 2003. Visualization of retroviral replication in living cells reveals budding into multivesicular bodies. Traffic https://doi.org/10.1034/j.1600-0854.2003.00135.x.
33. Nguyen DG, Booth A, Gould SJ, Hildreth JEK. 2003. Evidence That HIV Budding in Primary Macrophages Occurs through the Exosome Release Pathway. J Biol Chem

https://doi.org/10.1074/jbc.M309009200.
34. Klasse PJ. 2015. Molecular determinants of the ratio of inert to infectious virus particlesProgress in Molecular Biology and Translational Science.
35. Morales-Kastresana A, Telford B, Musich TA, McKinnon K, Clayborne C, Braig Z, Rosner A, Demberg T, Watson DC, Karpova TS, Freeman GJ, Dekruyff RH, Pavlakis GN, Terabe M, Robert-Guroff M, Berzofsky JA, Jones JC. 2017. Labeling extracellular vesicles for nanoscale flow cytometry. Sci Rep https://doi.org/10.1038/s41598-017-01731-2.
36. Zheng J, Sugrue RJ, Tang K. 2011. Mass spectrometry based proteomic studies on viruses and hosts - A review. Anal Chim Acta.
37. Chertova E, Chertov O, Coren L V., Roser JD, Trubey CM, Bess JW, Sowder RC, Barsov E, Hood BL, Fisher RJ, Nagashima K, Conrads TP, Veenstra TD, Lifson JD, Ott DE. 2006. Proteomic and Biochemical Analysis of Purified Human Immunodeficiency Virus Type 1 Produced from Infected Monocyte-Derived Macrophages. J Virol https://doi.org/10.1128/jvi.01013-06.
38. Saphire ACS, Gallay PA, Bark SJ. 2006. Proteomic analysis of human immunodeficiency virus using liquid chromatography/tandem mass spectrometry effectively distinguishes specific incorporated host proteins. J Proteome Res https://doi.org/10.1021/pr050276b.
39. Segura MM, Garnier A, Di Falco MR, Whissell G, Meneses-Acosta A, Arcand N, Kamen A. 2008. Identification of Host Proteins Associated with Retroviral Vector Particles by Proteomic Analysis of Highly Purified Vector Preparations. J Virol https://doi.org/10.1128/jvi.01909-07.
40. Woolley CF, Hayes MA, Mahanti P, Douglass Gilman S, Taylor T. 2017. Theoretical limitations of quantification for noncompetitive sandwich immunoassays. Anal Bioanal Chem https://doi.org/10.1007/s00216-015-9018-2.
41. Li Y, Holzgreve W, Kiefer V, Hahn S. 2006. MALDI-TOF mass spectrometry compared with real-time PCR for detection of fetal cell-free DNA in maternal plasma [7]. Clin Chem.
42. Cross TG, Hornshaw MP. 2016. Can LC and LC-MS ever replace immunoassays? J Appl Bioanal https://doi.org/10.17145/jab.16.015.
43. Doan M, Vorobjev I, Rees P, Filby A, Wolkenhauer O, Goldfeld AE, Lieberman J, Barteneva N, Carpenter AE, Hennig H. 2018. Diagnostic Potential of Imaging Flow Cytometry. Trends Biotechnol.
44. Hercher M, Mueller W, Shapiro HM. 1979. Detection and discrimination of individual viruses by flow cytometry. J Histochem Cytochem https://doi.org/10.1177/27.1.374599.
45. Brussaard CPD, Marie D, Bratbak G. 2000. Flow cytometric detection of viruses. J Virol Methods https://doi.org/10.1016/S0166-0934(99)00167-6.
46. Chen F, Lu JR, Binder BJ, Liu YC, Hodson RE. 2001. Application of digital image analysis and flow cytometry to enumerate marine viruses stained with SYBR Gold. Appl Environ Microbiol https://doi.org/10.1128/AEM.67.2.539-545.2001.
47. Martínez JM, Swan BK, Wilson WH. 2014. Marine viruses, a genetic reservoir revealed by targeted viromics. ISME J https://doi.org/10.1038/ismej.2013.214.
48. Nolte-‘t Hoen E, Cremer T, Gallo RC, Margolis LB. 2016. Extracellular vesicles and viruses: Are they close relatives? Proc Natl Acad Sci https://doi.org/10.1073/pnas.1605146113.
49. Brittain GC, Chen YQ, Martinez E, Tang VA, Renner TM, Langlois MA, Gulnik S. 2019.

A Novel Semiconductor-Based Flow Cytometer with Enhanced Light-Scatter Sensitivity for the Analysis of Biological Nanoparticles. Sci Rep https://doi.org/10.1038/s41598-019-52366-4.
50. Gaudin R, Barteneva NS. 2015. Sorting of small infectious virus particles by flow virometry reveals distinct infectivity profiles. Nat Commun https://doi.org/10.1038/ncomms7022.
51. Bonar MM, Tilton JC. 2017. High sensitivity detection and sorting of infectious human immunodeficiency virus (HIV-1) particles by flow virometry. Virology https://doi.org/10.1016/j.virol.2017.02.016.
52. Landowski M, Dabundo J, Liu Q, Nicola A V., Aguilar HC. 2014. Nipah Virion Entry Kinetics, Composition, and Conformational Changes Determined by Enzymatic Virus-Like Particles and New Flow Virometry Tools. J Virol https://doi.org/10.1128/jvi.01632-14.
53. Matter F. 2004. Overview of Immunity and the Immune System. Immunity.
54. Renner T, Bélanger K, Langlois M-A. 2018. Selective Isolation of Retroviruses from Extracellular Vesicles by Intact Virion Immunoprecipitation. BIO-PROTOCOL https://doi.org/10.21769/bioprotoc.3005.
55. Yáñez-Mó M, Siljander PRM, Andreu Z, Zavec AB, Borràs FE, Buzas EI, Buzas K, Casal E, Cappello F, Carvalho J, Colás E, Cordeiro-Da Silva A, Fais S, Falcon-Perez JM, Ghobrial IM, Giebel B, Gimona M, Graner M, Gursel I, Gursel M, Heegaard NHH, Hendrix A, Kierulf P, Kokubun K, Kosanovic M, Kralj-Iglic V, Krämer-Albers EM, Laitinen S, Lässer C, Lener T, Ligeti E, Line A, Lipps G, Llorente A, Lötvall J, Manček-Keber M, Marcilla A, Mittelbrunn M, Nazarenko I, Nolte-'t Hoen ENM, Nyman TA, O'Driscoll L, Olivan M, Oliveira C, Pállinger É, Del Portillo HA, Reventós J, Rigau M, Rohde E, Sammar M, Sánchez-Madrid F, Santarém N, Schallmoser K, Ostenfeld MS, Stoorvogel W, Stukelj R, Van Der Grein SG, Helena Vasconcelos M, Wauben MHM, De Wever O. 2015. Biological properties of extracellular vesicles and their physiological functions. J Extracell Vesicles.
56. Fujisawa R, McAtee FJ, Favara C, Hayes SF, Portis JL. 2001. N-Terminal Cleavage Fragment of Glycosylated Gag Is Incorporated into Murine Oncornavirus Particles. J Virol https://doi.org/10.1128/jvi.75.22.11239-11243.2001.
57. Renner TM, Bélanger K, Lam C, Gerpe MCR, McBane JE, Langlois M-A. 2018. Full-Length Glycosylated Gag of Murine Leukemia Virus Can Associate with the Viral Envelope as a Type I Integral Membrane Protein. J Virol https://doi.org/10.1128/jvi.01530-17.
58. Renner TM, Tang VA, Burger D, Langlois M-A. 2019. Intact Viral Particle Counts Measured by Flow Virometry Provide Insight into the Infectivity and Genome Packaging Efficiency of Moloney Murine Leukemia Virus. J Virol https://doi.org/10.1128/jvi.01600-19.
59. Cantin R, Diou J, Bélanger D, Tremblay AM, Gilbert C. 2008. Discrimination between exosomes and HIV-1: Purification of both vesicles from cell-free supernatants. J Immunol Methods https://doi.org/10.1016/j.jim.2008.07.007.
60. Kim SH, Lim K Il. 2017. Stability of retroviral vectors against ultracentrifugation is determined by the viral internal core and envelope proteins used for pseudotyping. Mol Cells https://doi.org/10.14348/molcells.2017.0043.
61. Trubey CM, Chertova E, Coren L V., Hilburn JM, Hixson C V., Nagashima K, Lifson JD,

Ott DE. 2003. Quantitation of HLA Class II Protein Incorporated into Human Immunodeficiency Type 1 Virions Purified by Anti-CD45 Immunoaffinity Depletion of Microvesicles. J Virol https://doi.org/10.1128/jvi.77.23.12699-12709.2003.
62. Arakelyan A, Fitzgerald W, Margolis L, Grivel JC. 2013. Nanoparticle-based flow virometry for the analysis of individual virions. J Clin Invest https://doi.org/10.1172/JCI67042.
63. Loret S, El Bilali N, Lippé R. 2012. Analysis of herpes simplex virus type I nuclear particles by flow cytometry. Cytom Part A https://doi.org/10.1002/cyto.a.22107.
64. El Bilali N, Duron J, Gingras D, Lippé R. 2017. Quantitative Evaluation of Protein Heterogeneity within Herpes Simplex Virus 1 Particles. J Virol https://doi.org/10.1128/jvi.00320-17.
65. Tang VA, Renner TM, Fritzsche AK, Burger D, Langlois MA. 2017. Single-Particle Discrimination of Retroviruses from Extracellular Vesicles by Nanoscale Flow Cytometry. Sci Rep https://doi.org/10.1038/s41598-017-18227-8.
66. Lippé R. 2017. Flow Virometry: a Powerful Tool To Functionally Characterize Viruses. J Virol https://doi.org/10.1128/jvi.01765-17.
67. Lippé R. 2017. Flow Virometry: A powerful tool to functionally characterize viruses. J Virol https://doi.org/10.1128/JVI.01765-17.
68. Arakelyan A, Fitzgerald W, Zicari S, Vagida M, Grivel JC, Margolis L. 2017. Flow virometry to analyze antigenic spectra of virions and extracellular vesicles. J Vis Exp https://doi.org/10.3791/55020.
69. Arakelyan A, Fitzgerald W, King DF, Rogers P, Cheeseman HM, Grivel JC, Shattock RJ, Margolis L. 2017. Flow virometry analysis of envelope glycoprotein conformations on individual HIV virions. Sci Rep https://doi.org/10.1038/s41598-017-00935-w.
70. Vlasak J, Hoang VM, Christanti S, Peluso R, Li F, Culp TD. 2016. Use of flow cytometry for characterization of human cytomegalovirus vaccine particles. Vaccine https://doi.org/10.1016/j.vaccine.2016.03.067.
71. Tang VA, Renner TM, Varette O, Le Boeuf F, Wang J, Diallo JS, Bell JC, Langlois MA. 2016. Single-particle characterization of oncolytic vaccinia virus by flow virometry. Vaccine https://doi.org/10.1016/j.vaccine.2016.08.074.
72. Musich T, Jones JC, Keele BF, Jenkins LMM, Demberg T, Uldrick TS, Yarchoan R, Robert-Guroff M. 2017. Flow virometric sorting and analysis of HIV quasispecies from plasma. JCI Insight https://doi.org/10.1172/jci.insight.90626.
73. Rein A. 2011. Murine leukemia viruses: Objects and organisms. Adv Virol.
74. Suomalainen M, Garoff H. 1994. Incorporation of homologous and heterologous proteins into the envelope of Moloney murine leukemia virus. J Virol https://doi.org/10.1128/jvi.68.8.4879-4889.1994.
75. Ding L, Derdowski A, Wang J-J, Spearman P. 2003. Independent Segregation of Human Immunodeficiency Virus Type 1 Gag Protein Complexes and Lipid Rafts. J Virol https://doi.org/10.1128/jvi.77.3.1916-1926.2003.
76. Waheed AA, Freed EO. 2010. The role of lipids in retrovirus replication. Viruses.
77. Hansen M, Jelinek L, Whiting S, Barklis E. 1990. Transport and assembly of gag proteins into Moloney murine leukemia virus. J Virol https://doi.org/10.1128/jvi.64.11.5306-5316.1990.
78. Dorfman T, Mammano F, Haseltine WA, Göttlinger HG. 1994. Role of the matrix protein in the virion association of the human immunodeficiency virus type 1 envelope

glycoprotein. J Virol https://doi.org/10.1128/jvi.68.3.1689-1696.1994.
79. Yu X, Yuan X, Matsuda Z, Lee TH, Essex M. 1992. The matrix protein of human immunodeficiency virus type 1 is required for incorporation of viral envelope protein into mature virions. J Virol https://doi.org/10.1128/jvi.66.8.4966-4971.1992.
80. Jalaguier P, Cantin R, Maaroufi H, Tremblay MJ. 2015. Selective Acquisition of Host-Derived ICAM-1 by HIV-1 Is a Matrix-Dependent Process. J Virol https://doi.org/10.1128/jvi.02701-14.
81. Qu K, Glass B, Dolezal M, Schur FKM, Murciano B, Rein A, Rumlová M, Ruml T, Kräusslich HG, Briggs JAG. 2018. Structure and architecture of immature and mature murine leukemia virus capsids. Proc Natl Acad Sci U S A https://doi.org/10.1073/pnas.1811580115.
82. Mattei S, Schur FK, Briggs JA. 2016. Retrovirus maturation - An extraordinary structural transformation. Curr Opin Virol.
83. Gorelick RJ, Henderson LE, Hanser JP, Rein A. 1988. Point mutants of Moloney murine leukemia virus that fail to package viral RNA: evidence for specific RNA recognition by a "zinc finger-like" protein sequence. Proc Natl Acad Sci U S A https://doi.org/10.1073/pnas.85.22.8420.
84. Yoshinaka Y, Katoh I, Copeland TD, Oroszlan S. 1985. Murine leukemia virus protease is encoded by the gag-pol gene and is synthesized through suppression of an amber termination codon. Proc Natl Acad Sci U S A https://doi.org/10.1073/pnas.82.6.1618.
85. Ragheb JA, Yu H, Hofmann T, Anderson WF. 1995. The amphotropic and ecotropic murine leukemia virus envelope TM subunits are equivalent mediators of direct membrane fusion: implications for the role of the ecotropic envelope and receptor in syncytium formation and viral entry. J Virol https://doi.org/10.1128/jvi.69.11.7205-7215.1995.
86. Opstelten D-JE, Wallin M, Garoff H. 1998. Moloney Murine Leukemia Virus Envelope Protein Subunits, gp70 and Pr15E, Form a Stable Disulfide-Linked Complex. J Virol https://doi.org/10.1128/jvi.72.8.6537-6545.1998.
87. Kuznetsov YG, Low A, Fan H, McPherson A. 2004. Atomic force microscopy investigation of wild-type Moloney murine leukemia virus particles and virus particles lacking the envelope protein. Virology https://doi.org/10.1016/j.virol.2004.02.023.
88. Zhu P, Chertova E, Bess J, Lifson JD, Arthur LO, Liu J, Taylor KA, Roux KH. 2003. Electron tomography analysis of envelope glycoprotein trimers on HIV and simian immunodeficiency virus virions. Proc Natl Acad Sci https://doi.org/10.1073/pnas.2634931100.
89. Stano A, Leaman DP, Kim AS, Zhang L, Autin L, Ingale J, Gift SK, Truong J, Wyatt RT, Olson AJ, Zwick MB. 2017. Dense Array of Spikes on HIV-1 Virion Particles. J Virol https://doi.org/10.1128/jvi.00415-17.
90. Arthur LO, Bess JW, Sowder RC, Benveniste RE, Mann DL, Chermann JC, Henderson LE. 1992. Cellular proteins bound to immunodeficiency viruses: Implications for pathogenesis and vaccines. Science (80-) https://doi.org/10.1126/science.1470916.
91. Fujisawa R, McAtee FJ, Zirbel JH, Portis JL. 1997. Characterization of glycosylated Gag expressed by a neurovirulent murine leukemia virus: identification of differences in processing in vitro and in vivo. J Virol https://doi.org/10.1128/jvi.71.7.5355-5360.1997.
92. Nitta T, Kuznetsov Y, McPherson A, Fan H. 2010. Murine leukemia virus glycosylated Gag (gPr80gag) facilitates interferon-sensitive virus release through lipid rafts. Proc Natl

Acad Sci U S A https://doi.org/10.1073/pnas.0908660107.
93. Low A, Datta S, Kuznetsov Y, Jahid S, Kothari N, McPherson A, Fan H. 2007. Mutation in the Glycosylated Gag Protein of Murine Leukemia Virus Results in Reduced In Vivo Infectivity and a Novel Defect in Viral Budding or Release. J Virol https://doi.org/10.1128/jvi.01538-06.
94. Rosales Gerpe MC, Renner TM, Bélanger K, Lam C, Aydin H, Langlois M-A. 2015. N - Linked Glycosylation Protects Gammaretroviruses against Deamination by APOBEC3 Proteins . J Virol https://doi.org/10.1128/jvi.03330-14.
95. Shi J, Xiong R, Zhou T, Su P, Zhang X, Qiu X, Li H, Li S, Yu C, Wang B, Ding C, Smithgall TE, Zheng Y-H. 2018. HIV-1 Nef Antagonizes SERINC5 Restriction by Downregulation of SERINC5 via the Endosome/Lysosome System. J Virol https://doi.org/10.1128/jvi.00196-18.
96. Li S, Ahmad I, Shi J, Wang B, Yu C, Zhang L, Zheng Y-H. 2018. Murine Leukemia Virus Glycosylated Gag Reduces Murine SERINC5 Protein Expression at Steady-State Levels via the Endosome/Lysosome Pathway to Counteract SERINC5 Antiretroviral Activity. J Virol https://doi.org/10.1128/jvi.01651-18.
97. Ahi YS, Zhang S, Thappeta Y, Denman A, Feizpour A, Gummuluru S, Reinhard B, Muriaux D, Fivash MJ, Rein A. 2016. Functional interplay between murine leukemia virus glycogag, serinc5, and surface glycoprotein governs virus entry, with opposite effects on gammaretroviral and ebolavirus glycoproteins. MBio https://doi.org/10.1128/mBio.01985-16.
98. Dragovic RA, Gardiner C, Brooks AS, Tannetta DS, Ferguson DJP, Hole P, Carr B, Redman CWG, Harris AL, Dobson PJ, Harrison P, Sargent IL. 2011. Sizing and phenotyping of cellular vesicles using Nanoparticle Tracking Analysis. Nanomedicine Nanotechnology, Biol Med https://doi.org/10.1016/j.nano.2011.04.003.
99. Van Der Pol E, Van Gemert MJC, Sturk A, Nieuwland R, Van Leeuwen TG. 2012. Single vs. swarm detection of microparticles and exosomes by flow cytometry. J Thromb Haemost https://doi.org/10.1111/j.1538-7836.2012.04683.x.
100. Goffinet C, Allespach I, Homann S, Tervo HM, Habermann A, Rupp D, Oberbremer L, Kern C, Tibroni N, Welsch S, Krijnse-Locker J, Banting G, Kräusslich HG, Fackler OT, Keppler OT. 2009. HIV-1 Antagonism of CD317 Is Species Specific and Involves Vpu-Mediated Proteasomal Degradation of the Restriction Factor. Cell Host Microbe https://doi.org/10.1016/j.chom.2009.01.009.
101. Iwabu Y, Fujita H, Kinomoto M, Kaneko K, Ishizaka Y, Tanaka Y, Sata T, Tokunaga K. 2009. HIV-1 accessory protein Vpu internalizes cell-surface BST-2/tetherin through transmembrane interactions leading to lysosomes. J Biol Chem https://doi.org/10.1074/jbc.M109.058305.
102. Van Damme N, Goff D, Katsura C, Jorgenson RL, Mitchell R, Johnson MC, Stephens EB, Guatelli J. 2008. The Interferon-Induced Protein BST-2 Restricts HIV-1 Release and Is Downregulated from the Cell Surface by the Viral Vpu Protein. Cell Host Microbe https://doi.org/10.1016/j.chom.2008.03.001.
103. Marin M, Pelegrin-Zurilla M, Bachrach E, Noël D, Brockly F, Piechaczyk M. 2000. Antiviral activity of an intracellularly expressed single-chain antibody fragment directed against the murine leukemia virus capsid protein. Hum Gene Ther https://doi.org/10.1089/10430340050015860.
104. Keele BF, Giorgi EE, Salazar-Gonzalez JF, Decker JM, Pham KT, Salazar MG, Sun C,

Grayson T, Wang S, Li H, Wei X, Jiang C, Kirchherr JL, Gao F, Anderson JA, Ping LH, Swanstrom R, Tomaras GD, Blattner WA, Goepfert PA, Kilby JM, Saag MS, Delwart EL, Busch MP, Cohen MS, Montefiori DC, Haynes BF, Gaschen B, Athreya GS, Lee HY, Wood N, Seoighe C, Perelson AS, Bhattacharya T, Korber BT, Hahn BH, Shaw GM. 2008. Identification and characterization of transmitted and early founder virus envelopes in primary HIV-1 infection. Proc Natl Acad Sci U S A https://doi.org/10.1073/pnas.0802203105.

105. Krementsov DN, Weng J, Lambelé M, Roy NH, Thali M. 2009. Tetraspanins regulate cell-to-cell transmission of HIV-1. Retrovirology https://doi.org/10.1186/1742-4690-6-64.
106. Grigorov B, Attuil-Audenis V, Perugi F, Nedelec M, Watson S, Pique C, Darlix JL, Conjeaud H, Muriaux D. 2009. A role for CD81 on the late steps of HIV-1 replication in a chronically infected T cell line. Retrovirology https://doi.org/10.1186/1742-4690-6-28.
107. Gordón-Alonso M, Yañez-Mó M, Barreiro O, Álvarez S, Muñoz-Fernández MÁ, Valenzuela-Fernández A, Sánchez-Madrid F. 2006. Tetraspanins CD9 and CD81 Modulate HIV-1-Induced Membrane Fusion. J Immunol https://doi.org/10.4049/jimmunol.177.8.5129.
108. Tardif MR, Tremblay MJ. 2005. Tetraspanin CD81 Provides a Costimulatory Signal Resulting in Increased Human Immunodeficiency Virus Type 1 Gene Expression in Primary CD4+ T Lymphocytes through NF-κB, NFAT, and AP-1 Transduction Pathways. J Virol https://doi.org/10.1128/jvi.79.7.4316-4328.2005.
109. Lane RE, Korbie D, Hill MM, Trau M. 2018. Extracellular vesicles as circulating cancer biomarkers: opportunities and challenges. Clin Transl Med https://doi.org/10.1186/s40169-018-0192-7.
110. Liao Z, Cimakasky LM, Hampton R, Nguyen DH, Hildreth JEK. 2001. Lipid rafts and HIV pathogenesis: Host membrane cholesterol is required for infection by HIV type 1. AIDS Res Hum Retroviruses https://doi.org/10.1089/088922201300343690.
111. Haeryfar SMM, Hoskin DW. 2004. Thy-1: More than a Mouse Pan-T Cell Marker. J Immunol https://doi.org/10.4049/jimmunol.173.6.3581.
112. de Mello Coelho V, Nguyen D, Giri B, Bunbury A, Schaffer E, Taub DD. 2004. Quantitative differences in lipid raft components between murine CD4+ and CD8+ T cells. BMC Immunol https://doi.org/10.1186/1471-2172-5-2.
113. Nitta T, Tam R, Kim JW, Fan H. 2011. The cellular protein la functions in enhancement of virus release through lipid rafts facilitated by murine leukemia virus glycosylated gag. MBio https://doi.org/10.1128/mBio.00341-10.
114. Roe T, Reynolds TC, Yu G, Brown PO. 1993. Integration of murine leukemia virus DNA depends on mitosis. EMBO J https://doi.org/10.1002/j.1460-2075.1993.tb05858.x.
115. Förster F, Medalia O, Zauberman N, Baumeister W, Fass D. 2005. Retrovirus envelope protein complex structure in situ studied by cryo-electron tomography. Proc Natl Acad Sci U S A https://doi.org/10.1073/pnas.0409178102.
116. Yeager M, Wilson-Kubalek EM, Weiner SG, Brown PO, Rein A. 1998. Supramolecular organization of immature and mature murine leukemia virus revealed by electron cryo-microscopy: Implications for retroviral assembly mechanisms. Proc Natl Acad Sci U S A https://doi.org/10.1073/pnas.95.13.7299.
117. Pizzato M. 2010. MLV glycosylated-gag is an infectivity factor that rescues Nef-deficient HIV-1. Proc Natl Acad Sci U S A https://doi.org/10.1073/pnas.1001554107.
118. Wu Y, Olety B, Weiss ER, Popova E, Yamanaka H, Göttlinger H. 2019. Potent

enhancement of HIV-1 replication by nef in the absence of SERINC3 and SERINC5. MBio https://doi.org/10.1128/mBio.01071-19.
119. Tartour K, Nguyen XN, Appourchaux R, Assil S, Barateau V, Bloyet LM, Burlaud Gaillard J, Confort MP, Escudero-Perez B, Gruffat H, Hong SS, Moroso M, Reynard O, Reynard S, Decembre E, Ftaich N, Rossi A, Wu N, Arnaud F, Baize S, Dreux M, Gerlier D, Paranhos-Baccala G, Volchkov V, Roingeard P, Cimarelli A. 2017. Interference with the production of infectious viral particles and bimodal inhibition of replication are broadly conserved antiviral properties of IFITMs. PLoS Pathog https://doi.org/10.1371/journal.ppat.1006610.
120. Ahi YS, Yimer D, Shi G, Majdoul S, Rahman K, Rein A, Compton AA. 2020. IFITM3 reduces retroviral envelope abundance and function and is counteracted by glycogag. MBio https://doi.org/10.1128/mBio.03088-19.
121. Hogue IB, Grover JR, Soheilian F, Nagashima K, Ono A. 2011. Gag Induces the Coalescence of Clustered Lipid Rafts and Tetraspanin-Enriched Microdomains at HIV-1 Assembly Sites on the Plasma Membrane. J Virol https://doi.org/10.1128/jvi.00743-11.
122. Goudsmit J, Smit L. 1990. CD11a/CD18 (LFA-1) epitopes involved in syncytium formation among CD4+ T-cells following cell free HIV-1 infection. Viral Immunol https://doi.org/10.1089/vim.1990.3.289.
123. Stoye JP. 2012. Studies of endogenous retroviruses reveal a continuing evolutionary saga. Nat Rev Microbiol.

6 CV

Mariam Maltseva

EDUCATION

Master's in Microbiology and Immunology **2018- Current**
University of Ottawa, Ottawa, ON
- Admission bursary
- Master's Supervisor: Dr. Marc-André Langlois
- Master's GPA: 10

Bachelor Honours in Biomedical Science - Minor in Health Sciences **2014-2018**
University of Ottawa, Ottawa, ON
- Admission bursary
- Merit Scholarship
- Honours Thesis Supervisor: Dr. John Bell
- CGPA last two years: 8.4

Pure and Applied Sciences **2012-2014**
Heritage College, Hull, QC
- Honours Roll
- Dean's List

AWARDS AND ACHIEVEMENTS

- **Exceptional Volunteering Services - 2 500 $** University of Ottawa
- **Dean's List –** University of Ottawa, 01/2017-06/2018
- **Merit Scholarship – $ 2000** University of Ottawa
- **Admission Scholarship - $ 1000** University of Ottawaa
- **2017 Passion for Science Scholarship** – 3rd Place Essay Winner
- **CRLA Regular tutoring certificate-** College Reading & Learning Association 2014

PROFESSIONAL EXPERIENCE

Master Candidate-Research Assistant **September 2018- September 2020**
Faculty of Medicine, University of Ottawa

Working on profiling ex vivo CD4 T cell surface antigens after infection with mouse lymphoma virus MLV using flow cytometry technique through surface and intracellular staining. Further characterization and profiling of surface markers on nascent virions from infected CD4 T cells using nanoscale flow cytometry. This experimental procedure will serve as proof of concept to answer key questions such as what receptors are taken up by MMLV during egress and whether there is conservation, selective upregulation and uptake of specific host antigens.

Undergraduate Student Researcher Bell Lab **September 2017- April 2018**
The Ottawa Hospital Research Institute

Worked on a yearlong Honours Research Project on innovative research in an immerging cancer immunotherapy field of oncolytic viruses at Dr. Bell's laboratory. Conducted experiments for virus harvesting and expansion, Alamar Blue Fluorescence Assay, Crystal Violet Staining Assay, viral tittering and homogenization. Characterized ten recombinant vaccinia viruses

through assessment of cytotoxicity and replication for potential novel platform of Vaccinia virus as oncolytic cancer therapeutic.

Science Laboratory Coordinator **September 2016- September 2018**

Faculty of Education, University of Ottawa

Coordinating the laboratory and a team of 3 technicians, closely working with the science professors, managing the laboratory and ensuring tasks are completed by the staff. Management of science materials, resources and equipment, maintaining inventory and ordering necessary materials within the budget of the department. Developed and managed the lab website, office management tools for materials, security, orders and database inventory at the lab. Performed one-on-one training with new technicians, ensured that the technician team worked cohesively and as group. Knowledge in health and safety in a laboratory and of techniques in a chemistry, biochemistry, biology, organic chemistry, physics and molecular biology laboratory. Organized a fundraising event for funding of the laboratory animals and plants.

Assistant for the Student Information System **May 2016- August 2016**

Human Resources, University of Ottawa and Deloitte

Assisted the Deloitte functional team with the admissions configuration and testing in Oracle, reviewed configuration and business process documentation for the admission to all cycles in the University of Ottawa's new Student Information System (SIS), uoCampus. Created new admission profiles, prepared them for testing and cleaned up data.

Lab Technician **May 2013- May 2014**

Heritage College, Gatineau, QC

Working within a science laboratory, preparing necessary materials, chemicals and equipment as instructed by science professors. Managing the inventory of science materials and data based inventory, assisting professors with demos in class. Managing general office administration, experience with materiel lists, stock requisitioning forms, counting items of stock or recording information on forms.

VOLUNTEER EXPERIENCE

Mentor for Graduate Students **Sept 1st, 2019-Present**

Organized by the BMI Association

Patient Ambassador - Team Leader **May 2016- Present**

Cancer Center, The Ottawa Hospital

- Provide guidance to the volunteer team for improving quality of care of patients. Assisted patients undergoing chemotherapy and their families. Ensured well-being of patients, and provided them with useful information.

Chemo Teach Instructor **May 2017-Present**

- Conducted one hour introductory sessions to recently diagnosed cancer patients on what to expect from chemotherapy treatments, participated in an answers and questions period along with other health professionals. Foster a unique relationship with the patients that are maintained during the shifts as a patient ambassador.

Relay for life for Canadian Cancer Society **Winter 2015**

- Raised awareness about the event, assisted in preparation of the event with University of Ottawa.

Blood Drive **2013-2014**

Heritage College, Hull, QC

- Delivered care and assistance to the donors to allow a safe donation and an enjoyable experience to more than 200 donors.

RESEARCH CONTRIBUTIONS:

Presentations:

Tyler Renner, Dr. Tang, Anna Fritzsche, **Mariam Maltseva**, Dr. Langlois. (2019). **Single Particle Viral Surface Antigen Phenotyping and Quantification by Nanoscale Flow Cytometry**. American Society for Virology, Minneapolis, Minnesota, United States

Mariam Maltseva, Tyler Renner, Dr. Tang, Dr. Langlois (2019). **Phenotypic Analysis of Retroviral Surface Markers by Nanoscale Flow Cytometry.** BMI Poster Day, University of Ottawa.

Andrew Norrie, **Mariam Maltseva**, Dr. Langlois (2019). Characterization of Viral & Immune Stimulated Release of Extracellular Vesicles & Endogenous Retroviruses from Murine Cells. BMI Poster Day, University of Ottawa.

Mariam Maltseva, Adrian Pelin, Dr. Le Boeuf, Dr. Bell (2018). Evaluating infectivity and toxicity of new chimeric Vaccinia Virus strains on suspension cells. BIM Poster Day, University of Ottawa.

Mariam Maltseva, Adrian Pelin, Dr. Le Boeuf, Dr. Bell (2018). Evaluating infectivity and toxicity of new chimeric Vaccinia Virus strains on suspension cells. 2nd Annual Research Connections Conference, University of Ottawa.

Mariam Maltseva, Adrian Pelin, Dr. Le Boeuf, Dr. Bell (2017). Evaluating infectivity and toxicity of new chimeric Vaccinia Virus strains on suspension cells. 13th Annual Canadian Undergraduate Conference on Healthcare 2017: Medicine in the Modern World, Queen's University, Canada.

Publications:

Vera Tang, Tyler Renner; Anna Fritzsche; **Mariam Maltseva** and Marc-André Langlois (2019). Profiling tetraspanin expression patterns on the surface of retroviruses and extracellular vesicles by nanoscale flow cytometry. ISEV2019 Abstract Book, Journal of Extracellular Vesicles, 8:sup1.

Mariam Maltseva, Adrian Pelin, Dr. Fabrice Le Boeuf, Dr. John Bell (2017). Evaluating infectivity and toxicity of new chimeric Vaccinia Virus strains on suspension cells. Williams et al. | URNCST Journal (2017): Volume 1, Issue 3.